



**DEPARTAMENTO DE FÍSICA**

Faculdade de Ciências e Tecnologia da  
Universidade de Coimbra

**DISSERTAÇÃO DE MESTRADO EM ENGENHARIA BIOMÉDICA**

**HEMODYNAMIC PARAMETERS ASSESSMENT**

**- An Improvement of Methodologies -**

**Vânia Maria Gomes de Almeida**

Setembro de 2009



## **DEPARTAMENTO DE FÍSICA**

Faculdade de Ciências e Tecnologia da  
Universidade de Coimbra

# **HEMODYNAMIC PARAMETERS ASSESSMENT**

## **- An Improvement of Methodologies -**

Dissertation presented to the University of Coimbra to  
complete the necessary requirements to obtain the  
degree of Master of Biomedical Engineering

### **Scientific Supervisors:**

Carlos Manuel Bolota Alexandre Correia

Luís Filipe Requicha Ferreira

**Vânia Maria Gomes de Almeida**

Coimbra, September 2009



## Research Unit

**CI-GEI**

**Centro de Instrumentação - Grupo de Electrónica e Instrumentação**

(<http://lei.fis.uc.pt>)



## Collaborations

**ISA –Intelligent Sensing Anywhere**

([www.isa.pt](http://www.isa.pt))



**IIFC- Instituto de Investigação e Formação Cardiovascular, S.A.**





*Ao meu avô Fernando Costa, que não  
teve tempo de estar aqui.*



**ABSTRACT**

The association between arterial stiffness and cardiovascular disease is an important research topic for the assessment at hemodynamic condition of the patients. Several indexes can be an indicator of arterial stiffness, the pulse wave velocity (PWV) and the augmentation index (AIx), are two examples. Other topics, as the wave reflections are a powerful marker in this context.

In this thesis are used piezoelectric sensors for record the waveform pressure and algorithms capable of rendering information about the certain hemodynamic parameters, as alternative at devices available in the market. The main motivation to search an alternative, to these devices, is related with the price for purchase these devices.

The development of a bench test capable of emulate the main characteristic of the dynamics of the arterial system constitute a powerful tool in the development of probes and in a validation of algorithms to extract clinically relevant information.

The augmentation index was the main parameters studied, this is evaluated by a new algorithm based in wavelet transform in comparison with others referenced in the literature. Its performance is assessed using realistic simulation based in exponential pulses as well using experimental data obtained from "clinical" tests in some volunteers.

**Keywords**

*Cardiovascular Diseases, Arterial Stiffness, Wavelet Transform, Augmentation Index, Piezoelectric Sensor.*





## RESUMO

A associação entre a rigidez arterial e as doenças cardiovasculares é um importante tópico de investigação com vista ao conhecimento da condição hemodinâmica dos pacientes. Vários índices podem ser um indicador da rigidez arterial, a velocidade da onda de pulso (VOP) e o índice de aumento, são dois exemplos. Outros tópicos relacionados com as ondas reflectidas são um poderoso indicador neste contexto.

Nesta tese são usados sensores piezoeléctricos para registar a forma da onda de pressão e algoritmos capazes de fornecer informação acerca de certos parâmetros hemodinâmicos, em alternativa aos dispositivos disponíveis no mercado. A principal motivação para procurar uma alternativa a estes dispositivos relaciona-se com o preço a que estes estão disponíveis.

O desenvolvimento de uma bancada de teste capaz de simular as principais características da dinâmica do sistema arterial constitui uma poderosa ferramenta com vista ao desenvolvimento de sondas e validação dos algoritmos usados para a extracção de informação clinicamente relevante.

O índice de aumento foi o principal parâmetro estudado, este foi avaliado por um novo algoritmo baseado na transformada de wavelet, em comparação com outros referenciados na literatura. O seu desempenho foi testado em pulsos a partir de uma simulação realista baseadas em exponenciais, bem como em dados experimentais obtidos em testes “clínicos” com alguns voluntários.

### **Palavras-chave**

*Doenças Cardiovasculares, Rigidez Arterial, Transformada de Wavelet, Índice de Aumento, Sensor Piezoeléctrico.*



## Acknowledgements

---

First, I must thank at my family, in special my parents that always encouragement my decisions.

At the team group of GEI, by their guidance, Prof. Dr. Carlos Correia, Prof. Dr. Requicha Ferreira, Dr. João Cardoso, Eng. Catarina Pereira, Eng. Elisabeth Borges, and my work colleague Tânia Pereira for your help along of this year. I must mention a special thanks to the Prof. Carlos Correia for their help and encourage throughout work.

Finally, a special thanks to my friends for their constant support and help.

Thank you all.

Vânia Maria Gomes de Almeida

September, 2009



---

## CONTENTS

---

<b>Abstract .....</b>	<b>vii</b>
<b>Resumo.....</b>	<b>ix</b>
<b>Acknowledgements.....</b>	<b>xi</b>
<b>Contents .....</b>	<b>xiii</b>
<b>List of Figures.....</b>	<b>xvii</b>
<b>List of Tables.....</b>	<b>xix</b>
<b>Acronyms .....</b>	<b>xxi</b>
<b>List of original papers .....</b>	<b>xxiii</b>
<b>1. Introduction.....</b>	<b>1</b>
1.1 Motivation .....	1
1.2 Main contributions.....	2
1.3 Hemodynamic project team .....	2
1.4 Contents by chapter.....	3
<b>2. Theoretical Background .....</b>	<b>5</b>
2.1 Anatomy of the Cardiovascular System .....	5
2.1.1 The Heart.....	5
2.1.2 Circulatory routes .....	6
2.2 Arterial stiffness .....	7
2.2.1 Proximal and distal arterial stiffness.....	7
2.2.2 Age .....	7
2.2.3 Measurement methods for arterial stiffness .....	8

---

2.3	Morphology of APW.....	11
2.3.1	“Incident” wave and Incisura.....	11
2.3.2	Reflection wave .....	12
2.4	Augmentation index (Alx) .....	13
2.5	Windkessel model .....	14
2.6	Clinical Applications.....	16
2.6.1	Atherosclerosis .....	16
2.6.2	Myocardial infarction and stroke.....	16
2.6.3	Factors associated with increase arterial stiffness .....	16
2.7	Piezoelectric sensors.....	17
2.7.1	General concepts .....	17
2.7.2	State of the Art.....	18
<b>3.</b>	<b>Wavelet Analysis.....</b>	<b>21</b>
3.1	General concepts .....	21
3.1.1	Wavelet Transform Vs. Fourier Transform .....	21
3.2	Scale and shifting .....	22
3.3	Continuous Wavelet Transform .....	23
3.4	Discrete Wavelet Transform (DWT) .....	24
3.5	State of the Art.....	25
<b>4.</b>	<b>Process Methodology.....</b>	<b>27</b>
4.1	Introduction.....	27
4.2	Acquisition system.....	27
4.2.1	PulScope Box Acquisition.....	28
4.2.2	Probes .....	29
<b>5.</b>	<b>Bench Test Systems .....</b>	<b>31</b>
5.1	Introduction.....	31
5.2	Deconvolution method.....	33
5.3	Test bench system I.....	34
5.3.1	First configuration .....	36
5.3.2	Second configuration .....	36
5.4	Bench test system II .....	38
5.4.1	Pressure sensors.....	39
5.4.2	Propagation of cardiac-like pressure wave .....	40
5.4.3	Inflection points.....	44

---

<b>6.</b>	<b>Synthesized Cardiac Waveforms .....</b>	<b>47</b>
6.1	Cardiac Pulses Synthesis .....	47
6.2	Augmentation Index.....	48
6.2.1	Reference values.....	50
6.2.2	Probability density function (PDF) .....	50
6.2.3	Bior1.3 mother wavelet.....	51
6.3	Results .....	53
<b>7.</b>	<b>Carotid Pressure Waveforms .....</b>	<b>55</b>
7.1	“Clinical” trials procedures .....	55
7.2	Data processing.....	55
7.3	Conclusions.....	58
<b>8.</b>	<b>Final remarks.....</b>	<b>59</b>
<b>9.</b>	<b>Appendix A – Specifications of DAQ modules.....</b>	<b>61</b>
<b>10.</b>	<b>Appendix B – Electronic Circuits Schematics .....</b>	<b>63</b>
<b>11.</b>	<b>Appendix C – Alx values from carotid signals.....</b>	<b>69</b>
<b>12.</b>	<b>Appendix D- Original Papers.....</b>	<b>71</b>
<b>13.</b>	<b>References.....</b>	<b>85</b>





---

## LIST OF FIGURES

---

Figure 2.1	The structure of the heart (an internal view) .....	6
Figure 2.2.	Pressure waves recorded along arterial tree .....	8
Figure 2.3	Schematic of the arterial tree .....	12
Figure 2.4	The typical arterial pressure waveforms.....	14
Figure 2.5	Windkessel models. ....	15
Figure 2.6	A sensor based on the piezoelectric effect.....	17
Figure 3.1	Fourier Transform and Wavelet Transform.....	22
Figure 3.2	Shifting a wavelet function .....	23
Figure 3.3	Schematic representation of wavelet analysis .....	23
Figure 3.4	Schematic drawing of the DWT .....	25
Figure 4.1	General system measurement architecture.....	28
Figure 4.2	Diagrammatic representation of the electronics box .....	29
Figure 4.3	Photos of PZ sensors.....	30
Figure 4.4	Photo of the PulScope Acquisition box, PZ sensors and pedal. ....	30
Figure 5.1	Schematic representation of the human arterial tree .....	32
Figure 5.2	Flowchart diagram of the deconvolution method. ....	34
Figure 5.3	Schematic drawing of the bench test I.....	35
Figure 5.4	Photo of the bench test system I .....	35
Figure 5.5	Raw and data deconvolved for the waves propagating in the tube.....	36

---

Figure 5.6	Result from the deconvolution method. ....	37
Figure 5.7	The signal processing process for a IR from a chirp signal .....	37
Figure 5.8	IR from a chirp signal .....	38
Figure 5.9	Schematic drawing of the bench test II.....	38
Figure 5.10	Photo of the bench test system II .....	39
Figure 5.11	Schematic of the pressure sensors (in detail).....	39
Figure 5.12	Pressure signals. ....	40
Figure 5.13	Raw data of a cardiac-like pressure waveform with duration of 250 ms.	42
Figure 5.14	Propagation of the Deconvolved PZ Signal along of tube (from 110 to 190 cm) .....	43
Figure 5.15	Determination of inflection points. ....	44
Figure 5.16	The real and imaginary parts of wavelet Cmor1-0.1 .....	45
Figure 5.17	Flowchart diagram of the Wavelet Method for determination of inflection points.....	46
Figure 6.1	Type A and type C waveforms resulted from synthesis process.....	49
Figure 6.2	Synthesized pressure waveform type B. ....	50
Figure 6.3	Flowchart diagram of PDF.....	51
Figure 6.4	Mother wavelet Bior1.3 and its center frequency based approximation. ....	52
Figure 6.5	Cardiac pulse and its WBior1.3 (scale 20) wavelet decomposition .....	52
Figure 6.6	Alx values for the three methods in analysis and errors for the wavelet and PDF methods. ....	54
Figure 7.1	Alx values from the carotid signals.....	56
Figure 7.2	PDF for an noisy signal. ....	57
Figure 7.3	Flowchart diagram of the first derivative method. ....	58

---

## LIST OF TABLES

---

Table I	Project team members .....	2
Table II	Gantt Diagram of project tasks .....	2
Table III	Pulse wave velocity in different vessels .....	9
Table IV	Devices based on measurement of Pulse Transit Time .....	10
Table V	Classification for the waveforms proposed by Murgó .....	13
Table VI	Effect of scaling wavelets.....	22
Table VII	Anatomical data of model for human arterial system proposed by Avolio	32
Table VIII	Parameters description used in the synthesis of the cardiac-like pulses .....	48
Table IX	Example of a set of parameters used in the synthesis of cardiac pulses for evaluate the algorithms.....	53
Table X	Statistical analysis of noisy signals. ....	57



**ACRONYMS**

CVD	Cardiovascular Diseases
PWV	Pressure Wave Velocity
AIx	Augmentation Index
PZ	Piezoelectric
PDF	Probability Density Function
APW	Arterial Pressure Waveform
DWT	Discrete Wavelet Transform
CWT	Continuous Wavelet Transform
AV	Atrioventricular
CV	Cardiovascular
PTT	Pulse Transit Time
ECG	Electrocardiogram
SBP	Systolic Blood Pressure
DBP	Diastolic Blood Pressure
DAQ	Data Acquisition
WIA	Wave Intensity Analysis
IR	Impulse Response
FFT	Fast Fourier Transform
IFFT	Inverse Fast Fourier Transform
Cmor	Wavelet Complex Morlet
WBior1.3	Mother Wavelet Bior1.3
RMSE	Root Mean Square Error



---

## LIST OF ORIGINAL PAPERS

---

Parts of this thesis have been published in the following papers:

- I. Programmable test bench for hemodynamic studies. H.C. Pereira, J.M. Cardoso, **V.G. Almeida**, T. Pereira, E. Borges, E. Figueiras, L.R. Ferreira, J.B. Simões, C. Correia. Accepted to WC2009 (World Congress 2009- Medical Physics and Biomedical Engineering), 7-12 Sept, Munich, 4 pp.
  
- II. Synthesized cardiac waveform in the evaluation of augmentation index algorithms. **Vânia Almeida**, Tânia Pereira, Elisabeth Borges, Edite Figueiras, João Cardoso, Carlos Correia, Helena Catarina Pereira, José Luís Malaquias and José B. Simões. 2009. Submitted to Biostec - Biosignals (The International Joint Conference on Biomedical Engineering Systems and Technologies), 20-23 Jan, Valencia, 7 pp.

In the following presentation, the papers above will be referred to by the Roman numerals I and II.

Paper I focuses a test bench capable of emulating some of the properties of the cardiovascular system.

Paper II discusses a technique of synthesizing cardiac-like waveforms by summing three exponentially shaped sub-pulses that represent the main components of cardiac waveform, and a new wavelet based algorithm for Augmentation Index (AIx) determination.





# 1. INTRODUCTION

## 1.1 Motivation

Cardiovascular diseases (CVD) are one of the leading causes of death. According to the World Health Organization, 17.5 million people died from CVD in 2005, and is expected that this number rises to 20 million in 2015 [1]. In Portugal, they are the main cause of death, with 36570 casualties in 2005 [2], (34% of all deaths registered).

In recent years great emphasis has been placed on the role of arterial stiffness in the development of CVD, resulting of its association with diseases, as the arteriosclerosis [3 , 4]. Several indexes have been established as indicator of arterial stiffness: the pulse wave velocity (PWV) and the augmentation index (AIx) are two examples. Other topics, such as wave reflections, are also powerful markers in this context.

Methods based on invasive blood pressure measurements are generally used in hospitals, especially in intensive care units, however, it is well known that these methods, in addition to discomfort, carry some risk for patients. So, noninvasive methods that offer a similar degree of accuracy and real time operation in a continuous mode can be an alternative to avoid these risks without compromising accuracy.

The main equipments available in the marker for determining arterial stiffness are the Complior ® (Colson) [5], and Shygmocor ® (AtCor) [6], but the use of these devices, probably due to their cost, remains restricted to research centers and did not succeed to reach a regular clinical level of operation.

In this context, this work demonstrates the capabilities of a new moderate-cost instrumentation, capable of rendering relevant clinical information. The instrumentation developed is based in piezoelectric (PZ) sensors, but the determinant factor for success of this project is the development of reliable algorithms for hemodynamic parameters extraction.

## 1.2 Main contributions

The main contribution of this thesis is the development of PZ probes and new algorithms for hemodynamic parameters assessment. A new type of programmable test bench for probe and algorithm validation can also be accounted for as relevant.

This work is a continuity project with the ultimate goal of developing a consistent apparatus capable of reliably evaluating the major descriptors of the cardiovascular system.

## 1.3 Hemodynamic project team

This work was developed at *Grupo de Electrónica e Instrumentação* (GEI), one of the research groups of *Centro de Instrumentação* (CI) of the University of Coimbra, in the framework of a partnership with *Instituto de Investigação e Formação Cardiovascular* (IIFC) and *Intelligent Sensing Anywhere* (ISA).

Table I shows an overview of the projects currently running at GEI and of the associated staff and students.

Table I Project team members.

<i>Team members</i>	<i>Contribution or main area of research</i>	<i>Institution</i>
<i>Prof Dr. Carlos Correia</i>		<i>GEI</i>
<i>Prof Dr. Luís Requicha</i>	<i>Scientific and Technical</i>	<i>GEI</i>
<i>Doctor. João Cardoso</i>	<i>Supervisors</i>	<i>GEI</i>
<i>PhD Student Catarina Pereira</i>		<i>GEI/ISA</i>
<i>MSc Student Vânia Almeida</i>	<i>Hemodynamic Parameters</i>	<i>GEI</i>
<i>MSc Student Tânia Pereira</i>		<i>GEI</i>
<i>MSc Elisabeth Borges</i>	<i>Bioimpedance</i>	<i>GEI</i>
<i>PhD Student Edite Figueiras</i>		<i>GEI</i>
<i>MSc Student Vera Loureiro</i>	<i>Blood Perfusion in Microcirculation</i>	<i>GEI</i>
<i>MSc Student Rita Domingues</i>		<i>GEI</i>
<i>MSc Student Rita Sérgio Brás</i>	<i>Oxymetry</i>	<i>GEI</i>

## 1.4 Contents by chapter

This work reported in this thesis developed in three stages along time. In the first one the theoretical background was studied and, simultaneously, the hardware was developed (electronic acquisition box and probes).

In the second stage a test bench with was built with two major characteristics: firstly it should be able to replicate some of the main characteristics of the cardiovascular (CV) system. Secondly it should be able to produce programmable, arbitrary pressure waveforms.

Finally, in the third stage, new signal processing techniques were studied to extract relevant information from the probes. A new algorithm for identifying the inflection points that determine Alx has been developed and successfully tested. This algorithm, based on the wavelet transform, was tested in both, synthesized and in carotid pressure waveforms. Results are compared with the probability distribution function (PDF) method, and with a method based in the first derivative of the waveform pressure. For the synthesized signals only, results are compared with the “real” value (derived from synthesis). All comparisons show the good performance of the new algorithm.

Table II illustrates the weekly chronogram of the main tasks developed during project course.

The second chapter, **Theoretical Background**, addresses the basic concepts associated to anatomical structure of CV system, the theoretical concepts associated to arterial stiffness, as well as it identifies the main components of the arterial pressure waveform (APW). The main indexes used to estimate the arterial stiffness are also reviewed, with special focus on Alx. A brief description of the Windkessel model is presented. , followed by a review of the physics characteristics of piezoelectric sensors.

In the chapter 3, the two approximations to **Wavelet Analysis**, the discrete wavelet transform (DWT) and the continuous wavelet transform (CWT), are reviewed, and an explanation is given about the way wavelet analysis is used in context of this thesis. Other studies, where wavelet analysis was applied to physiological signals, are also discussed.

Chapter 4, **Process Methodologies**, describes the instrumentation developed for “clinical” data acquisition, the measurement probes and the *PulScope* acquisition box are presented.

Chapter 5, **Bench Test Systems**, describes the two test benches developed. Results from these setups demonstrate that it is possible to emulate many important aspects of the dynamics of the CV system.

Chapter 6, **Synthesized Cardiac Waveforms**, describes the synthesis of cardiac-like pulses using a weighted combination of exponentially pulses. These waveforms are used to evaluate the performance of a new wavelet transform based algorithm to calculate  $Alx$ . Ideal values taken from the synthesized waveforms are used as reference. Results are also compared with values derived from the PDF method.

In chapter 7, **Carotid Pressure Waveforms**, the previous methods, and a method based in derivatives is applied to carotid pressure waveforms collected from some volunteers, to calculate  $Alx$

Finally, in Chapter 7, **Final Remarks**, some conclusions are drawn that summarized the most important contribution of this work. The developments foreseen in a near future and applications of the described techniques are also mentioned.

**Table II** Gantt Diagram of project tasks.

ID	Task name	Start	Finish	Duration	2008					2009						
					Ago	Set	Out	Nov	Dez	Jan	Fev	Mar	Abr	Mai	Jun	Jul
1	Study of the State of Art	08-09-2008	19-12-2008	15w	■											
2	Hardware developmet	13-10-2008	19-12-2008	10w	■											
3	Construction and data analysis of the Bench Test I	07-01-2009	27-02-2009	7,6w						■						
4	Construction and data analysis of the Bench Test II	02-03-2009	23-04-2009	7,8w						■						
5	Wavelet analysis	27-04-2009	26-06-2009	9w						■						
6	Paper II	09-07-2009	22-07-2009	2w						■						
7	Project Report	23-07-2009	25-08-2009	4,8w						■						

## 2. THEORETICAL BACKGROUND

*This chapter begins with an overview of cardiovascular system and the role of arterial stiffness in cardiovascular diseases. Different methods and indexes for measuring arterial stiffness are presented. A brief description of Windkessel model is presented. Section 2.7 describes the basic principles of the piezoelectric (PZ) sensors used in development of our instrumental prototypes.*

### 2.1 Anatomy of the Cardiovascular System

#### 2.1.1 The Heart

The human heart is a muscular pump, which circulates the blood through the body in order to provide oxygen to and remove carbon dioxide from the body's various systems.

The walls of the left ventricle are thicker than those of the right ventricle, thus it is able to develop a much higher pressure, pumping blood through the entire body.

The interior of the heart is divided into four chambers, left and right atria and left and right ventricles. The atria contracts and empty simultaneously into the ventricles, which also contracts in unison. The atria are separated from each other by the thin, muscular interatrial septum, while the ventricles are separated from each other by the thick, muscular interventricular septum. Atrioventricular (AV) valves lie between the atria and ventricles. Semilunar valves are located at the bases of the large vessels leading heart. The heart valves maintain a one-way flow of blood. Figure 2.1 depicts an internal view of the structure of the heart.

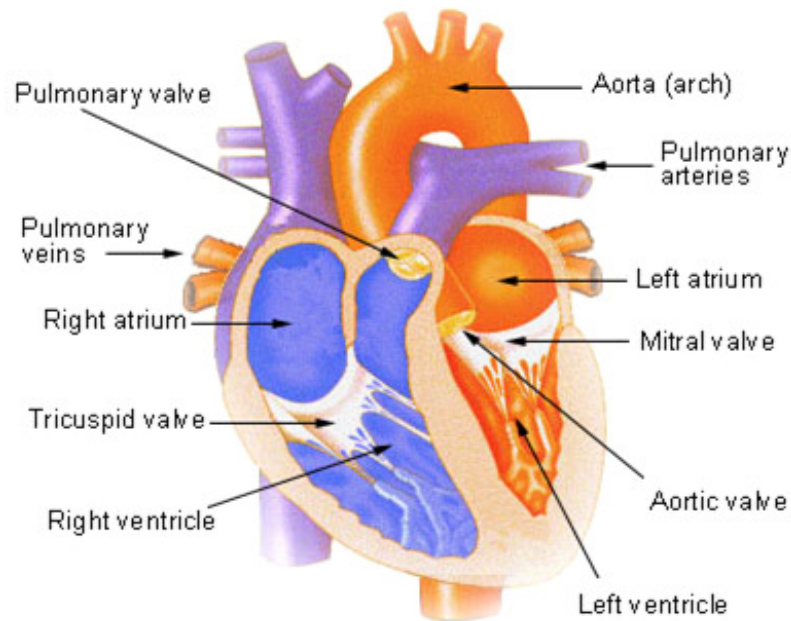


**Figure 2.1** The structure of the heart (an internal view) [7].

## 2.1.2 Circulatory routes

The blood flow is divided into two circuits, one to move the blood through the body, and one to move the blood through the lungs for oxygenation.

### 2.1.2.1 Pulmonary circulation

The right atrium receives deoxygenated blood from the superior and inferior vena cavae. This blood passes through the right AV valve (also called tricuspid valve) to fill the right ventricle. Most of the blood passes directly from the atrium into the ventricle, but a small percentage passes after contraction of the atria. Ventricular contraction causes the closure of the right AV valve and blood leaves the right ventricle through the pulmonary trunk (it follows the capillaries of the lungs). In the base of the pulmonary trunk, a pulmonary semilunar valve, also called the pulmonary valve, prevents the backflow of ejected blood into the right ventricle. The blood is oxygenated in the lungs and is transported to the left atrium.

### 2.1.2.2 Systemic circulation

The left atrium receives oxygenated blood from the lungs. The blood passes from the atrium into the ventricle through the left AV valve (also called the bicuspid valve or mitral valve). When the ventricle contracts, the valve closes to prevent the backflow of blood into the atrium. During contraction of the ventricles, the blood leaves the left ventricle through the aortic valve, and follows to all parts of the body. This valve closes when the left ventricle relaxes, and thus prevents the backflow of blood into the relaxed ventricle [8 pp. 547-552].

### **2.1.2.3 Coronary Circulation**

The wall of the heart has its own supply of systemic blood vessels to meet its vital needs. The myocardium is supplied with blood by the right and left coronary arteries. These arteries arise from the ascending part of the aorta and encircle the heart.

## **2.2 Arterial stiffness**

Recent studies demonstrated that arterial stiffness is a marker of CV risk [3]. The interest in this area increased in recent years, related with the rigidity of the arterial walls.

Regional arterial stiffness can be measured at various arterial sites, but the aorta is the major site of interest. The measure of arterial stiffness can be done by several different methods; some will be discussed in section 2.2.3.

### **2.2.1 Proximal and distal arterial stiffness**

The elastic properties of conduit arteries vary along the arterial tree, while the proximal arteries are more elastic, the distal arteries are stiffer. This is consequence of the different cellular, molecular and histological structure of the arterial wall along arterial tree.

It is inaccurate to use brachial or radial pulse pressure as a surrogate for central pulse pressure, particularly in young subjects.

Along a viscoelastic tube avoid of reflection sites, a pressure wave is progressively attenuated, with an exponential decay along the tube, but a pressure wave which propagates along a same viscoelastic tube with numerous branches is progressively amplified from central to distal conduit arteries due at wave reflections. In the peripheral arteries the pressure wave is more amplified because reflection sites are closer to peripheral sites than to central arteries and, so, PWV, is higher in peripheral stiffer artery [3].

### **2.2.2 Age**

In the elderly humans with arterial degeneration the pressure wave in the ascending aorta is almost identical to the pressure wave in the iliac artery (see figure 2.2).

While, the central arteries of younger subjects are more elastic than peripheral arteries, for elderly humans this gradient can be reversed [3]. In younger healthy



vessels the aorta is more elastic and maintains a smaller pulse pressure. In older patients the arteries are less compliant (as a rigid tube), resulting in the increase of the systolic pressure at each contraction of the aorta [9].

So, the peripheral amplification is lower in older humans than in young subjects [10]. For the elderly humans the increase of central and peripheral pressure is caused by increased of forward wave amplitude, rather than reflection wave [11].

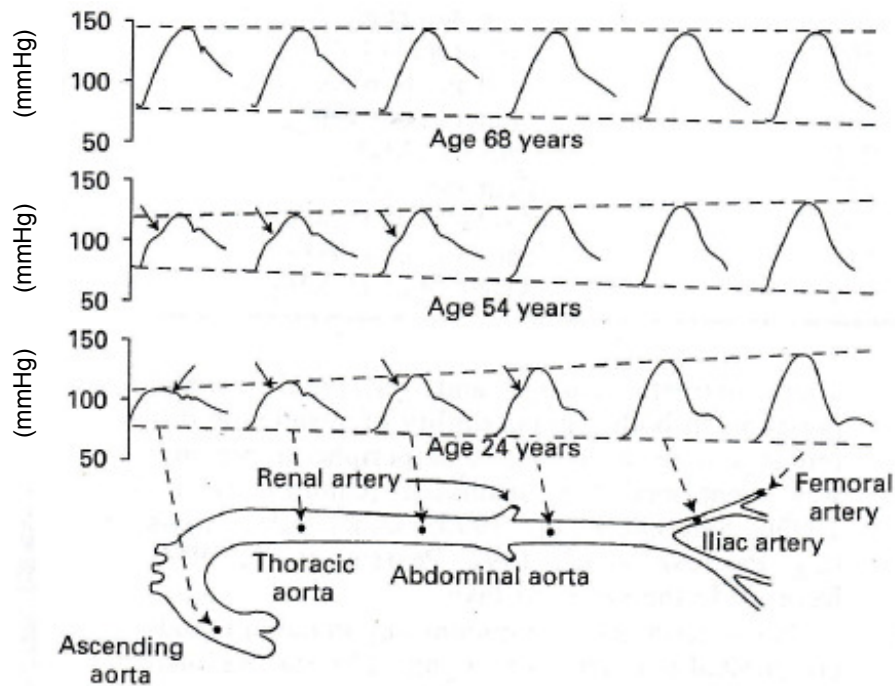


**Figure 2.2** Pressure waves recorded along arterial tree from the proximal ascending aorta to femoral artery in three humans aged 24, 54, and 68 years. The oldest subject there is little amplification in the pressure wave propagation; however in the youngest subject the amplification of the pressure wave increases approximately 60 %. Taken from [10 p. 91].

### 2.2.3 Measurement methods for arterial stiffness

There are several different methods for assessing arterial stiffness with information about systemic arterial stiffness or local arterial stiffness. The main devices used in clinical laboratories and experimental studies were presented by Bruno Pannier [12], these have remained unchanged in last years.

#### 2.2.3.1 Pulse pressure

The pulse pressure is the difference between systolic and diastolic pressures, and depends on the cardiac output, large artery stiffness and wave reflections. It is one of the simplest techniques for measure arterial stiffness, and easily practicable in clinical setting. A high pulse pressure is often a sign that the heart is working harder than the normal to maintain the circulation [9].

Pulse pressure can be measured using standard sphygmomanometer in the periphery arteries. Pulse pressure alone is inadequate to assess arterial stiffness accurately; the main problem is the amplification of pressure wave in the periphery [13].

### 2.2.3.2 Pulse wave velocity (PWV)

The PWV is the speed at which the forward wave is transmitted along the arterial tree. Moens and Korteweg formulated the following relationship, where  $E$  is the elastic modulus of the arterial wall,  $h$  is the thickness,  $r$  is the radius and  $\rho$  is the blood density.

$$PWV = \sqrt{\frac{Eh}{2r\rho}} \quad (2.1)$$

The assessment involves the measurement of time transit ( $\Delta T$ ) and distance ( $D$ ) between two points.

$$PWV = \frac{D}{\Delta T} \quad (2.2)$$

The main problems of this technique are related with the inaccessibility of the central arteries, and the difficulty in accurately estimating the distance between recording sites, using surface measurements only, and not taking into account the curvature of the arteries. Several references can be found in the literature for different measurement sites, the carotid-femoral pathway is the most common.

The value of PWV rises along arterial tree [13, 12], according to the table III. The “amplification phenomenon” described in section 2.2.1 can overestimate PWV in peripheral sites, particularly in young subjects.

The main devices based in pressure sensors used in clinical practice was the Complior System® (Colson, Les Lilas, Paris), developed by Asmar and co-workers, the Sphygmocor® System (ArtCor, Sydney, Australia) developed by O’Rourke and co-workers [16 p. 58], and the most recent device is the PulsePen® (Diatecne, Milano, Italy) [14, 15]. A brief description of these devices is presented in table IV.

**Table III** Pulse wave velocity in different vessels [3].

Ascending aorta	4-5 m/s
Abdominal aorta	5-6 m/s
Iliac and Femoral arteries	8-9 m/s

**Table IV** Devices based on measurement of pulse transit time (PTT) [12 , 17]..

Device	Arterial Measurement
<i>Complior</i> ®	<p>This system gives an automated measurement of PWV for one or two arterial segment simultaneously. The signal is acquired during 10 seconds with mechanotransducers (PZ sensors). The operator needs to confirm the quality of pressure waves.</p>
<i>Sphygmocor</i> ®	<p>Pulse transit time (PTT) between arterial sites is determined in relation to the R wave of the electrocardiogram. The signal is recorded by applanation tonometer (Millar ®) in two sites, a proximal (carotid artery) and distal (radial or femoral) sites sequentially. Transit time is obtained by subtraction from the delays between electrocardiogram (ECG) and both pulses.</p>
<i>PulsePen</i> ®	<p>PulsePen ® is composed of one tonometer and, an integrated ECG unit realizes two consecutive measurements in the carotid and femoral arteries, both synchronized by ECG. The main functions of this device are related with the measurement of the PWV, an assessment of arterial pulse wave contours, an estimation of reflection waves, and an estimation of the central blood pressure values.</p>

### 2.2.3.3 Arterial waveform

The morphology of arterial pressure waveform (APW) allows extracting clinically relevant information. Techniques of record APW have been developed to extract this information using non-invasive methods that can replace catheterization. Along the years, this quest opened new fields of investigation with development of sensing and algorithms capable of faithfully rendering this information at major arteries sites (carotid, brachial, femoral and radial, mainly).

APW analysed at the central level, ascending aorta surrogate the true load imposed to the left ventricle. The measure of APW at peripheral sites, as, the radial or brachial arteries uses a transfer function to reconstruct aortic waveform while, the measurement at carotid arteries requires a higher degree of technical expertise, but a

transfer function is not necessary. The carotid arteries are very close to central artery, so their waveforms are similar.

The use of transfer function decreases the accuracy of data, but this technique may be useful in subjects when is difficult access at carotid artery (obese subjects or in patients with major atherosclerotic plaques).

The techniques of collect still rely almost exclusively on applanation tonometry. Tonometer compresses the artery against the underlying bone allowing record a high fidelity pressure waveform [13]. This technique is easily portable and, thus useful in clinical settings. The main problem of this technique is the difficulty in obtain efficient transfer functions capable of rendering the central APW from peripheral data. Some authors as, McConnel [18] and Chen-Huan [19] advocating its accurate while other show caution, Hope demonstrate that transfer functions can not be universally applicable to both genders [20].

Photoplethysmography has been used to record the digital volume pulse. This technique measures the transmission of infrared light through the finger and ear detecting changes in volume. The analysis of the blood volume waveform allows evaluate parameters as, the Alx or the reflection index.

## 2.3 Morphology of APW

The arterial pressure waveform is a composite of a forward pressure created by ventricular contraction and a reflected wave. From the measurement of wave reflections can derive parameters as the Alx.

### 2.3.1 “Incident” wave and Incisura

The main component of pulse waveform is the forward travelling “incident” wave determined by blood ejection of left ventricle. The characteristics of the incident wave depend largely upon the elastic properties of the central aorta.

After the closure of the aortic valve the pressure in the ascending aortic increase accompanied by a sudden cessation of the flow. This pressure rise is called the incisura and, corresponds to the reaction of the aortic pressure to the closure of the aortic valve (related with effect of aortic reservoir described by Windkessel model – section 2.5). The incisura is identified approximately 300 ms after upstroke [21].

### 2.3.2 Reflection wave

The large arterial system can be properly represented as a bifurcation tree. In the bifurcations is generated a reflection wave, and its propagation depends of the elastic properties of the arterial tree.

The increased arterial stiffness, observed, for example, in older subjects or hypertensive patients increases PWV, and reflected wave travels more rapidly along the arterial tree. Thus, peripheral reflecting sites contribute to early reflected waves which arrive in early systole, superimpose on the forward wave.

The main reflections occur at iliac arteries [3 , 22], but these are inaccessible, so it is common the measurement of pressure waveforms along carotid-femoral pathway, as represented in figure 2.3.

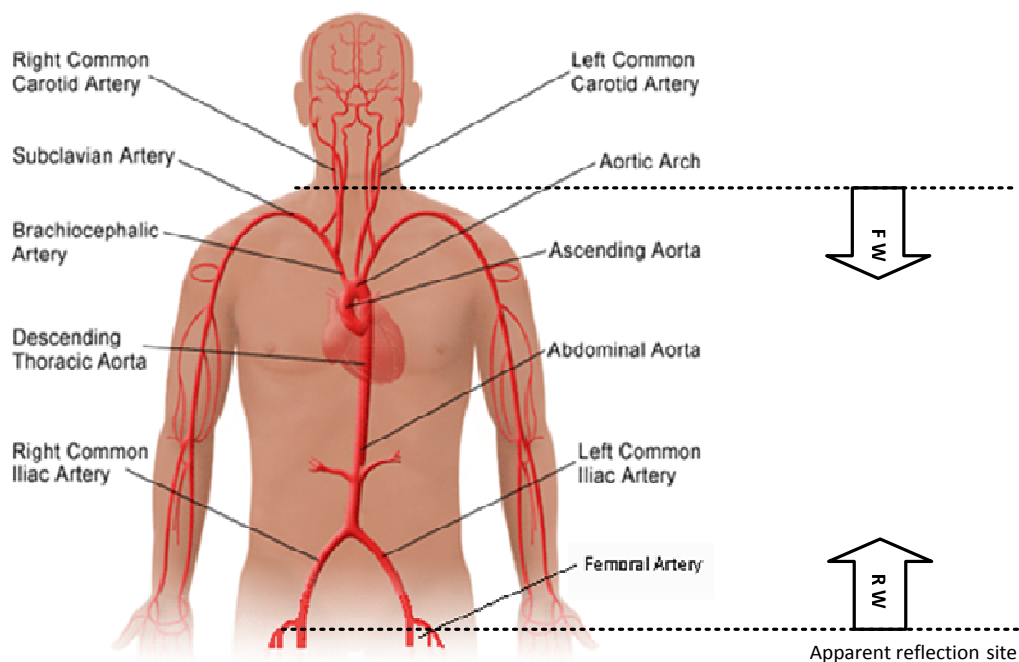


**Figure 2.3** Schematic of the arterial tree. Carotid-femoral pathway is a direct measurement of pressure waveform, but clinically relevant is the pressure central at the aorta artery. FW- forward wave, RW- reflected wave. Adapted from [23].

Figure 2.4 (p. 14) illustrates physiological cases: when the reflected wave arrives early during the systolic upstroke, producing an augmentation effect, (a) and (d), when its arrival occurs shortly after close the systolic peak (b) and when it arrives during late systole (c).

The determinant factor in the morphology of the arterial wave is the wave reflection that becomes more significant with increase age and can be related to augmentation of the risk for develop CVD.

## 2.4 Augmentation index (Alx)

Alx is one of the most widely used indices to quantify the arterial stiffness: it represents a measure of the strength of the reflected wave relative to the total pressure waveform. According to the criteria proposed by Murgu (1980) the pressure waveform can be classified into one of four types [24] (see table V and figure 2.4). The key point to estimate Alx is identifying the inflection point that the reflected wave imparts to the pressure waveform.

Despite several studies, there is still no consensus on the prognostic value of Alx over the general population.

The main problem was reported by McEniery et al. who demonstrates that Alx tends to reach a plateau value of 50 % around the age of 60. In elderly subjects the increase of forward wave amplitude is greater than the amplitude of the reflected wave (section 2.2.2). This is one limitation of index for clinical purpose [25]. Use of other index based in augmentation of pressure instead Alx can resolve this problem [26].

Several methods are used in the literature to assess the above referred inflection point, the fourth derivate is just one of them, but it cannot be used to process noisy pressure waveforms [27 , 28]. The use of filters to remove noise is no solution since it also removes useful information for the determining the inflection point.

The probability density function (PDF) method [28] can be effective although it tends to be time consuming in computational terms

**Table V** Classification proposed by Murgu (1980) [24].

<b>Type A</b>	The inflection point occurs before peak systolic. The value of Alx is positive representing larger stiffness artery. $Alx = \frac{P_S - P_i}{P_S - P_D}$
<b>Type B</b>	Indicates smaller arterial stiffness, when the inflection point occurs shortly before of the peak systolic. Same definition of type A.
<b>Type C</b>	The inflection point occurs after peak systolic. The value of Alx is negative representing that the artery is relatively elastic and healthier. $Alx = \frac{P_i - P_S}{P_S - P_D}$
<b>Type D</b>	Waveform similar to A, but inflection point cannot be observed visually because reflected wave arrives early in systole and merge with the incident wave Same definition of the type A.

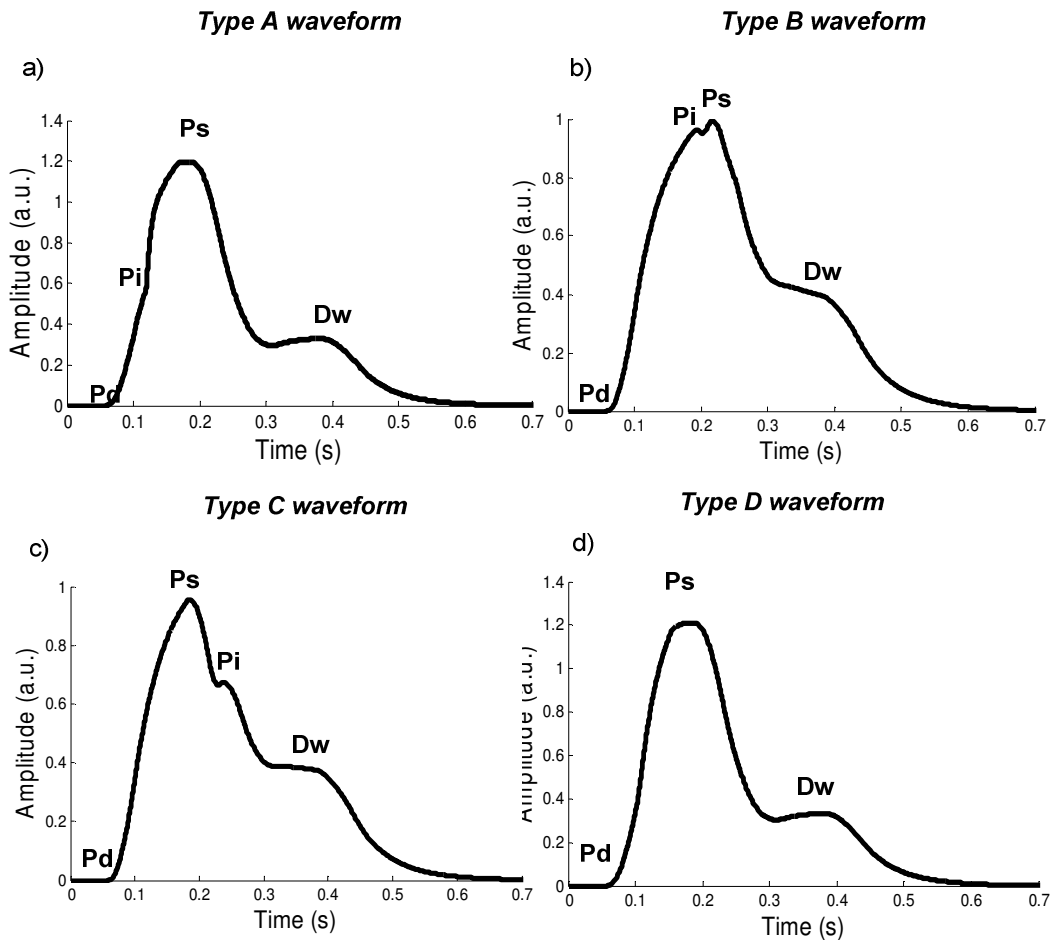


**Figure 2.4** The typical arterial pressure waveforms. Pd -diastolic pressure, Ps - systolic pressure, Pi - inflection point, Dw - dicrotic wave.

The comparison of Alx and PWV, the “gold standard” method for measure arterial stiffness, demonstrates a dissociation of results in consequence of factors as diabetes or aging process. McEniery et al. demonstrated that changes in Alx are more prominent in younger individuals (<50 years), whereas the changes in aortic PWV are more marked in older individuals (> 50 years) [25]. New techniques must be developed for a better quantification of wave reflections.

## 2.5 Windkessel model

The Windkessel model describes the whole arterial system, in terms of a pressure-flow relation at its entrance, or the effect of aortic reservoir. The blood flow from the heart enters the aorta (an elastic vessel) through a one-way valve, entering more rapidly than it can leave because the peripheral vessels are narrow.

This model is easily expressed in equations, the valve prevents backward flow, and fluid is driven through the resistance  $R$ , results of pressure,  $P$ , within the chamber vessel. The outflow,  $Q$ , is the decrease in chamber volume,  $V$ , per unit time,  $Q = dV/dt$ . Resistance is defined as the ratio of pressure to flow,  $R = P/Q$ , and the volumetric compliance of the chamber,  $C$ , is defined by  $C = dV/dP$ . The quantity  $RC$  is then,

$$\frac{1}{RC} = -\frac{dP}{P} \cdot \frac{dV}{dt} \quad (2.3)$$

Integration of this equation with respect to time of outflow shows that pressure in the chamber declines exponentially from its initial value  $P_0$  [29 p. 202].

$$P(t) = P_0 \exp\left(-\frac{t}{RC}\right) \quad (2.4)$$

This model simulates the behaviour of elastic arteries, but its simplicity can be a limitation for the quantitative physiological data, wave transmission and wave travel cannot be studied, as well the blood flow distribution along of the arterial tree.

The first Windkessel model, Frank's Windkessel, had only the pressure aortic in consideration, simulation uses a RC circuit, a capacitor and a resistor in parallel, however this model was improve by adding characteristic impedance,  $Z_c$ , necessary to describe pressure and flow throughout the entire cardiac cycle [30], this resistor can be interpreted as the resistance of the conduit arteries [31]. Figure 2.5 depicts these models.

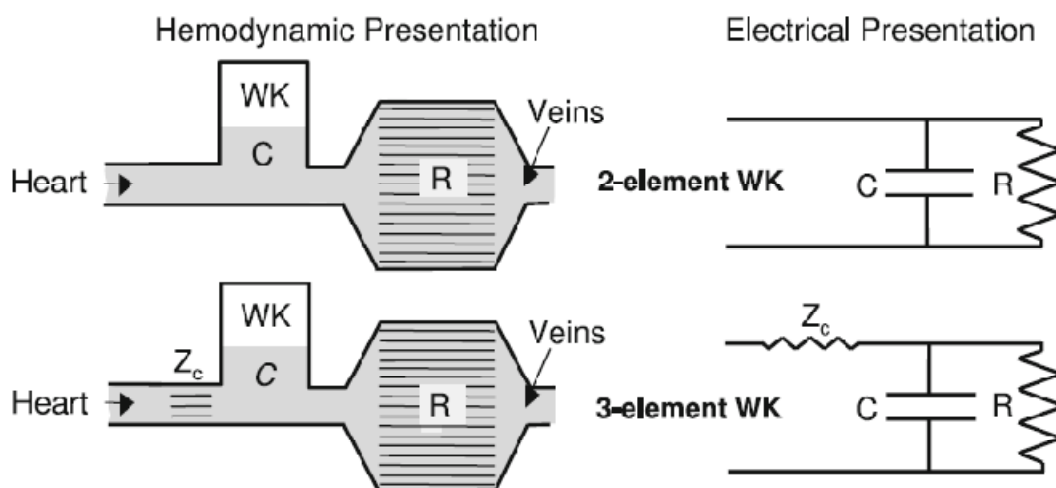


**Figure 2.5** The two and three element Windkessel models presented in hydraulic and electrical forms. Taken from [30].



## 2.6 Clinical Applications

A major reason for measuring arterial stiffness and wave reflections in clinical practice derives from recent studies that demonstrate that arterial stiffness is a marker of CV risk. An increase of arterial stiffness causes a premature return of reflected waves, increasing central pulse pressure and, thus systolic blood pressure (SBP).

### 2.6.1 Atherosclerosis

Atherosclerosis is a disease affecting arteries in which plaque constitute by fatty material builds up on the inside of the arteries. The plaque is made up of fat, cholesterol, calcium, and other substances founded in the blood.

Over time, plaque hardens and narrows arteries and reduces the amount of blood and oxygen that is delivery to vital organs [32 , 33].

Several studies reported the relation between arterial stiffness and atherosclerosis at various sites in the arterial tree [4].

Atherosclerosis can affect any artery in the body, leading to the development of different diseases depending on which artery is affected. The main arteries affected by atherosclerosis are the aorta, carotid and arteries in the legs, arms and pelvis [32].

### 2.6.2 Myocardial infarction and stroke

Stiffening of arterial tree leads to an increased SBP and, simultaneously, to a decreased diastolic blood pressure (DBP), resulting in wide pulse pressure. The increased SBP has a negative effect on the heart due to an increased workload, and the decreased DBP may limit a coronary perfusion. These effects may explain the association between arterial stiffness and myocardial infarction. So, the increased pulse pressure is a strong predictor of coronary disease [34].

The risk of a stroke (a situation where blood blow to the brain is decreased or stopped) can result from an increase of arterial stiffness. Several mechanisms can contribute to the stiffening: increase in central pulse pressure, increase of carotid wall thickness or the development of stenoses and plaque [3 ,35].

### 2.6.3 Factors associated with increase arterial stiffness

Several publications reported various pathophysiological conditions associated with increased arterial stiffness and wave reflections. Apart from the dominant effect of aging, factors as gender, obesity, smoking, hypertension, diabetes and genetic background, among other, can contribute for increase of arterial stiffness [3].

## 2.7 Piezoelectric sensors

### 2.7.1 General concepts

In the last decades piezoelectric sensors have proven to be a versatile tool for the measurement of various processes. Currently, they are used for assessing pressure, acceleration, strain or force in different application areas.

PZ sensors are characterized by having a transduction element made of a piezoelectric material. A mechanical deformation of the PZ material produces a proportional electric charge as output - “piezoelectric effect”, discovered in the 1880's by the Curie brothers. The PZ effect occurs when the charge balance within the crystal is disrupted. When no stress is applied to the material, positive and negative charges are evenly distributed and no potential difference is established. If a force is applied to the PZ crystal a disruption in the orientation of electrical dipoles occurs and so, the charge is not completely canceled. The new charge distribution results in a voltage  $V$ ,

$$V = \frac{Q_f}{C} \quad (2.5)$$

where  $Q_f$  is the charge resulting from a force applied and  $C$  is the capacitance of the device. Figure 2.6 illustrates a drawing of a sensor based on the piezoelectric effect.

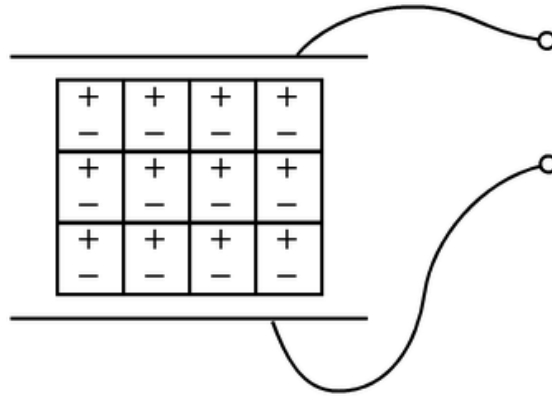


**Figure 2.6** A sensor based on the piezoelectric effect. Taken from [36; 37].

Based on PZ technology, various physical variables can be measured, the most important include pressure and acceleration. The force sensor is the basic type of sensor; pressure and acceleration are only particular designs of the force sensors.

Pressure sensors usually have a sensing diaphragm which transmits the fluid pressure to the transduction element. The effective area of diaphragm is constant and therefore, the force transmitted to the transduction element is directly proportional to the acting pressure. The force is converted in a proportional electric charge.

$$F = P \cdot A \quad (2.6)$$

In the acceleration sensors a seismic mass is attached to the crystal elements. When accelerated this mass, owing to its inertia, exerts a force on the sensor. The seismic mass is constant and so the force and correspondent output in the form of electric charge are proportional to the acting acceleration, according Newton's second law [38].

$$F = m \cdot a \quad (2.7)$$

A PZ transducer acts as a differentiator since its equivalent circuit is basically an RC network [37 , 39].

### 2.7.2 State of the Art

Several references can be found in the literature on the use of PZ sensors in hemodynamic studies. Akhila Tadinada proposes a blood pressure monitoring system for continuous ambulatory blood pressure measurement. This system is based in PZ film sensors. Two sensors are placed on the wrist and mid arm and the signal from both the sensors are then compared to compute the arterial pulse delay. The implemented device is based on Chen et al, US Patent No. 6,599,251 which expresses the arterial pulse delay proportional to blood pressure.

$$P = a + b \ln(T) \quad (2.8)$$

where P is the blood pressure, T is time delay (ms), *a* and *b* are constants depending on the nature of the subject and the signal detection device. The constants *a* and *b* are calibrated for each patient using a single pair of reference blood pressure from a standard instrument and corresponding elapse time. The method of computing *a* and *b* was not yet optimized (reference at December 2007) [40].

McLaughlin, J. et al proposes a peripheral measurement of PWV based in determination of pulse transit time between from radial to brachial arteries. The pressure pulse detection is taken by using two thin film piezoelectric sensors of Polyvinylidene fluoride (PVDF) [41].



## 3. WAVELET ANALYSIS

*This chapter presents the main concepts associated at wavelet analysis. The application of this transform at physiological signals is discussed in section 3.5.*

### 3.1 General concepts

Wavelet transform is a time-scale representation based on multiresolution signal decomposition which allows one to follow the temporal evolution of the spectrum of the frequencies contains in the signal. This transform uses long time intervals for precise regions of low frequency and shorter regions to analyse high frequency [42].

#### 3.1.1 Wavelet transform vs. Fourier transform

Fourier transform decompose a signal into its sine and cosine components. The output of this transform represents the signal in the frequency domain, where the Fourier coefficients represents the contribution of each sine and cosine at each frequency. This transform is indicated to analyse stationary signals due the nature of waves, sinusoids have not limited duration and tends to be smooth and predictable.

The wavelet transform consists in decomposing the signal into shifted and scaled versions of the original (or mother) wavelet. The figure 3.1 illustrates the analysis of a signal with this transform and compare with the analysis by the Fourier transform. A wavelet is a waveform of limited duration that has an average value of zero, and tends to be irregular and asymmetric. Starting by an initial function “mother wavelet” a family of functions can be build by dilation and translocation. Shifted versions of the mother wavelet allow analysing the signal in the time domain, and scaled versions allow analyse in frequency domain.

Conversely to Fourier analysis that has not time information, wavelet analysis allows follow the temporal evolution of the spectrum of frequencies contained in the signal [42 , 43].

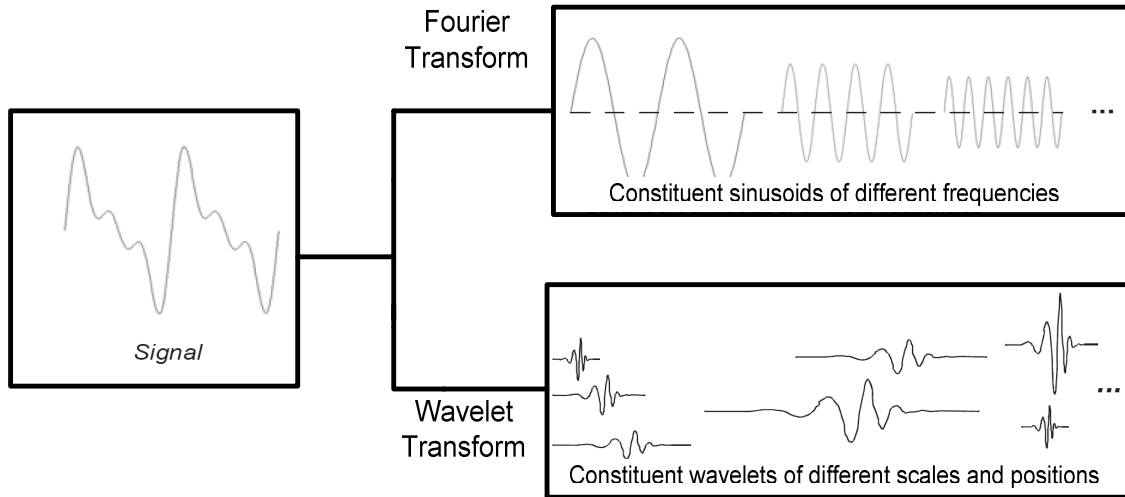


**Figure 3.1** Fourier transform vs Wavelet transform. Fourier transform yields the constituent sinusoidal components of the original signal and wavelet transform yields the constituent wavelets of the original signal in function of different scales and positions. Adapted from [44].



### 3.2 Scale and shifting

The scale of a wavelet is related with its compression or stretching, low scales correspond to high frequencies and higher scales correspond to low frequencies, as represented in table VI. At each scale corresponds a pseudo-frequency,

$$F_a = \frac{F_c}{a \cdot \Delta} \quad (3.1)$$

where  $a$  is the scale,  $F_a$  is the pseudo-frequency that corresponds to the scale  $a$  (in Hz),  $\Delta$  is the sampling period and  $F_c$  is the center frequency of a wavelet (in Hz). The center frequency corresponds at main wavelet oscillation.

**Table VI** Effect of scaling wavelets. Adapted from [44].

Low scale	Higher scale
	
<i>Compressed wavelet</i>	<i>Stretched wavelet</i>
<i>High frequency</i>	<i>Low frequency</i>

Shifting a wavelet consist in delaying or hastening its onset. Mathematically, delaying a function by  $k$  (time) is represented by:  $f(t - k)$ , as represented in figure 3.2. The schematic representation of wavelet analysis is represented in figure 3.3.

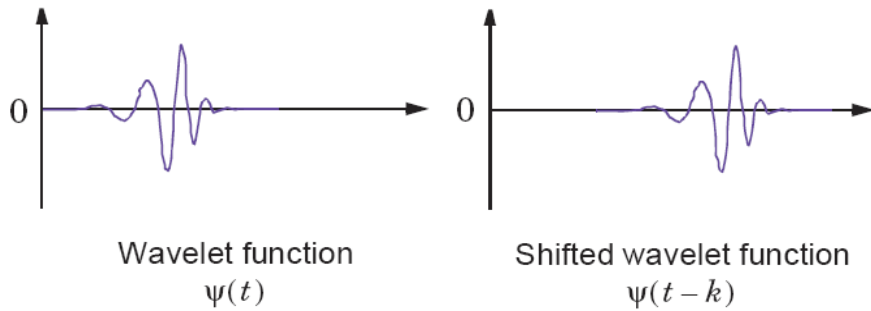


**Figure 3.2** Shifting a wavelet function. Adapted from [44].

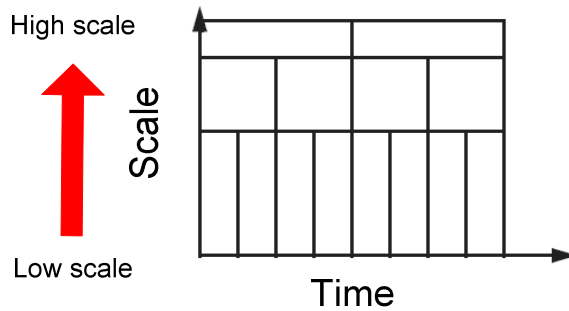


**Figure 3.3** Schematic representation of wavelet analysis. Adapted from [44].

### 3.3 Continuous Wavelet Transform

The continuous wavelet transform (CWT) is an integral transform that decomposes the signal into a family of functions. The signal under analysis  $f(t)$  is decomposed by a “mother wavelet“. The family of functions, or “wavelet frame“, is built by,

$$W_f(s, \tau) = \int_{-\infty}^{+\infty} f(t) h_{s,\tau}^*(t) dt \quad (* \text{ is the complex conjugate}) \quad (3.2)$$

Where,  $h_{s,\tau}(t)$  is the set of basic functions derived from mother wavelet, which are function of scale and position.



$$h_{s,\tau}(t) = \frac{1}{\sqrt{s}} h\left(\frac{t-\tau}{s}\right) \quad (3.3)$$

$S$  is the scaling factor that allows the expansion and the contraction of the wavelet function  $h_{s,\tau}(t)$  in time, and  $\tau$  is the factor that shifts the wavelet function in time, and  $t$  is the abscissa on which the signal is analysed (time) [42].

The list of wavelet coefficients  $W_f(s, \tau)$  represents the evolution of correlation between the signal  $f$  and the chosen wavelet at different scale values.

Several families can be studied,

- Haar,
- Daubechies,
- Biorthogonal,
- Coiflets,
- Symlets,
- Morlet,
- Mexican Hat,
- Meyer,
- Complex wavelets

The complex wavelets are a particular class defined by a real and an imaginary part. Some complex wavelet families are available in the Wavelet Toolbox of Matlab®, Gaussian derivatives, Morlet, Frequency B-Spine and Shannon [44].

### 3.4 Discrete Wavelet Transform (DWT)

The DWT is based in orthogonal dyadic functions that can be expressed as,

$$h_{i,k}(t) = 2^{i/2} h(2^i t - k \tau_0) \quad (3.4)$$

where  $i$  and  $k$  are integers. Eq. 3.4 is derived from Eq. 3.3 by choosing the dilation parameter  $s = 2^{-i}$  and restricting the translation parameter  $\tau$  to the discrete set of sampling points  $\tau_{i,k} = \frac{k}{2^i} \tau_0$ , where  $\tau_0$  is a fixed constant called the sampling rate [42].

In 1988, Mallat developed an efficient way to implement this scheme using filters, the signal passes through the filters and emerges as two signals [44 , 45].

Figure 3.4-a) depicts the process, starting from  $S$ , the first step produces two sets of coefficients: approximation coefficients  $cA_1$ , and detail coefficients  $cD_1$ . These vectors are obtained convolving  $S$  with a low-pass filter for approximation coefficient, and with a high-pass filter for detail coefficient. The coefficients  $cA_1$  and  $cD_1$  are produced by downsampling, so their length is half of the length of the original signal. The decomposition process can be iterated, with successive approximations (figure 3.4-b) [44].

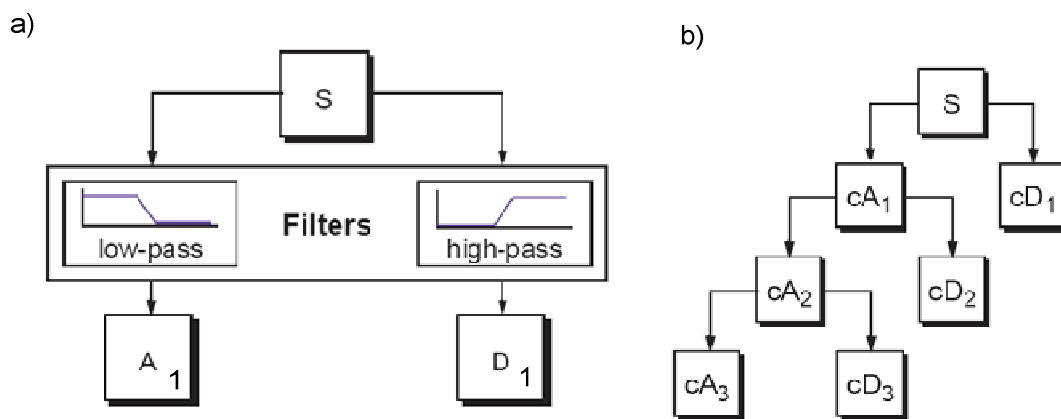


**Figure 3.4** Schematic drawing of the DWT **a)** level 1, **b)** level 1 to 3. Adapted from [44].

### 3.5 State of the Art

Physiological signals, such as blood pressure and ECG are nonstationary, depending on patient condition and heart rate. The wavelet transform is an appropriate tool to rapidly locate changes in the signals.

Some researchers focus on the study of arterial blood pressure waveform by wavelet transform analysis. De Melis et al. studied the morphological features of the pressure waveform in carotid artery using DWT (“mother” wavelet Db4), and the potential role of this transform in ascertaining the dynamics of temporal properties of APW. The wavelets details are used to identify specific features related with wave reflection and aortic valve closure. The information of wavelet details can be used for waveform classification [42]. Pulse transit time (PTT) is calculated in [46] using wavelet transform modulus maxima (WTMM) to estimate blood pressure. Antonelli et al. developed a method of accurately and consistently extracting the dicrotic notch from

the aortic blood pressure signal based in wavelet transform [47]. The detection of the dicrotic notch and systolic peak is successful determined in [48] for noisy signals.

Moghadam et al. studied the application of wavelet transforms in special complex wavelet transforms (Complex Morlet Wavelet and Complex Frequency B-Spline Wavelet) to detect QRS complex of ECG. The complex wavelets were combined to generate a hybrid wavelet transform with good performance in R peak detection [49]. Other authors also applied CWT for determine the starting points and endpoints of the P wave, QRS complex and T wave [50].

## 4. PROCESS METHODOLOGY

---

*The hardware development, probes and acquisition boxes constituted the first stage of this project. The electronic circuit schematics were developed in a previous stage.*

### 4.1 Introduction

The development of instrumentation and algorithms for pulse wave assessment started more than two years ago. Two types of sensors were used, accelerometers and PZ sensors. This work focuses the use of PZ sensors. The results obtained in previous studies demonstrate the feasibility and versatility of the PZ sensors in assessment of some hemodynamic parameters [37 , 51].

The objective of this project aims at developing and testing of probes and algorithmic basis of a non-invasive device.

### 4.2 Acquisition system

The schematic of measurement system developed is shown in figure 4.1. It can be divided into three different blocks, the PZ probe, the Pulscope box with data acquisition (DAQ) module, and the data processing block (data logging and data processing).

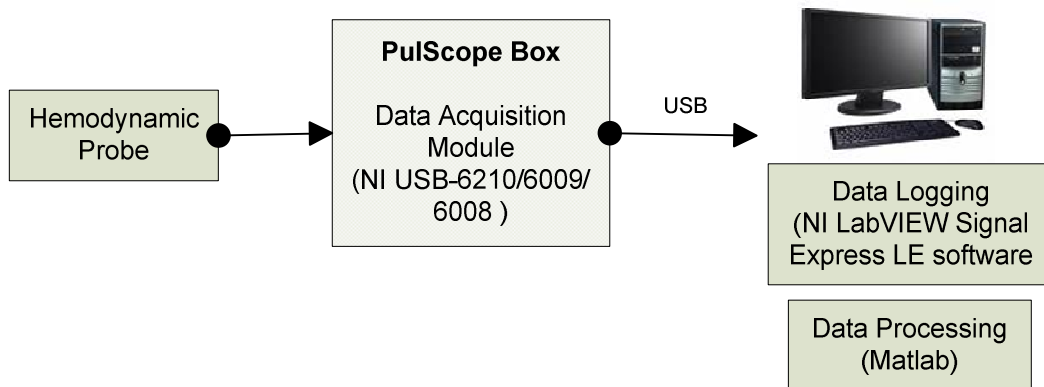


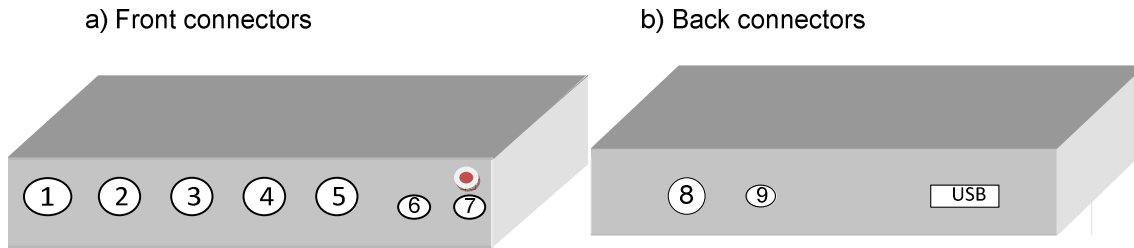
**Figure 4.1** General system measurement architecture.

#### 4.2.1 PulScope Box Acquisition

The circuit of Pulscope box is designed to amplify the signals originated at the hemodynamic probes and to convey them to a data acquisition module. The probes supported are:

- PZ+Accelerometer
- Dual Piezo Probe
- Single Piezo Probe
- Respiration thermal probe
- ECG
- Pressure sensors.

Figure 4.2 represents the schematic of PulScope box with reference at position of connectors. The circuit also supports an external switch that starts the acquisition and logging of signals. DAQ modules in use are NI USB 6210, NI USB 6008 or NI USB 6009 (see appendix A - DAQ specifications). A photo of the PulScope box, with a pedal to start the acquisition and probes is visibility in the figure 4.4.



- 1- Single PZ+Accelerometer Probe
- 2- PZ Probes
- 3- Respiration
- 4- Pedal
- 5- Pressure Sensor 1
- 6- DAQ output 1
- 7- DAQ output 2
- 8- Pressure sensor 2
- 9- Sync

**Figure 4.2** Diagrammatic representation of the electronics box showing the position of the connectors, **a)** front panel, **b)** back panel.

#### 4.2.2 Probes

The PZ probes, PZ single and PZ double, developed are based in PZ sensors (MURATA 7BB-12-9 Sounder, and MURATA 7BB-20-3CA0 Sounder, with 12 mm and 20 mm of diameter, respectively). The schematic of these probes are presented in appendix B. The probe's covering consist in a plastic box (OKW (ENCLOSURES) - B9002107). The interface between the transducer and artery (or silicon tube) is done by a PVC piece (in form of a "champignon", with 15 mm diameter in top). Two versions of these probes were used, a simple probe and a collar probe, shown in figure 4.3 and figure 4.4.

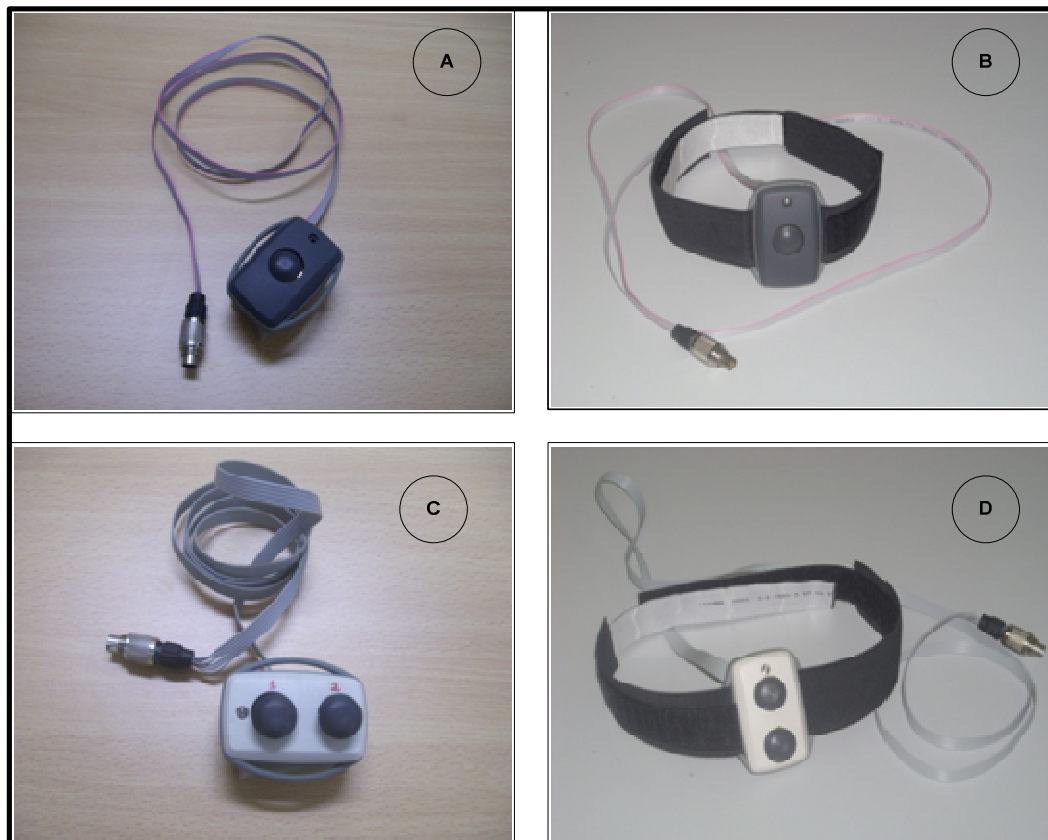


**Figure 4.3** Photos of PZ sensors. **A-** PZ single, **B-**PZ single with collar, **C-** PZ double, **D-**PZ double with collar.



**Figure 4.4** Photo of the PulScope acquisition box, PZ sensors and pedal.

## 5. BENCH TEST SYSTEMS

*The bench test system plays a fundamental role in this project, with objective of emulate the dynamics of arterial system, especially the propagation of the arterial pulse wave (APW).*

*Two benches test were developed. The bench test II is an upgrade of bench test I, with differences in the total length and in number of pressure sensors.*

*The system developed is a powerful tool in the development of probes and in a validation of algorithms to extract clinically relevant information. Results of bench test system I were accepted for presentation in WC2009 (World Congress 2009-Medical Physics and Biomedical Engineering). See appendix D- "Programmable test bench for hemodynamic studies".*

### 5.1 Introduction

A test bench was constructed with the possibility of generate a programming pressure waveforms; this is based on the combination of a programmable pressure wave generator with a flexible tube. With the use of non-invasive probes (see section 4.2.2) is possible recover the propagating pressure waveform along of the tube.

The physiological characteristics of the arterial wall exert a major influence over blood flow, and these are a determinant factor in measurement of parameters as the PWV. Latex vessels have been studied by Walker et al. proving their adequacy for use in arterial flow models [52]. In our study, a silicon rubber tube (Lindeman, 8 mm inner diameter, 0.5 mm wall thickness) is used for simulate the arteries vessels. The tube of 82 cm simulates the large vessels, aortic-iliac pathway. In comparison with a model of the human arterial system proposed by Avolio [53], the 8 mm of diameter of our system are between the range of values of the Avolio model (14.5cm - 5.7cm), but the thickness of our tube (0.5 mm) is inferior in comparison with values registered in



arterial tree (1.63-0.76 mm). Figure 5.1 illustrates the schematic of the model proposed by Avolio, and the anatomical values of segments are presented in table VII.

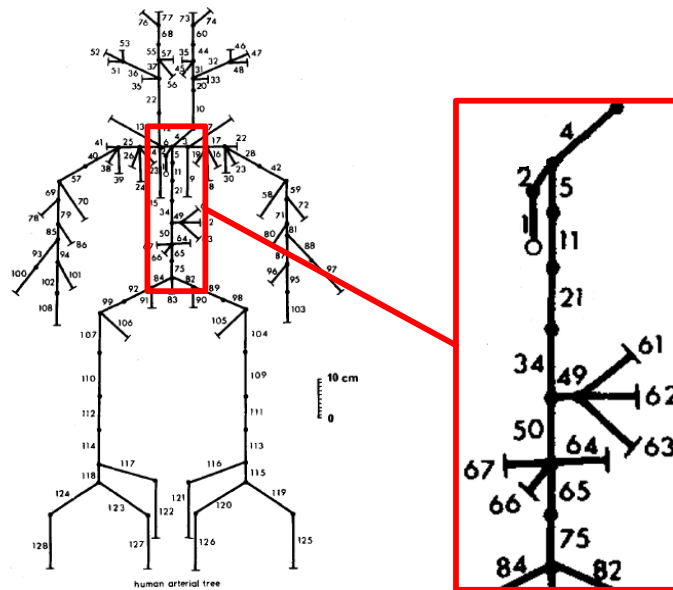


**Figure 5.1** Schematic representation of the human arterial tree. The red box corresponds at main segment used to study reflections (ascending aorta-iliac arteries). Segments numbers corresponds to arteries listed in table VII. Adapted from.[53].

**Table VII** Anatomical data referred to figure 5.1. Adapted from [53].

	<b>Number in the figure</b>	<b>Radius (mm)</b>	<b>Wall thickness (mm)</b>
<i>Ascending aorta</i>	1	14.5	1.63
<i>Aortic arch</i>	2	11.2	1.32
<i>Aortic arch</i>	5	10.7	1.27
<i>Thoracic aorta</i>	11	10.0	1.2
<i>Thoracic aorta</i>	21	9.5	1.16
<i>Thoracic aorta</i>	34	9.5	1.16
<i>Abdominal aorta</i>	50	8.7	1.08
<i>Abdominal aorta</i>	65	5.7	0.8
<i>Abdominal aorta</i>	75	5.7	0.8
<i>Common iliac</i>	82, 84	5.2	0.76

Several authors address wave separation studies based in test benches. Swillens et al. describe a sophisticated silicon model for pressure and flow wave simulation and measurement. Reflections were analysed using linear wave separation analysis and wave intensity analysis. A mixture of water and glycerine in the proportion of 60-40 was used to approximate the dynamics viscosity of blood [54]. In our model were used two solutions, water and a mixture of water and glycerine (same proportion).

The main hemodynamic parameters studied were the PWV and the AIx through of the determination of inflection points.

Other hemodynamic parameters must be studied. Wave intensity is a hemodynamic index, which is the product of changes in pressure and velocity across the wave-front. This technique allows the separation of running waves into their forward and backward directions. Feng and Khir constructed an experimental setup made of a piston pump connected at a latex tube. There were used flow and diameter probes and pressure transducers. They conclude that this index can be determined using diameter of flexible tube's wall and flow velocity instead of traditional measurements of pressure and velocity [55].

Wave intensity analysis (WIA), technique developed by Parker and Jones is a convenient time domain method for studying the propagation of waves in elastic tubes and the arterial system. Studies in literature with bench tests show that WIA can be useful in the interpretation of non-periodic waves in elastic vessels [56 , 57].

## 5.2 Deconvolution method

The objective of the deconvolution method is reversing the effect that a system exerts in an input signal. The output signal  $y(t)$  is relates with input signal  $x(t)$  by a convolution product,

$$y(t) = x(t) * h(t) \tag{5.1}$$

Where,  $h(t)$  is the impulse response (IR) of the system. In the frequency domain,

$$Y(jw) = X(jw) * H(jw), \tag{5.2}$$

Where,  $H(jw)$  is the transfer function of the system.

In this case study,  $y(t)$  is the response of PZ probe,  $x(t)$  is the APW, and  $h(t)$  is the impulse response that characterizes the probe. The impulse response can be obtained in two different setups, in response a Dirac impulse or in response a sweep signal. Figure 5.2 shows a flowchart with all mathematical operations performed on the data to get the APW. The IR and PZ signal are filtered before of the deconvolution.

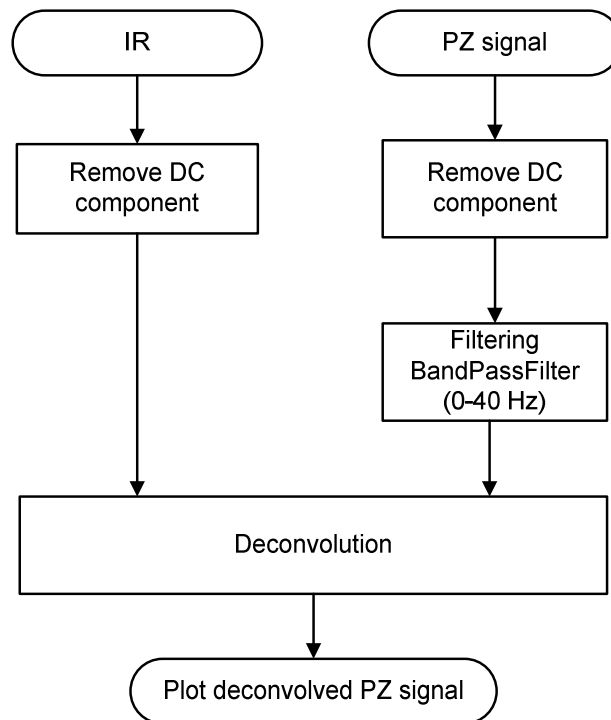
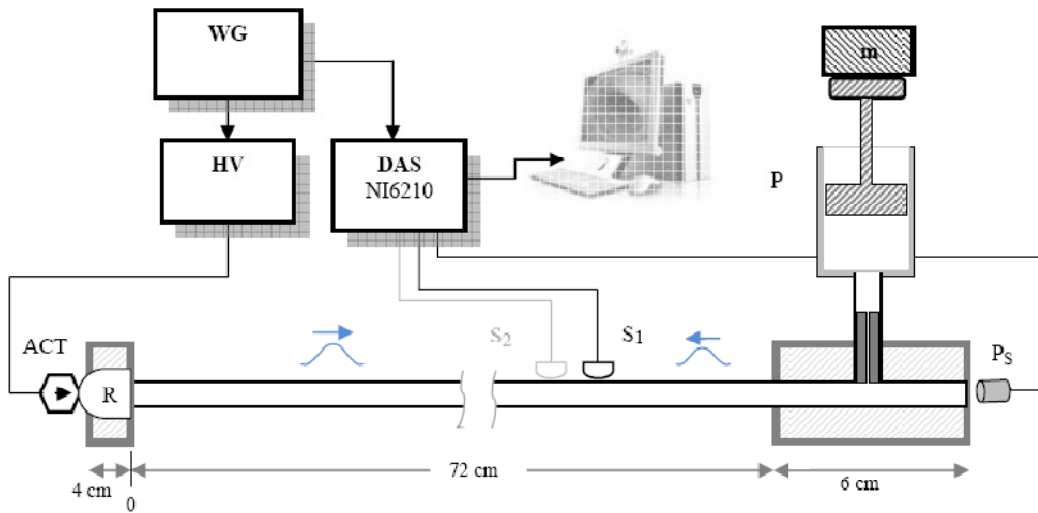


Figure 5.2 Flowchart diagram of the deconvolution method.

### 5.3 Test bench system I

In this setup, figures 5.3 and 5.4, an 82 cm long silicon tube is kept under a DC level by piston (**P**) at its right extremity. In the other extremity, a pressure waveform is generated by an actuator driven by a high voltage power driver (**HV**). This extremity is terminated by a rubber membrane (**R**). A pressure sensor is placed at the other extremity (Honeywell &C-40PC015G1A).

Two version of this system have been set up. One that generates a short duration pulse-like pressure wave from an actuator operated in a switcher mode, and another using a long stroke actuator, linearly operated under program control. This actuator is capable of generating complex pressure waveforms, such as a cardiac-like waveform. Both configurations are controlled by an Agilent 33220A arbitrary waveform generator that also delivers the synchronizing signal that triggers the DAQ.



**Figure 5.3** Schematic drawing of the bench test I. The longitudinal pressure wave is imposed by actuator (ACT) at the rubber interface (R), piston (P) and mass (m) set a DC level of 50 mm Hg. Sensors S1, S2 are placed along the tube and pressure sensor (Ps) at its end.

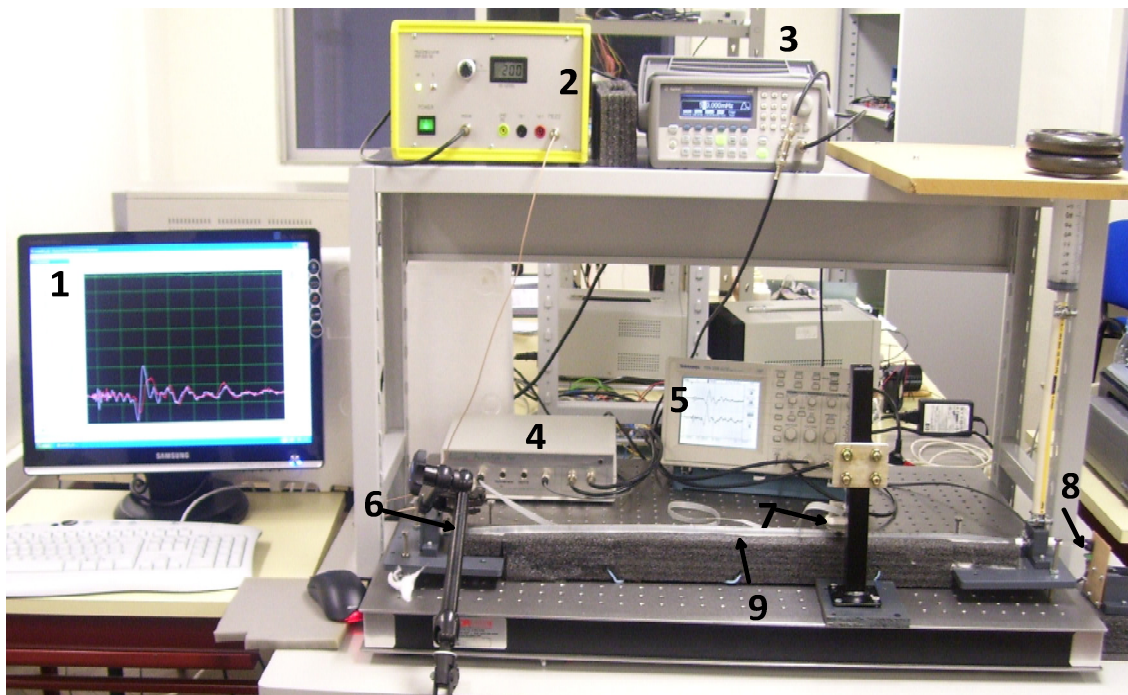


**Figure 5.4** Photo of the bench test system I. 1) Personal computer, 2) HV (power switcher), 3) WG (waveform generator), 4) PulScope acquisition box, 5) Oscilloscope, 6) PZ actuator, 7) PZ double, 8) Pressure sensor, 9) Silicon tube.

### 5.3.1 First configuration

The first configuration uses a very short pressure wave (100  $\mu\text{s}$  width, 0.5 Hz frequency) generated by a 70  $\mu\text{m}$  stroke actuator (Piezomechanik, PSt-HD200/10/45 VD 15) driven by a power switcher (Piezomechanik, HVP200/500). One of the purposes of this configuration was the characterization of this bench test. Figure 5.5 shows two different representations of the data, (raw and deconvolved) collected along the tube with 2 cm intervals, using short pulses of 100 $\mu\text{s}$  width and 0.5 Hz frequency. The forward and backward waves are clearly visible, with higher contrast on the deconvolved data panel. A very faint evidence of a possible transversal component of the forward wave is visible and denoted by **3** in figure 5.5.

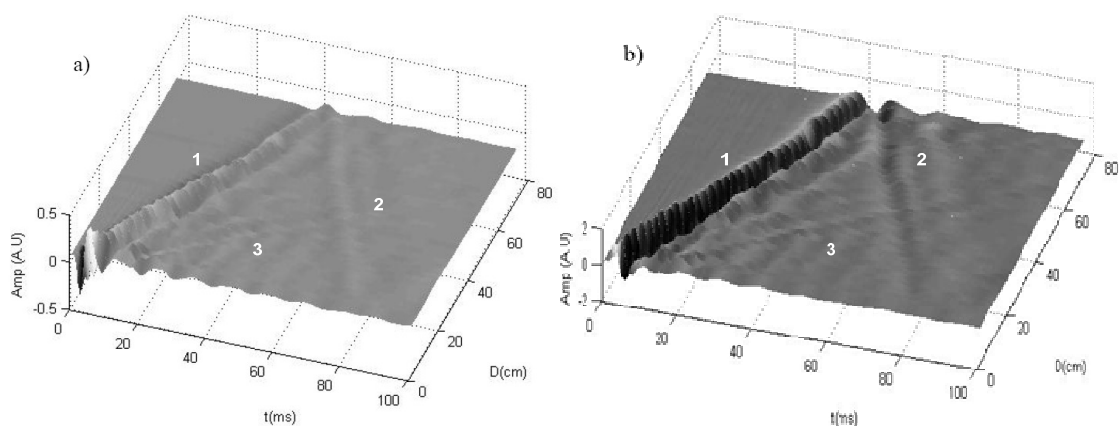


**Figure 5.5** Raw and data deconvolved represented in **a)** and **b)** respectively. 1-forward wave, 2-backward wave, 3-transversal component of the forward wave.

#### 5.3.1.1 IR obtained in an experimental setup

This configuration was used to experimentally obtain the IR of the probe by sending a Dirac like mechanical pulse, followed by a direct reading of se probe output. The experimental setup showed up difficult to operate, with results not reproducible. Hence, a new technique has been developed to obtain the IR of the system based on a different configuration of this test bench [37 p. 39].

### 5.3.2 Second configuration

For the second configuration a 700  $\mu\text{m}$  actuator (Physik Instrument GmbH, P-287) is connect to the high-voltage linear amplifier. A cardiac-like pressure waveform was synthesized and delivered to the system and deconvolution was used to recover the initial pressure waveform. Figure 5.6 shows the result of this operation when the probe is placed at the middle of the tube and clearly demonstrates the recovery capability of the concept.

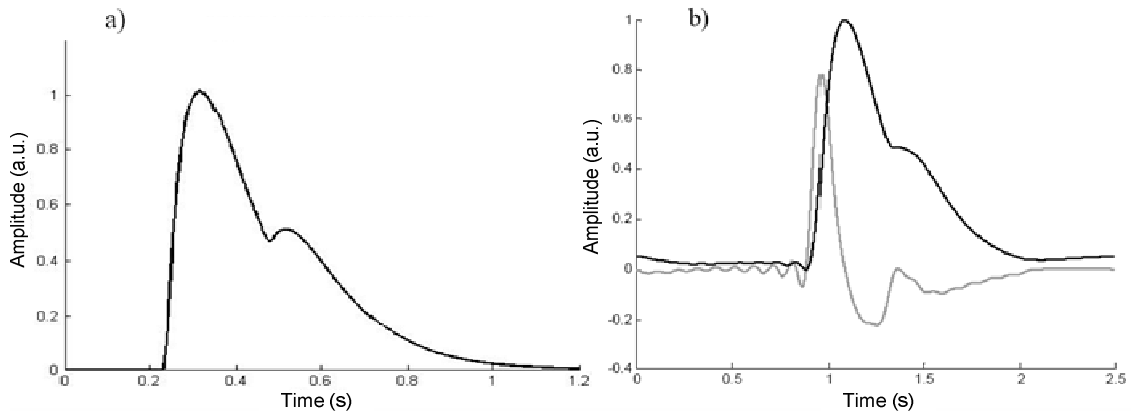


**Figure 5.6** **a)** Programmed cardiac-like pressure wave generated by the actuator, **b)** Probe output (gray), and its deconvolved output (black).

### 5.3.2.1 IR obtain from a chirp signal

This technique uses a chirp signal that sweeps the interesting range of frequencies (from approximately DC to 1 to 2 kHz). The main problem associated at this technique is the computational efficiency.

This technique is the most efficient technique for the IR extraction. The signal processing is illustrated by the figure 5.7. A linear sweep is generated by a waveform generator and is fed to the actuator and recorded by the probe. The spectrums (FFT-Fast Fourier Transform) of the probe output and of the sweep are computed, and is calculated the transfer function of the system. This frequency response is transformed back to the time domain by the Inverse Fast Fourier Transform (IFFT) [58]. Figure 5.8 depicts the frequency response of PZ single (a) obtained for a linear sweep from 10 mHz to 1kHz in 500s, and the respective IR (b).

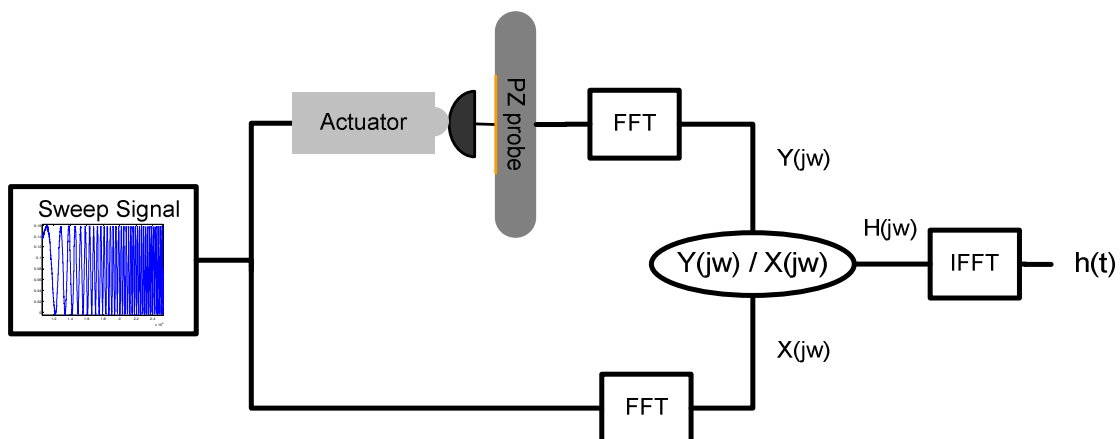


**Figure 5.7** The signal processing process.

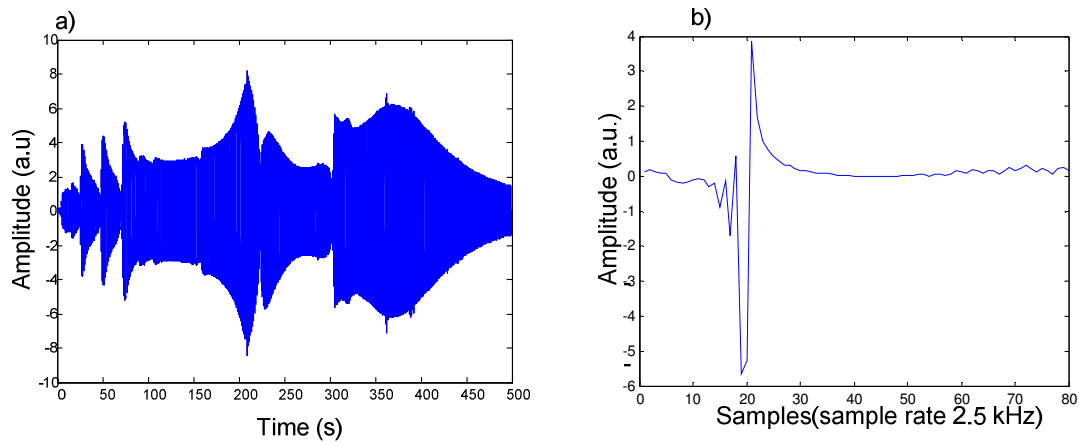


**Figure 5.8** IR from a chirp signal. **a)** Frequency response of PZ single for a linear sweep (10 MHz - 1kHz, Sweep Time - 500s), **b)** IR

## 5.4 Bench test system II

The bench test II, figures 5.9 and 5.10, is an upgrade of bench test I. The main differences are the total length of silicon tube (2 m instead of 82 cm of bench test I) and the use of two pressure sensors to monitor pressure at the beginning and end of tube.

The long tube allows better discrimination of reflected waves, and the pressure sensors are used as reference for velocity determination.

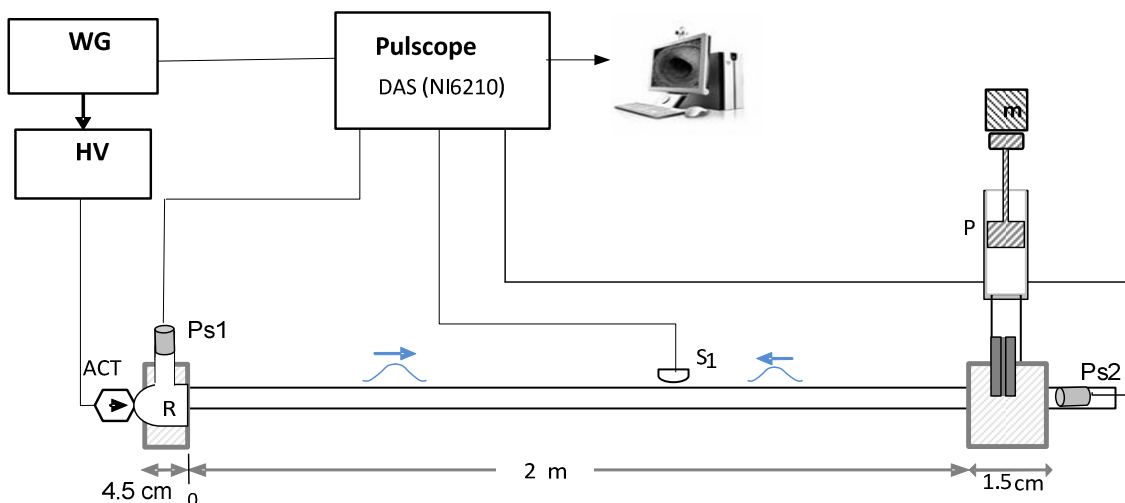


**Figure 5.9** Schematic drawing of the bench test II. Two pressure sensors are used and a long silicon tube of 2 m replaces the silicon tube of the bench test I.

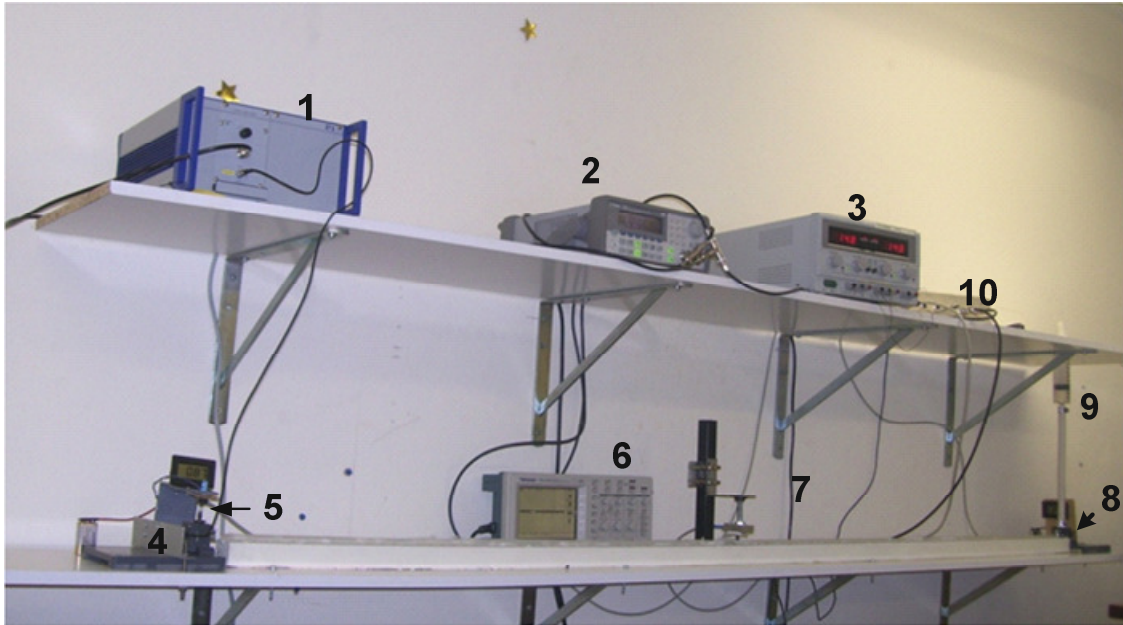


**Figure 5.10** Photo of the bench test system II. 1-HV (high voltage linear amplifier), 2-WG, 3-Power supply, 4-Actuator, 5-Pressure sensor 1, 6-Oscilloscope, 7-PZ Single, 8-Pressure sensor 2, 9- Piston, 10-Pulscope acquisition box.

#### 5.4.1 Pressure sensors

Two pressure sensors (Honeywell S&C-40PC015G1A) monitor pressure at the extremities of the tube, figure 5.11. Pressure sensor 1 (pressure at begin of tube), **Ps1**, is placed transversely to the silicon tube and pressure sensor 2, **Ps2**, longitudinally.

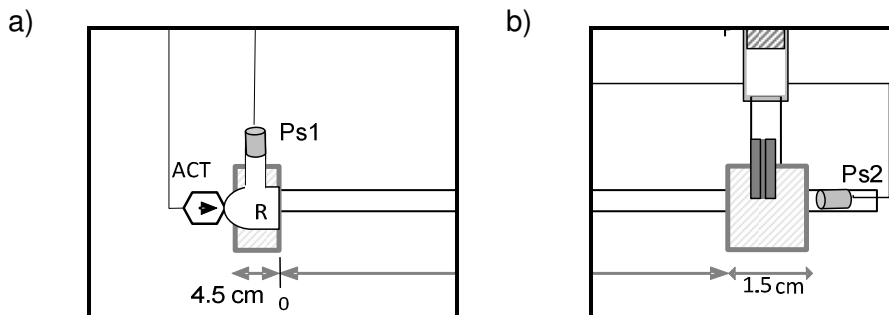


**Figure 5.11** The pressure sensors in detail. a) Pressure sensor 1, b) Pressure sensor 2.

Figure 5.12 depicts the output of pressure sensors for a triangular wave with duration of 500 ms.

Problems with noise that affects these signals are satisfactorily attenuated using a moving average filter, as shown in figure 5.12.



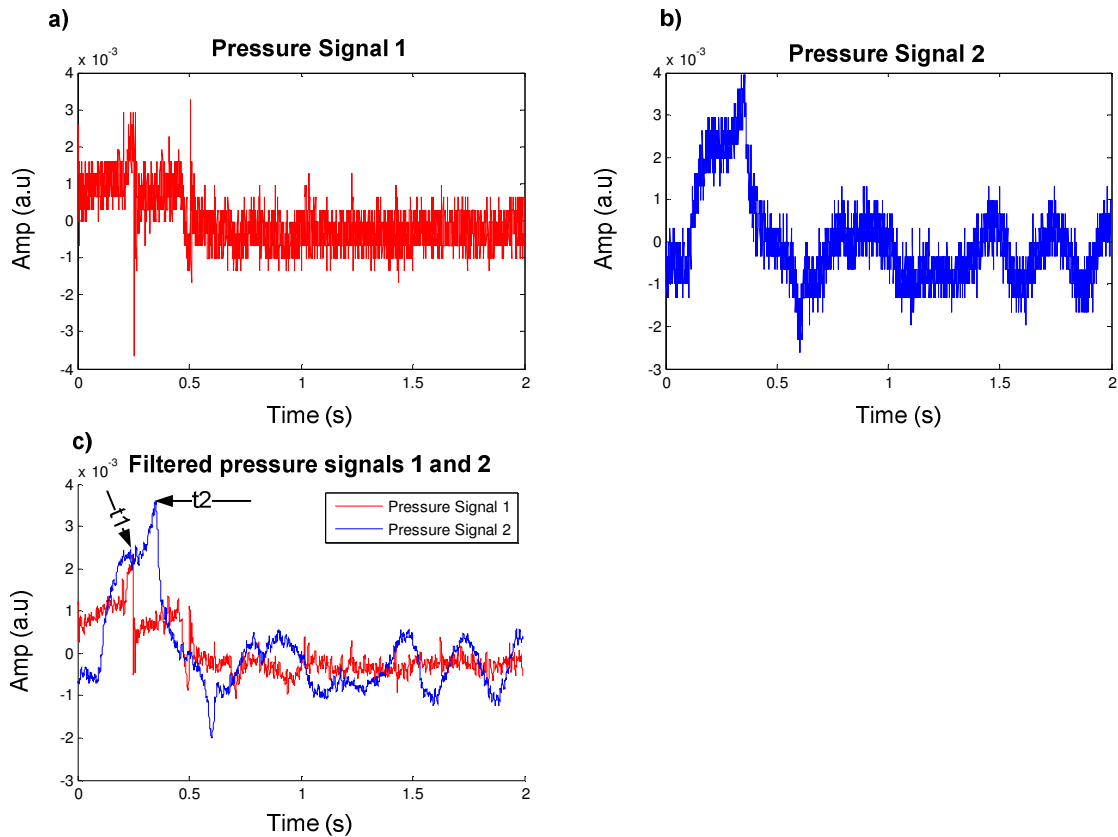


**Figure 5.12** Pressure signals. **a)** PS1, **b)** PS2, **c)** Filtered pressure signals (Filter: MovAvg-15ptos).

Velocity is defined by,

$$v = \frac{d}{\Delta t} \quad (5.3)$$

where  $d$  is distance (in m) and  $\Delta t$  is time (in s). Distance between PS1 and PS2 is 2.06 m and  $\Delta t$  is time difference between peaks of PS1 and PS2 ( $t_2 - t_1$ ), represented in figure 5.12. The computed value of velocity is 19.58 m/s.

This velocity measurement method suffers from imprecision; the measured value is only used as an estimate. Other techniques were studied for PZ double (See D dissertation-Tânia Pereira).

#### 5.4.2 Propagation of cardiac-like pressure wave

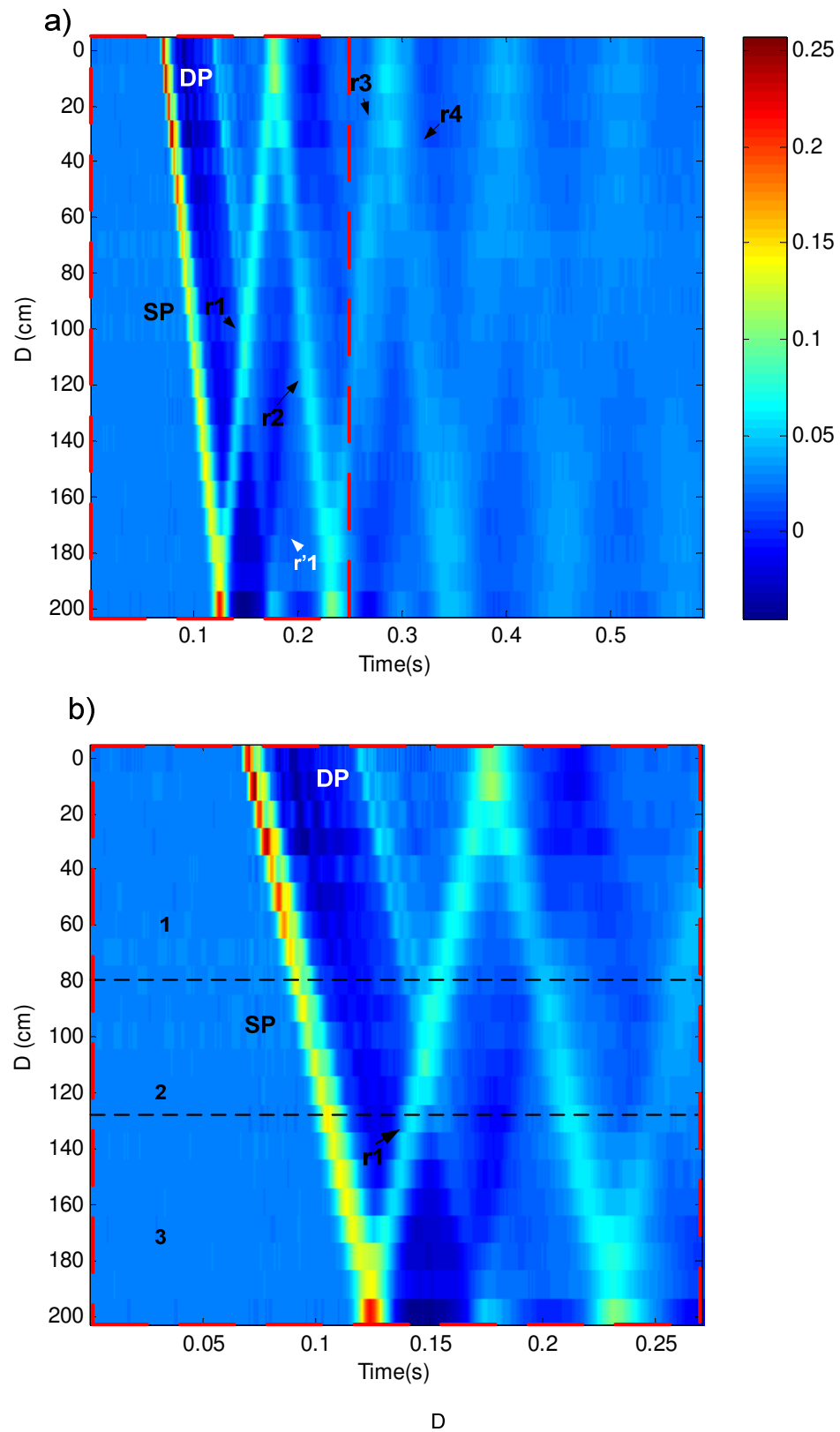
Figure 5.13 a) represents the propagation of a cardiac-like pressure waveform with duration of 250 ms along the silicon tube. The main components are the systolic peak (SP) and the diastolic peak (DP), while the SP is reflected several times with little attenuation ( $r_1, r_2, r_3, r_4$ ) the reflection of DP is much attenuated ( $r'1$ ).

Figure 5.13 b) represent in detail the propagation of waves during 250 ms. In a restricted location in the middle of tube (approximately between 80 and 120 cm) the

reflection of SP is coincident with DP (zone 2). This is the best area to acquire a "clean" signal without reflections.

In zone 1 reflection of SP arrives after of DP and in a zone 3 the reflection arrives before PD. This chapter focuses the zone 2 and 3, in 1 an oscillatory signal is detected and the reflections are not visible.

The long duration of signal causes other reflections in the signal.



**Figure 5.13** a) Raw data of a cardiac-like pressure waveform with duration of 250 ms. b) Zoom of a). DP - dicrotic peak, SP - systolic peak,  $r_1, r_2, r_3, r_4$ - successive reflections of SP,  $r_1'$ -reflection of DP. 1, 2 and 3 represents different regions on the tube.

Figure 5.14 depicts PZ signals deconvolved and the input pressure wave, in a) are represented the deconvolved PZ signals since 110 to 190 cm in the tube. In the middle of tube the PZ signal deconvolved and the programmed pressure wave are similarities (figure 5.14 b), but in the end of tube, figure 5.14 c), SP reflection ( $r_1$ ) occur before DP, the input signal cannot be fully recovered.

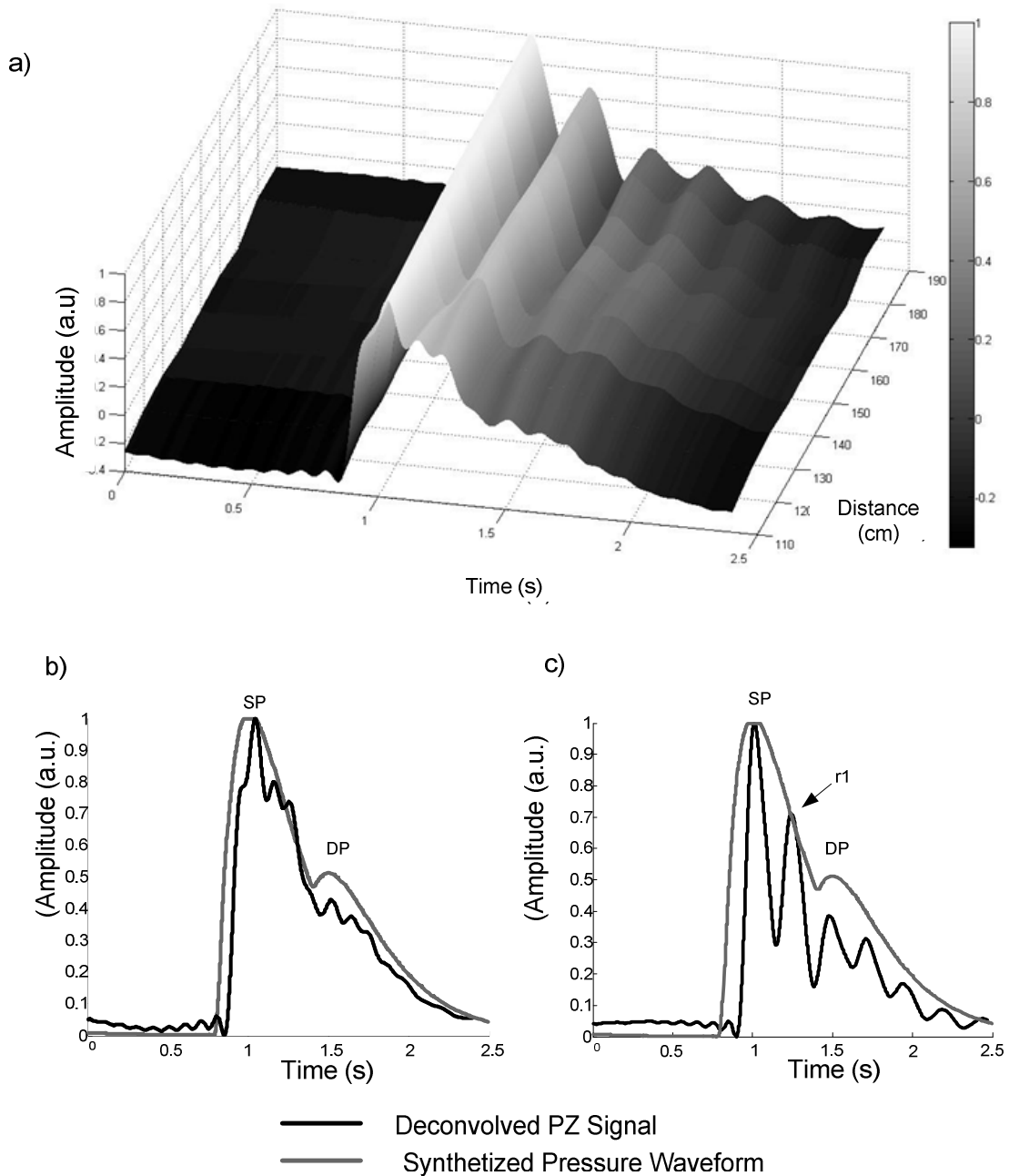


**Figure 5.14** a) Deconvolved PZ signals along of tube (from 110 to 190 cm), b) Deconvolved PZ signal at 110 cm, c) Deconvolved PZ signal at 190 cm.

### 5.4.3 Inflection points

Determining the inflection points originated by the reflected wave can be a difficult task. Preliminary results, however, demonstrate that the method based in different wavelets can be effective and, hence, a powerful tool.

The time of arrival of the waves reflected at the two extremities was computed using the previously determined value of the wave propagation velocity. These values were then compared with the ones produced by the method based in wavelets.

Figure 5.15 depicts a PZ signal in the middle of tube for a 500 ms triangular input. The blue points in figure 5.15 a) and b) are obtained using the Cmor1-0.1<sup>1</sup> mother wavelet (see flowchart of this method - figure 5.17), while the red circles, represented in b), result from velocity/distance computation.

The main disadvantage of this method is the necessity of using a trial-and-error method to select the wavelet scale. The inflection points are obtained through peak detection (maximum) in the signal that results from wavelet decomposition. The abscissas of the peaks correspond to inflection points in pressure waveform. Figure 5.16 represents the real and imaginary parts of this wavelet, from which just the real part is used in the analysis. Figure 5.17 is a flowchart of the process for determining the inflection points.

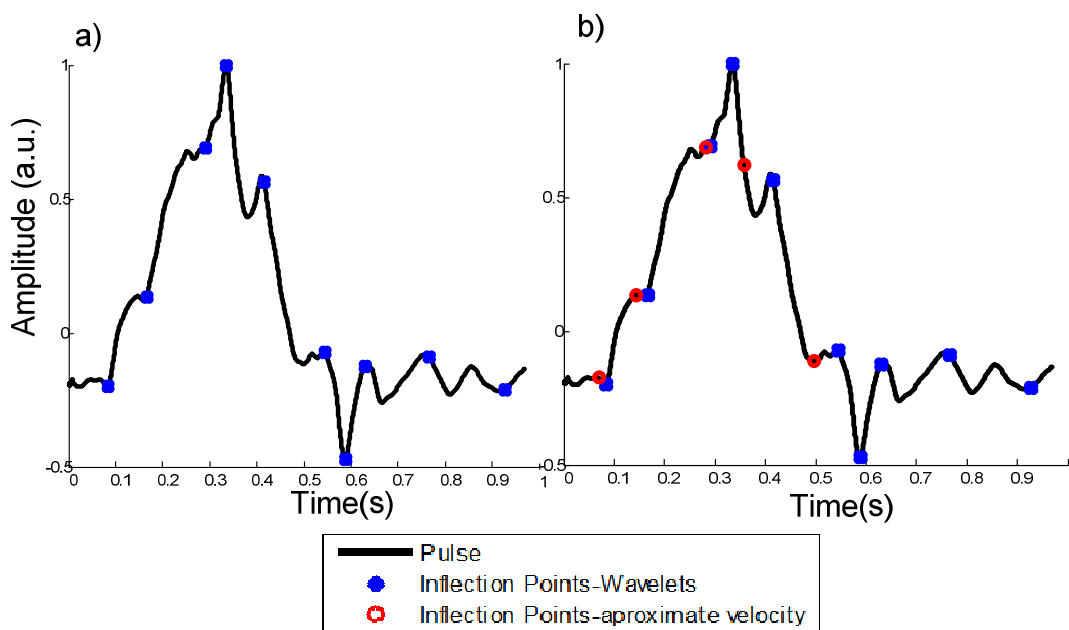


**Figure 5.15** Determination of inflection points. **a)** Method based in wavelets (Cmor1-0.1, scale13), **b)** comparison of method based in wavelets with method of velocity measurement.

<sup>1</sup> Wavelet name: Cmor"Fb"-Fc", where Fb is the bandwidth parameter and Fc is the wavelet center frequency

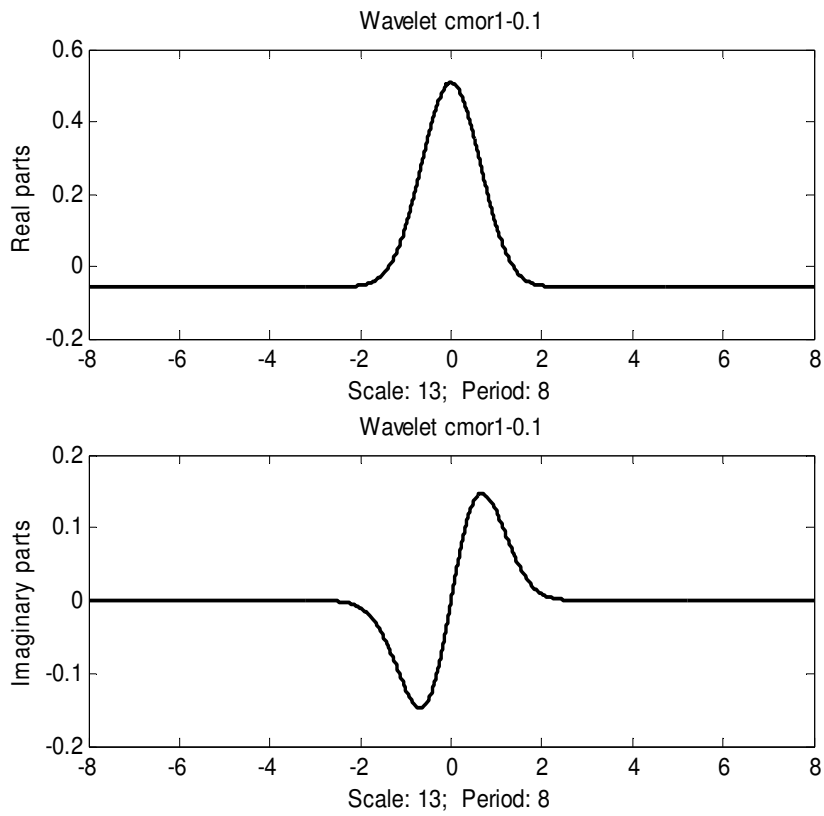


**Figure 5.16** The real and imaginary parts of wavelet Cmor1-0.1

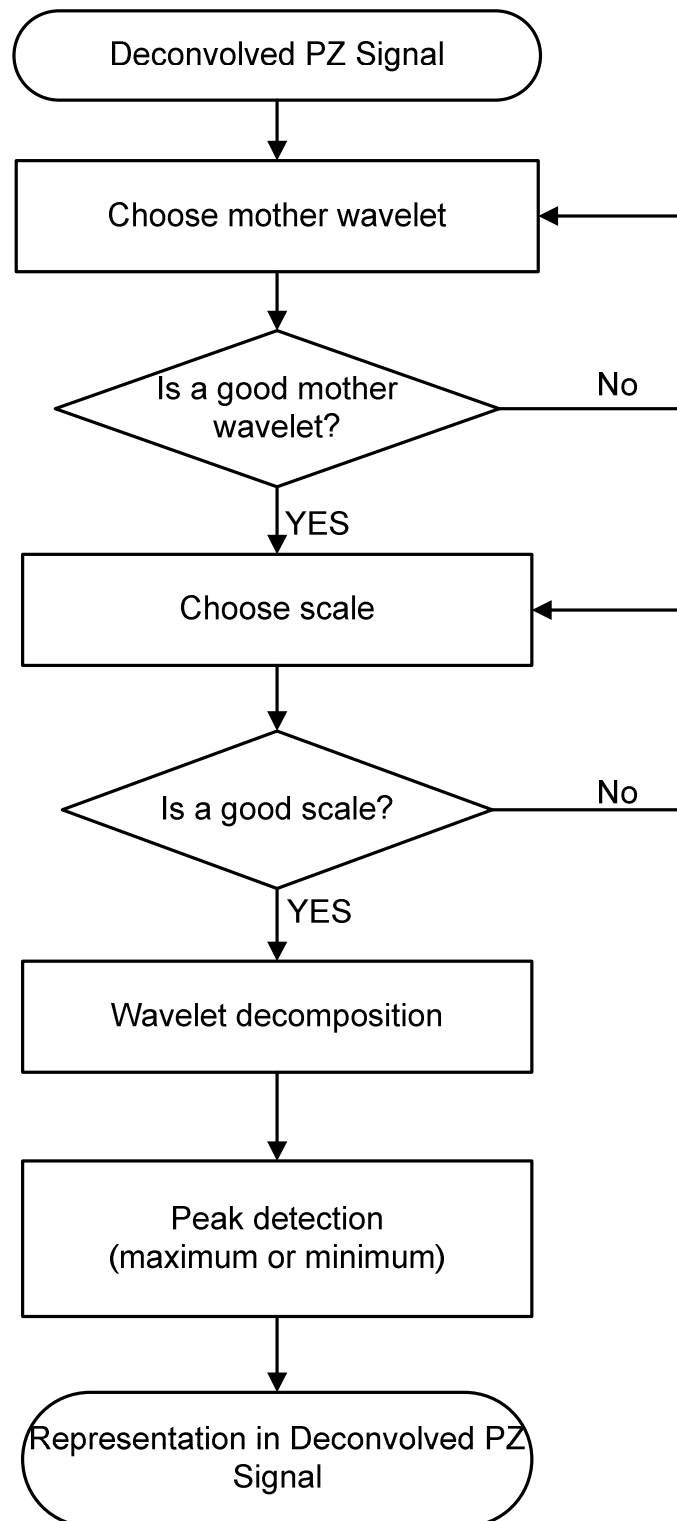


**Figure 5.17** Flowchart diagram depicting the wavelet method for determine the inflection points.

## 6. SYNTHESIZED CARDIAC WAVEFORMS

*In this chapter, cardiac-like pressure waves were synthesized using a weighted combination of exponentially shaped sub-pulses representing the main physiological components of the real cardiac pulse. These pulses were tested using a new wavelet based algorithm for AIx determination. The results were compared with the ones derived from the method based in the probability density function and with the values computed directly from the synthesized waveform.*

*The results from this chapter resulted in a paper submitted to BIOSIGNALS 2010 – Third International Conference on Bio-inspired Systems and Signal Processing. (See Appendix D- “Synthesized cardiac waveform in the evaluation of augmentation index algorithms”).*

### 6.1 Cardiac Pulses Synthesis

The synthesis of the cardiac-like pulse  $c(t)$ , is achieved by summing three exponentially shaped sub-pulses that represent the components of the cardiac waveform. They represent, respectively, the systolic stroke, the reflected wave, and finally the aortic reservoir or Windkessel effect that occurs when the aortic valve closes.

Each sub-pulse is built up by two successive exponential curves for the rising and falling edges. The general expression of the synthesized pulse is,

$$c(t) = \sum_{k=1}^3 A_k \left( \varepsilon^{-\frac{t-D_{Rk}}{\tau_{Rk}}} - \varepsilon^{-\frac{t-D_{Fk}}{\tau_{Fk}}} \right)$$

(6.1)



Prior to summing, the sub-pulses are submitted to a moving average filtering process in order to smooth the corners, that, otherwise, would show up in  $c(t)$ .

The table below describes the parameters used in equation 6.1.

**Table VIII** Parameter definition for equation 6.1. k=1-systole, k=2-reflection wave, k=3-windkessel effect.

Parameter Description	
$A_k$	Amplitude
$D_{Rk}$	Delay of rising exponential
$\tau_{Rk}$	Rising exponential time constant
$D_{Fk}$	Delay of falling exponential
$\tau_{Fk}$	Falling exponential time constant

The analysis of the contour of the blood pressure wave is an important factor to take into account to synthesize the behaviour of the cardiovascular system. Rubins fits the systolic wave and the diastolic wave with the sum of two Gaussian functions [59].

Other authors describe the APW with a pure exponential decay [60].

The set of synthesized waveforms are obtained by gradually varying of its parameters, in such a way that a range of interesting conditions are swept. The range of synthesized waveforms should contain the interesting situations, namely the ones that occur during positive to negative transitions of Alx.

## 6.2 Augmentation Index

Alx is an index widely used to quantify the arterial stiffness and evaluate the cardiovascular risk. (See section 2.4). Although commonly used, it has not yet revealed strong prognostic value in general population. This is a consequence of its definition.

Alx is computed by,  $Alx = \frac{P_S - P_i}{P_S - P_D}$ , if the inflection point occurs before the systolic peak, and by  $Alx = \frac{P_i - P_S}{P_S - P_D}$ , otherwise.

This definition can originate misleading situations in what concerns the physiological meaning of Alx. In fact, it should be related with increment in systolic peak (P), and not with the increment of the inflection point (Pi). Figure 6.1 illustrates this situation for type A and type C waveforms, respectively. The augmentation of pressure should be expressed by  $Alx = \frac{P_S - P}{P_S - P_D}$  in a) and in b) no physical augmentation occurs. As the value of P is unknown, or, at least, very hard to obtain, Alx is computed

as a simplification of real augmentation of systolic peak. The value  $\epsilon$  corresponds to error resulting from this simplification.

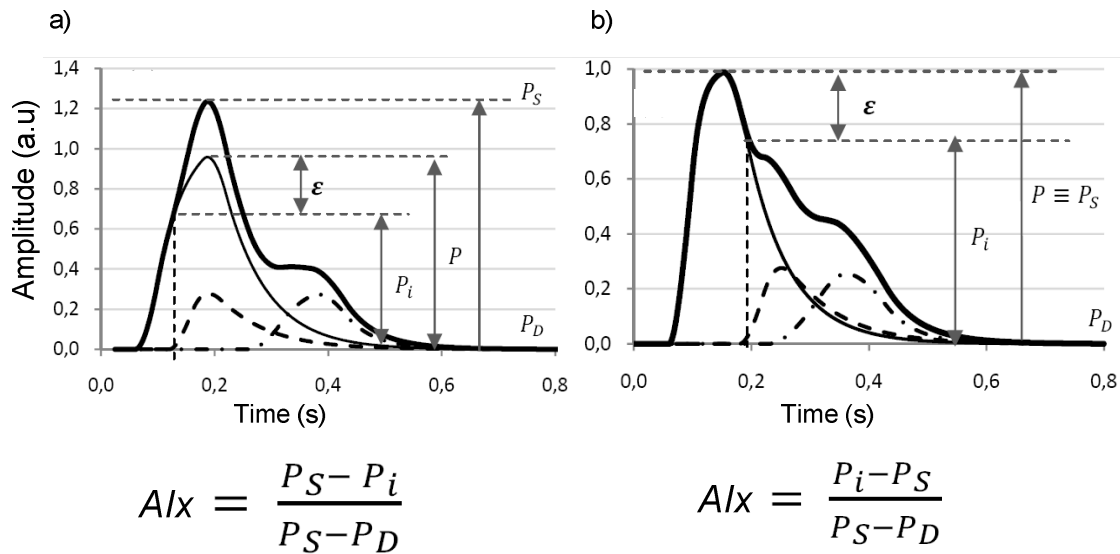


**Figure 6.1** Two waveforms resulting of synthesize process. a) Type A, b) Type C.

Thin solid line-systolic pressure wave, dashed wave - reflected wave, dash-point line - aortic reservoir or Windkessel effect, Thick solid line - APW.  $P_S$  - APW peak pressure,  $P_i$  - pressure at inflection point,  $P_D$  - diastolic pressure and  $P$  - increment in pressure imparted to  $P_D$  by the systolic stroke alone.

A similar situation occurs when the reflected wave arrives shortly after the systolic peak (type B waveform). The formula yields a negative  $Alx$ , but physical augmentation still occurs. So, small negative values of  $Alx$  yet, correspond at physical augmentation in the systolic peak. The figure 6.2 illustrates this situation.

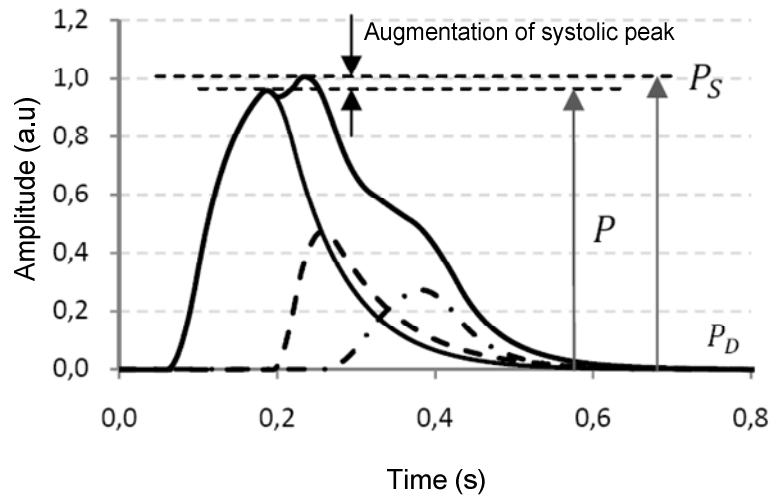


**Figure 6.2** Synthesized pressure waveform type B. Thin solid line-systolic pressure wave, Dashed wave - reflected wave, Dash-point line - aortic reservoir or Windkessel effect, Thick solid line - APW.  $P_S$  - APW peak pressure,  $P_D$  - diastolic pressure and  $P$  - increment in pressure imparted to  $P_D$  by the systolic stroke alone.

### 6.2.1 Reference values

The key feature of any AIx algorithm is its ability to identify the inflection points associated to the arrival of the reflected wave. The values of AIx derived from the synthesized waveform are taken as the reference in all measurements of this chapter, since these values are not affected by any error in identification of the inflection point. This methodology will be used to evaluate the performance of two algorithms, the PDF and the Bior1.3 wavelet one.

### 6.2.2 Probability density function (PDF)

The principle of this method is based on the property that associates high PDF values to the inflection points. In other words, local maximum of PDF are created at the inflection point sites. Unfortunately, other maxima are also created whenever the signal amplitude is slow varying, as happens close to its peaks. For some waveforms these peaks can occur in amplitudes of the same order of magnitude of the inflection point, making the algorithmic identification task very hard to accomplish.

Figure 6.3 depicts a flowchart diagram of this method, the pressure pulse amplitude is normalized to setting the peak systolic blood pressure =1 and minimum diastolic pressure=0, the signal normalization does not affect the estimation of AIx because this is a dimensionless ratio. The inflection point is identified by a maximum of PDF; a cursor based interaction is used to identify this point.

If the inflection point occurs before the absolute maximum, AIx is defined by  $AIx = 1 - P_i$  (%), and if occurs after  $AIx = P_i - 1$  (%) where  $P_i$  is the ordinate of

inflection point (amplitude). These equations derive from Table IV,  $P_S = 1$  and  $P_S - P_D = 1$ .

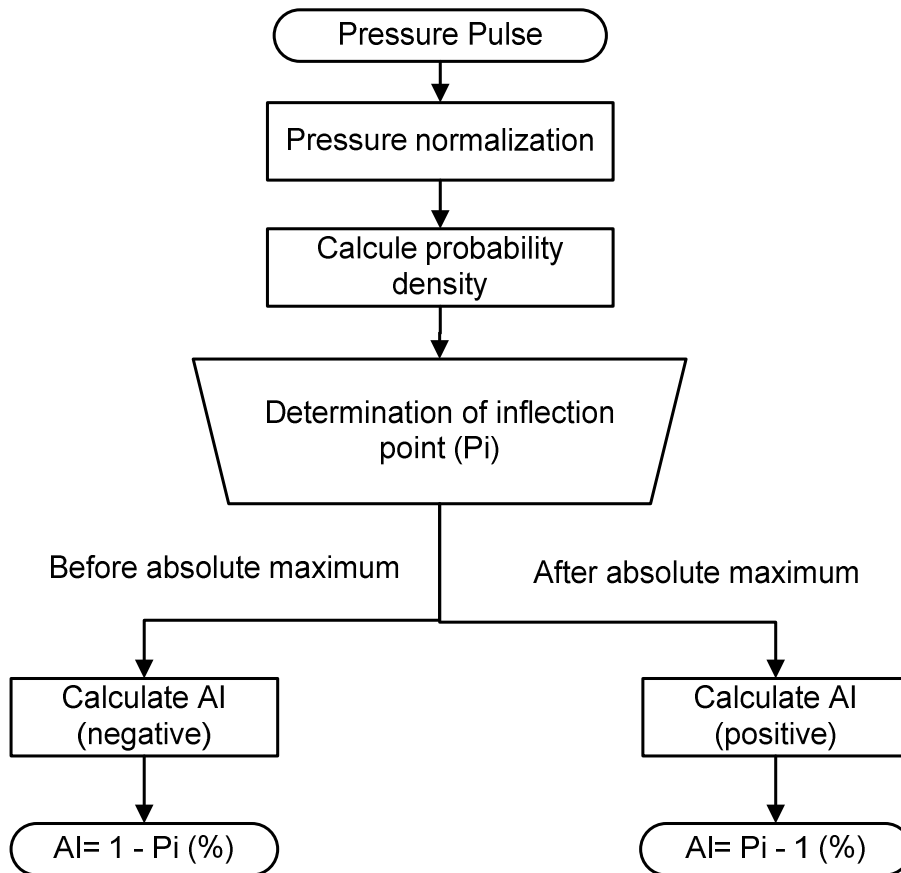


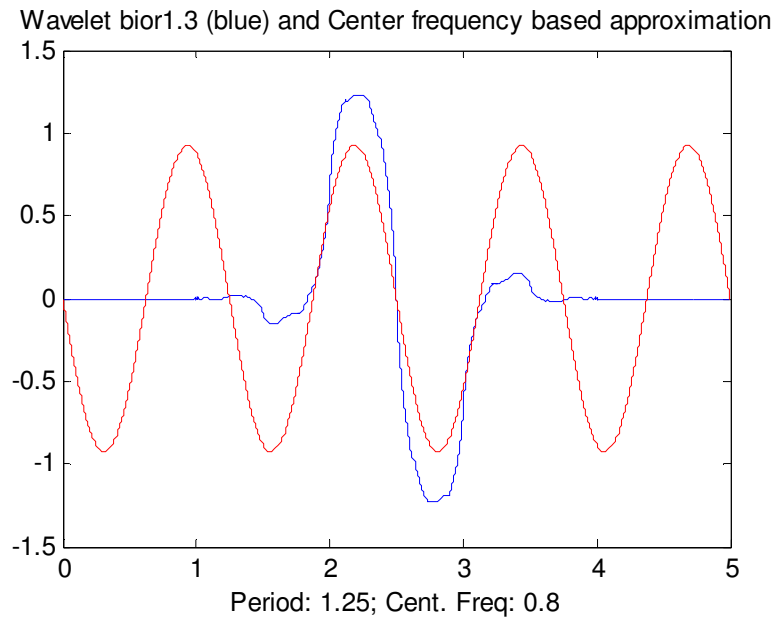
Figure 6.3 Flowchart diagram of PDF.

### 6.2.3 Bior1.3 mother wavelet

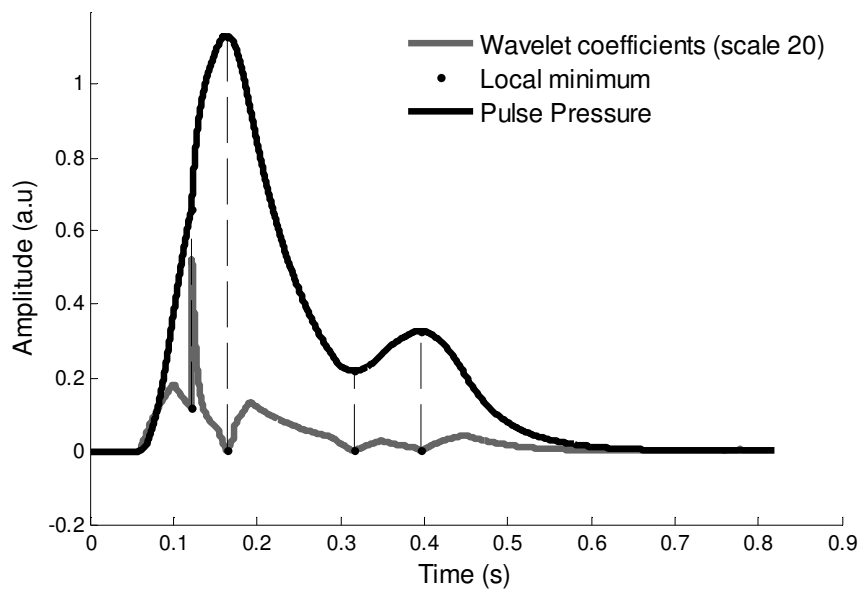
The Bior1.3 mother wavelet represented in figure 6.4 was selected among a few candidates, in a trial-and-error basis, for its capacity of identifying the inflection points. In the selection process, an appropriate scale is a key factor to obtain good results. For these signals, a scale of 20 yields the best performance. The inflection points result from the peak identification in the wavelet coefficient, at a selected scale. (See section 3.3) The wavelet coefficient represents the correlation between the signal and the wavelet under analysis. So, depending on the signal and mother wavelet, different analysis can be done, i.e., the inflection points can be identified for a minimum or a maximum peak.

Figure 6.4 depicts the Bior1.3 mother wavelet at scale 20, and its frequency (main wavelet oscillation),  $F_c$ . The pseudo-frequency corresponding to the scale 20 is computed by equation 3.1, where  $F_c$  is 0.8 Hz, and the sampling time is 1/20000 s.

The figure 6.5 represents a typical detection event characterized by its distinctive narrow peak located in coincident (vertically aligned) with inflection points. In this case the inflection points correspond at minimum of the wavelet coefficient.



**Figure 6.4** Mother wavelet Bior1.3 and its center frequency based approximation.



**Figure 6.5** Cardiac pulse and its WBior1.3 (scale 20) wavelet decomposition (gray curve). Vertical dashed lines show local peaks detected by the WBior1.3.

### 6.3 Results

Tests were carried out by feeding a set of cardiac pulses as the input to the PDF and WBior1.3 algorithms in order to calculate  $A_{Ix}$ . These results are compared with the values obtained directly from the synthesized waveforms. Table IX describes the parameters used to generate a family of cardiac pulses, the reflected wave sweeps the interesting area (crosses the systolic peak).

**Table IX** Parameters used for evaluate the algorithms. For the reflected wave,  $w = 1:30$ .

	<b>Systole</b> <b>(<math>k = 1</math>)</b>	<b>Reflected wave</b> <b>(<math>k = 2</math>)</b>	<b>Windkessel effect</b> <b>(<math>k = 3</math>)</b>
<b>A (a. u)</b>	1	0.2	0.3
<b>D<sub>R</sub> (s)</b>	0.1	$0.1201 + (w \times 0.0033)$	0.35
<b><math>\tau_R</math> (s)</b>	0.001	0.01	0.001
<b>D<sub>F</sub> (s)</b>	0.192	$0.1701 + (w \times 0.0033)$	0.45
<b><math>\tau_F</math> (s)</b>	0.0007	0.0006	0.001

Figure 6.6 shows the results for this set of cardiac waveforms, a discontinuity point is created around the systolic peak as a result of the definition. This discontinuity was also identified by other authors, Tsui et al. (2007) [28].

The magnitude of errors shown in the middle and lower panels demonstrates the superior performance of WBior1.3. Errors are less than 0.5 %, while the PDF method yields errors above 2%.

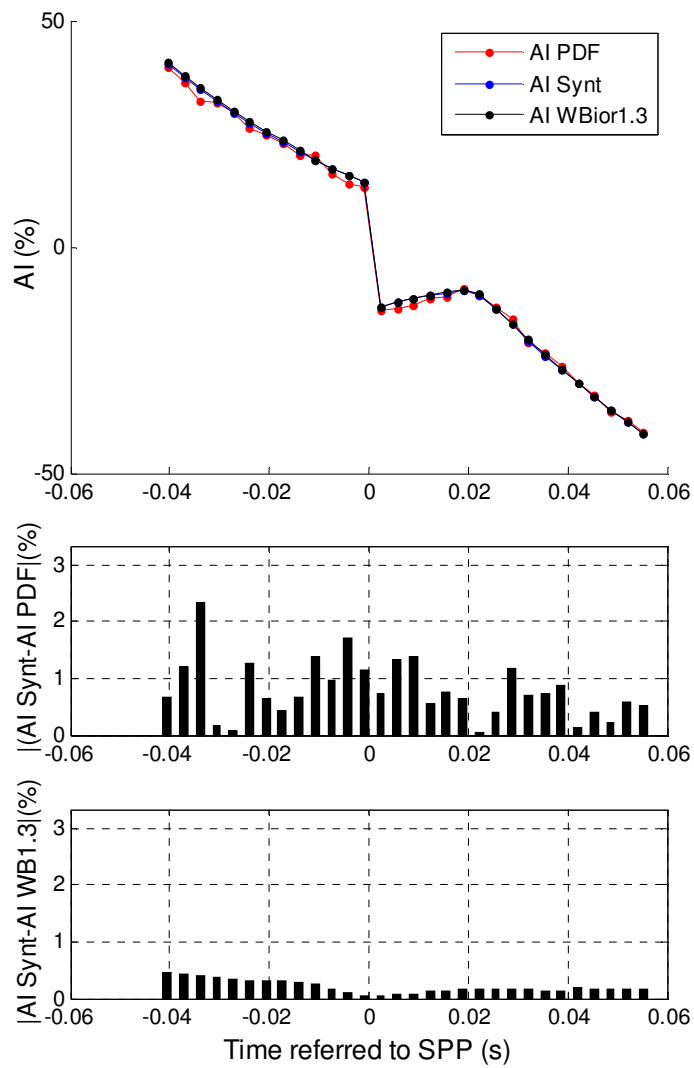


**Figure 6.6** AIx results yielded by the three methods (upper panel) and plot of errors of PDF and WBior1.3 algorithms (middle and lower panels, respectively). The time scale is referred to the systolic peak pressure (SPP).

# 7. CAROTID PRESSURE WAVEFORMS

*The analysis of carotid signals was the final step of the work. Due to time limitations, only a small number of volunteers were studied.*

## 7.1 “Clinical” trials procedures

A total of 10 volunteers without known cardiovascular diseases have participated in this study. Before the measurements, the subjects were asked to relax in a supine position for 5 min. Measurements were performed continuously during 1 min, while the subject was in a supine position.

The signals were recorded at 2.5 KSpss in the carotid artery site; single pulses are obtained with the *Pulsoft* software pack [37].

AI was computed by three different methods, PDF, WBior1.3 and a method based in first derivative of pressure waveform. The data recorded are presented in Appendix C.

## 7.2 Data processing

Several references in the literature focus the use of derivatives to identify the augmentation point (figure 7.3 shows a flowchart diagram of this method, for the test of noise performance). For noisy signals, this technique requires the use of a filter; which also causes loss of useful information, the same problem can be reported when wavelets are used in the analysis. The PDF allows the estimation of AI<sub>x</sub> using poorer-quality pressure waveform, without application of filters in the signal processing, but this analysis tends to be inaccurate.

Figure 7.1 a) shows the relationship between AI<sub>x</sub> (x), obtained using Bior1.3 wavelet analysis, and using the first derivative of pressure waveform, AI<sub>x</sub> (y). The



relationship between AIx obtained from PDF and first derivative of pressure waveform is shown in figure 7.2 b). The methods have a good linear dependence,  $y = 0.9563x + 0.4965$ , and,  $y = 0.9295x - 0.0973$  respectively. The correlation coefficient is greater in wavelet analysis 0.9348, versus 0.9291 in PDF. This implies that wavelet analysis or PDF perform as well as the technique of first derivative in estimating AIx.

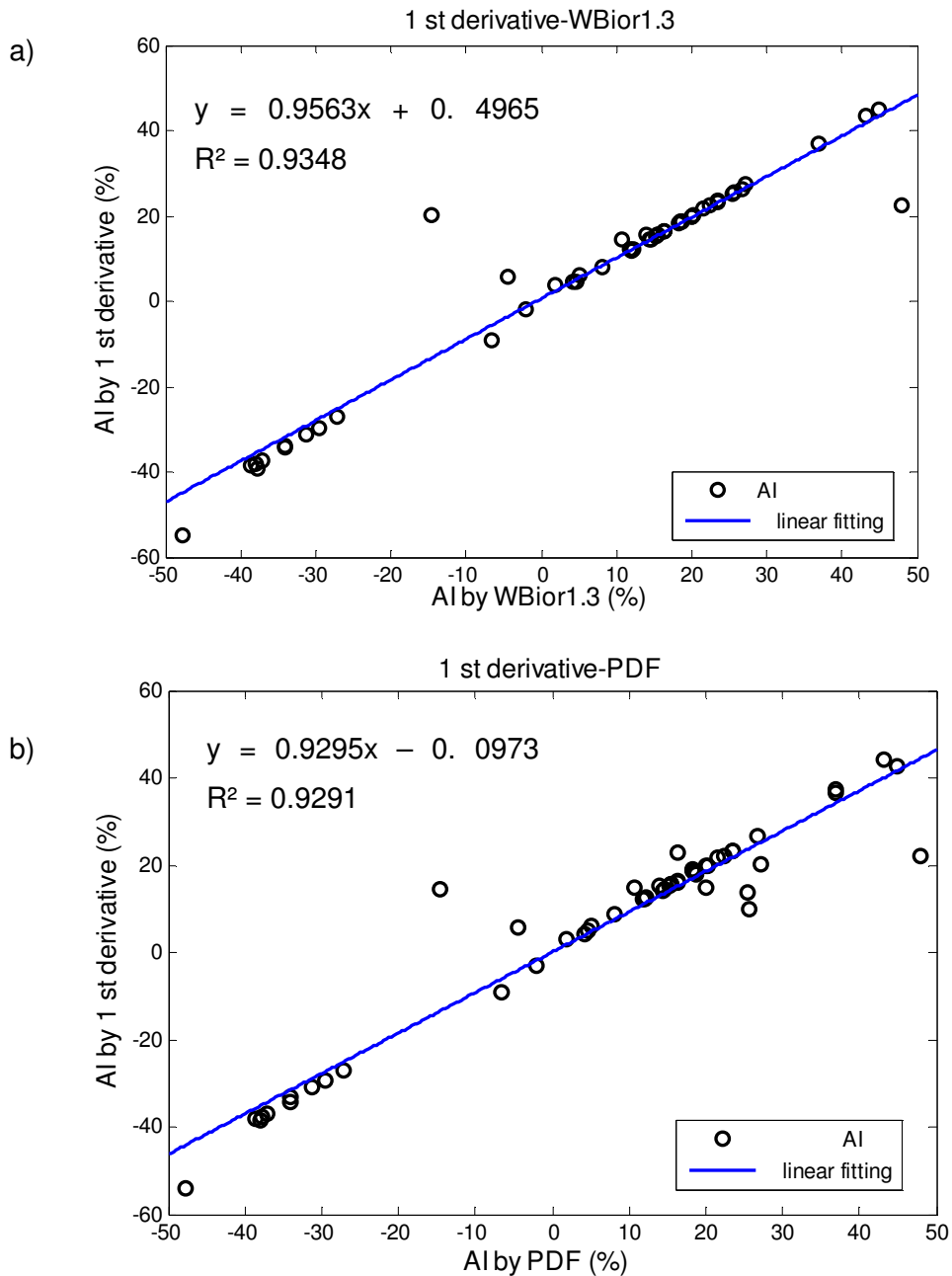


**Figure 7.1** a) The relationships between AIx obtained from 1 st derivative of pressure and WBior1.3, b) the relationships between AIx obtained from 1 st derivative of pressure waveform and PDF.

The performance of the algorithms is impaired by noise added to the carotid pulses (see flowchart of this process in figure 7.3). Alx was calculated using the same three methods, for 37 dB SNR signals.

In some situations, all algorithms are unable to estimate Alx. In the PDF method this limitation resides in the operator. Figure 7.2 shows an example of this situation. In the other two methods, the error results from the algorithm's incapacity in determining the inflection point.

The root mean square error (RMSE) is calculated relative to noise-free signals, for all methods, table X.

**Table X** Statistical analysis of noisy signals.

Method of determination Alx	Error or uncertain	RMSE
<i>1<sup>st</sup> derivative of pressure waveform</i>	1.92%	3.66%
<i>PDF</i>	30.77%	1.94%
<i>WBior1.3</i>	17.31%	1.96%

The PDF exhibits a greater uncertainty, 30.77% versus 1.92 % for the first derivative. The WBior1.3 shows an error of 17.30 % in determining the inflection point.

The RMSE is similar in PDF and WBior1.3, 1.94% and 1.96 % respectively, while the first derivative method is less accurate in the presence of noise, RMSE of 3.66%.

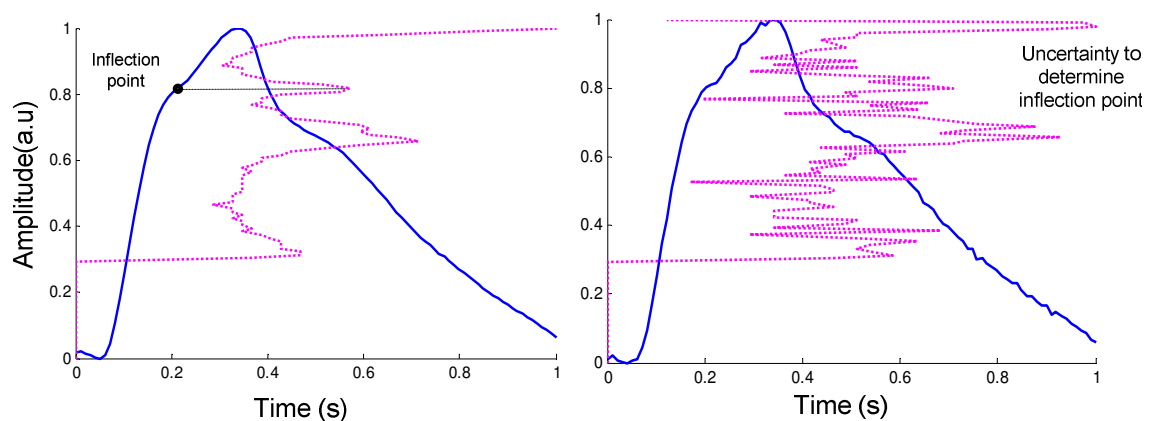


**Figure 7.2** Probability density function, **a)** APW, **b)** APW with noise added (SNR=37 dB).

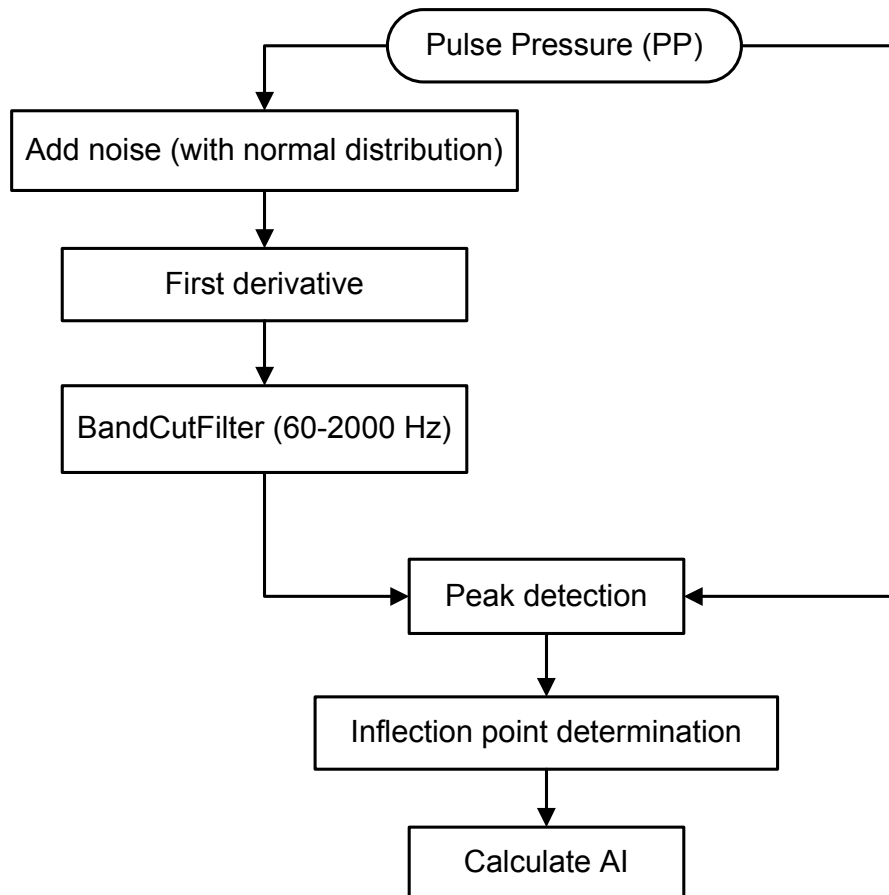


**Figure 7.3** Flowchart of the first derivative method, by noisy signals (in this case by noise added).

### 7.3 Conclusions

This analysis must be carried out in a larger population that includes healthy as well as cardiovascular disease bearer subjects. The majority of cases in this study were type A and C pressure waveform types. Type B waveforms, are important case-studies that could not be included in this study and should be analysed.

Data demonstrates that PDF and WBior1.3 perform well in the presence of noise, but PDF has a greater uncertainty associated. The first derivative method has less error associated. Thus, in future, analysis of inflection points should integrate more than one method, such as wavelet and first derivative. Other order derivatives must be analysed, as well other mother wavelets. The PDF must be optimized to automatic detection of inflection points.

## 8. FINAL REMARKS

The role of arterial stiffness in the development of CV diseases is the focus theme of this thesis. In this context, several techniques and algorithms for hemodynamic parameters extraction can be developed, as well as bench tests for emulating the dynamics of the cardiovascular system.

The developed probes demonstrate good performance in acquiring carotid and test bench signals with excellent signal-to-noise ratio and large bandwidth (the results focus only the PZ Single probe).

In order to help the compression of the dynamics of the arterial system two test bench were developed. The results from the first test bench allowed testing the deconvolution method with excellent results. For test bench II, the dynamics of the flow propagation is more complex and results from this setup demonstrate an oscillatory behaviour in the beginning of tube that not allowing to recover the original pressure waveform. The determination of the inflection points and the study of the wave propagation was the main themes studied, other situations must be simulated in order to emulate other properties of the arterial system, as the augmentation of the pressure caused by an occlusion of an artery.

The synthesis of a cardiac like-pressure was performed using a weighted combination of exponentially shaped sub-pulses representing the main physiological components of the waveform. Although of the new method based in the mother wavelet Bior1.3 shows good results, other mother wavelets, eventually at different scales, must be tested in order to seek an increase in performance of this algorithm.

The results with carotid signals are limited by the database of volunteers available for this study. Preliminary results show good accuracy for the Bior1.3 mother wavelet in comparison with other methods. They also demonstrate that the association of different methods, e.g. derivatives and wavelet transform, can be an interesting theme for future developments.

The results from the influence of collar probe are inconclusive due to the limited database.

Augmentation Index has been addressed in this work almost exclusively. Although it is one of the most clinically relevant hemodynamic parameters, this analysis must be extended at other parameters.

### ***Future work***

The results of this work demonstrate the feasibility of the use of PZ probes for assessing hemodynamic parameters. The results obtained from test bench systems were very interesting; however the results from flow propagation must be explored further for test and calibration of the sensors. This test bench will be a powerful tool in the testing of the efficiency of the algorithms from which the hemodynamic parameters are derived.

Clinical tests are an important factor for the success of this project. It is important collect a database with significant number of patients, with and without pathologies for proper evaluation of the algorithms.

A statistical analysis of the signals from the developed probes must be done, as well as test on reproducibility, accuracy, and other statistical parameters. It is also necessary a comparison with results from the golden standard devices (Complior ® and Sphygmocor ®).




Other themes must be studied, in spite of much controversy they rise in the literature. One such theme is the use of transfer functions for obtaining central pressure from measurements in peripheral sites. Transfer functions can also be useful in special situations, as is the case in obese subjects or in patients with major atherosclerotic plaques, when the carotid site is not an option.

Wave reflections are an important issue for they supply a great deal information about the cardiovascular system. The “method of characteristics”, proposed by Parker, allows the separation of forward and backward running waves. This method is an important tool for analyzing one-dimensional waves in the time domain instead of the frequency domain [61 , 62].

The electronic implementation, based in a microcontroller, was referred in article II, but a thorough study must be carried out to eliminate current limitations: the reduced real time capacity and software inflexibility bugs of the NI USB 6210 ®,

## 9. APPENDIX A - SPECIFICATIONS OF DAQ MODULES

### DAQ Modules [63].

NI USB 6008	NI USB 6009	NI USB 6210
		
<b>8 analog inputs (12-bit, 10 kS/s)</b>	<b>8 analog inputs (14-bit, 48 kS/s)</b>	<b>16 analog inputs (16-bit, 250 kS/s)</b>
<b>2 analog outputs (12-bit, 150 S/s)</b>	<b>2 analog outputs (12-bit, 150 S/s)</b>	-----
<b>12 digital I/O</b>	<b>12 digital I/O</b>	<b>8 digital I/O (4 Digital Input/4 Digital Output)</b>
<b>32-bit counter</b>	<b>32-bit counter</b>	<b>two 32-bit counter</b>

### USB bus type

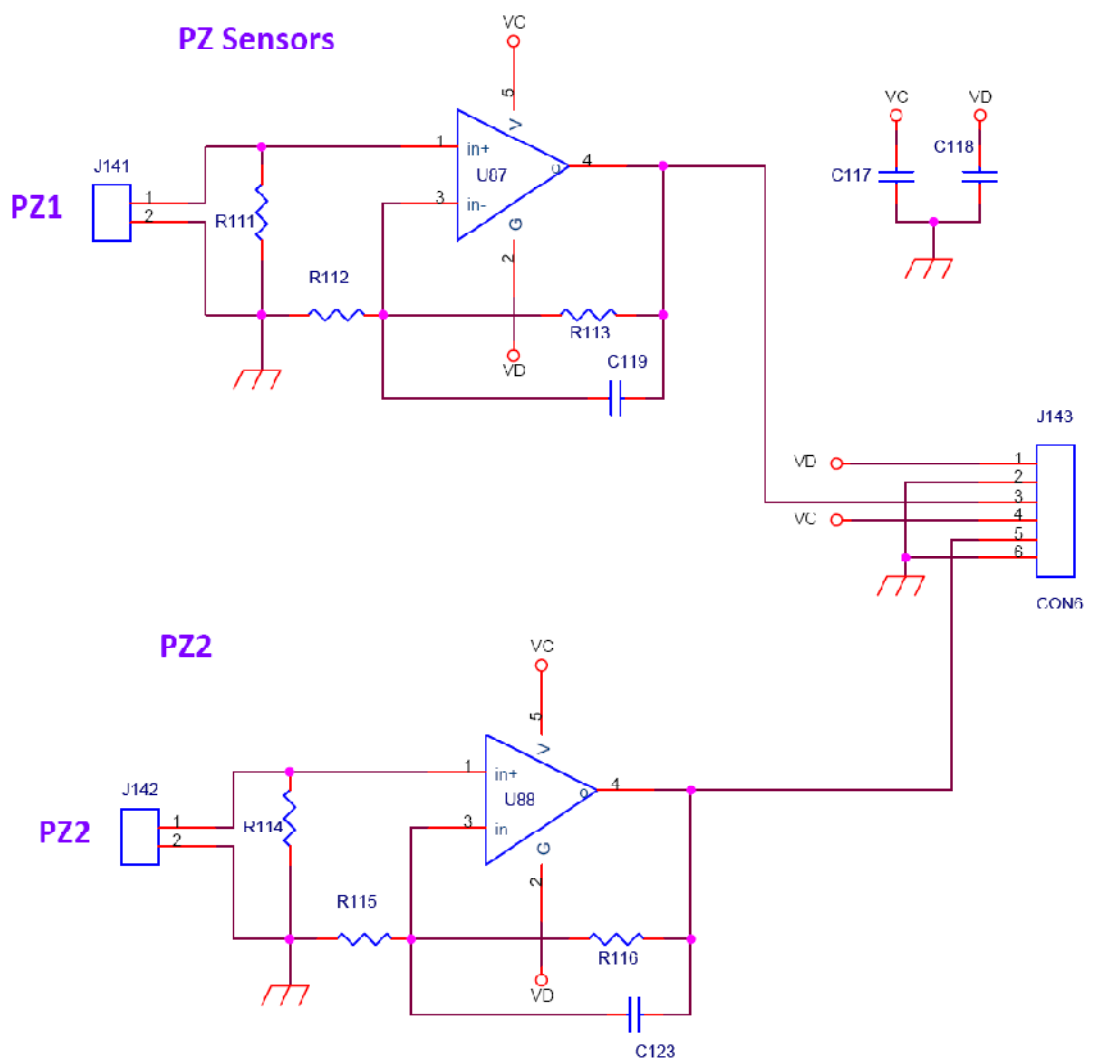
**NI-DAQmx driver software and LabVIEW SignalExpress LE interactive data-logging**



# 10. APPENDIX B - ELECTRONIC CIRCUITS

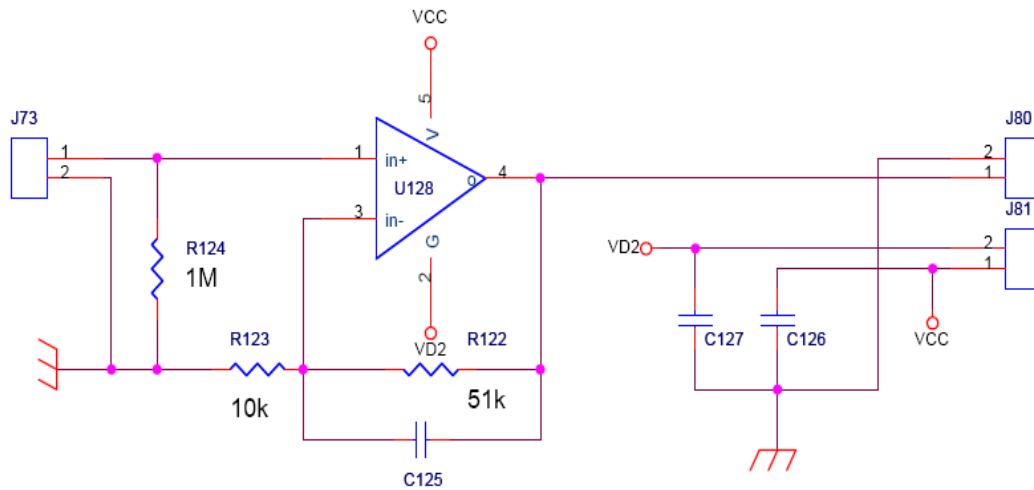
## SCHEMATICS

### a) PZ Double



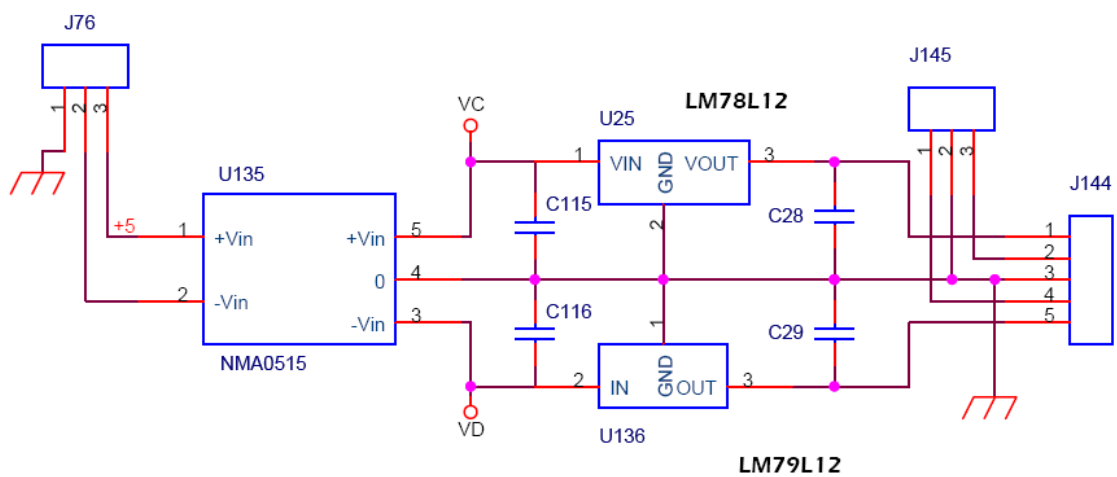


## b) PZ Simple

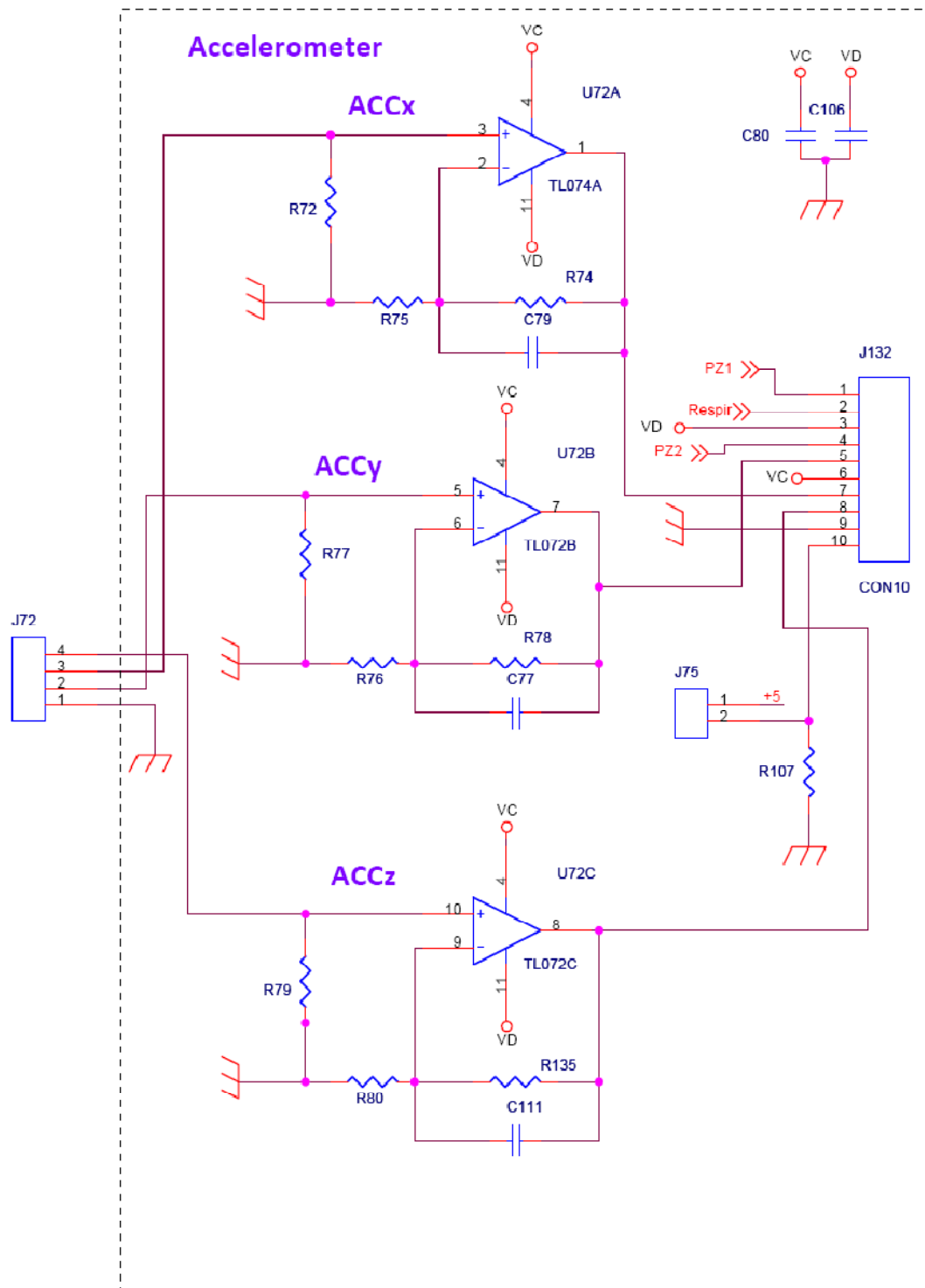


## c) Signal Condition PulScope Box

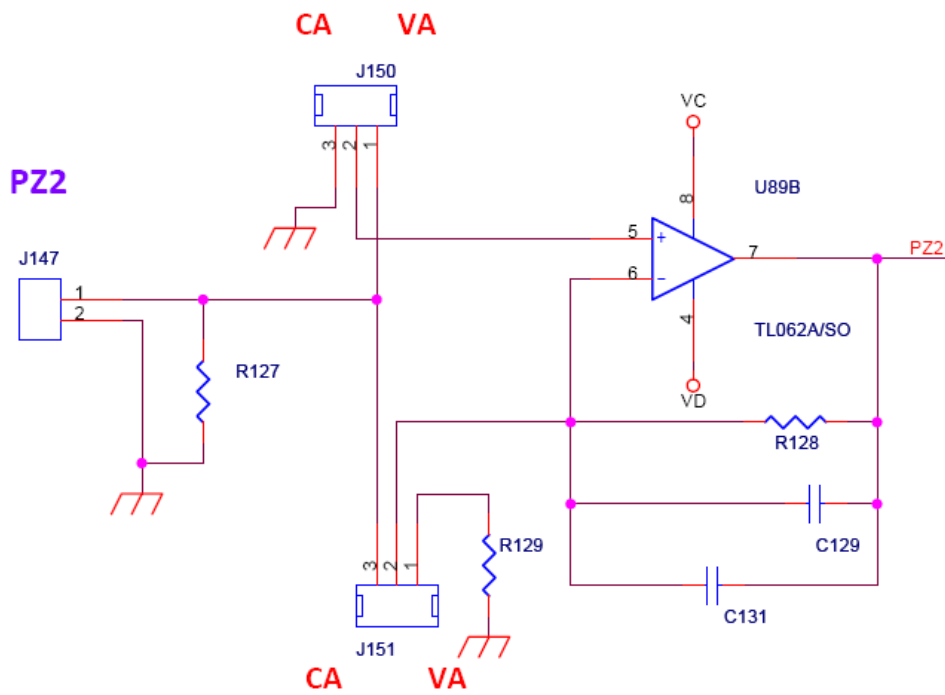
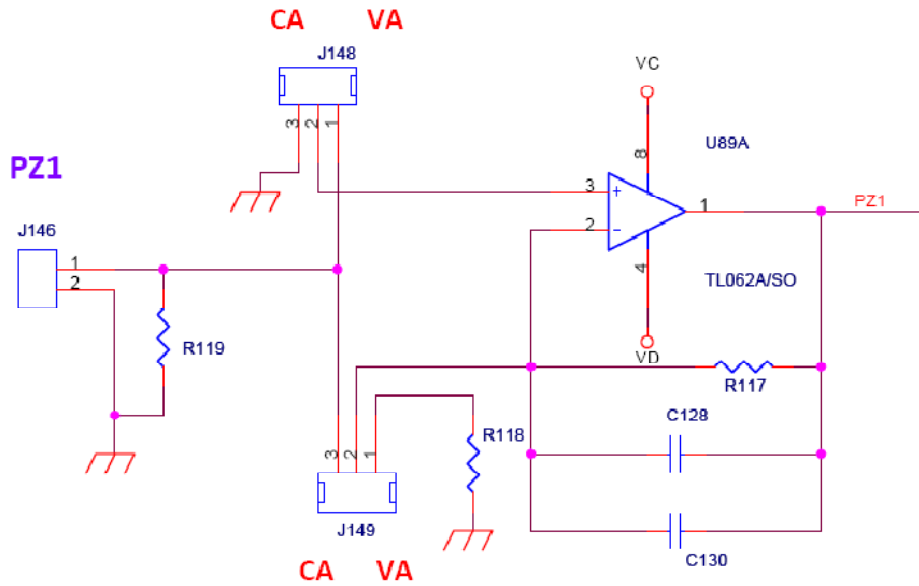
i)



ii) Accelerometer

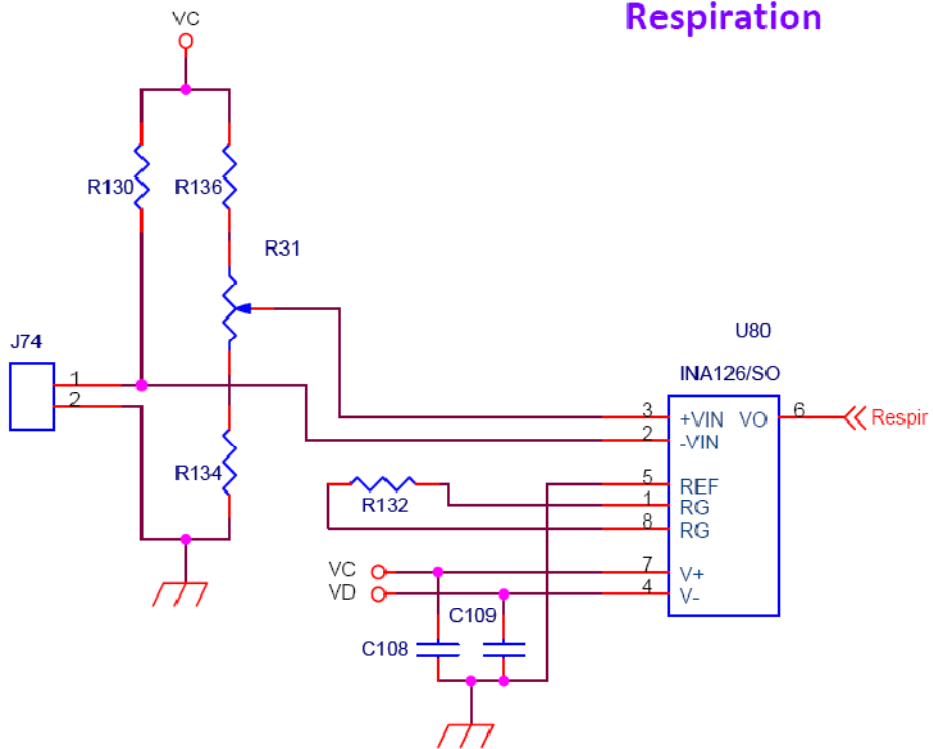


## iii) PZ Sensors



iv) Respiration

Respiration





# 11. APPENDIX C - AIX VALUES FROM CAROTID

## SIGNALS

	<i>Without noise</i>			<i>With noise 37 dB</i>		
	PDF	WB1.3	1 <sup>st</sup> derivate	PDF	WB1.3	1 <sup>st</sup> derivate
1-1-1	18.20	18.48	18.48	Uncertain	19.60	19.87
1-1-2	18.58	18.44	18.44	18.97	19.64	19.07
1-1-3	18.97	18.40	18.40	18.58	18.86	19.08
1-1-4	19.73	19.83	19.83	20.11	12.40	20.76
1-1-5	15.52	15.57	15.57	16.67	15.90	17.05
1-1-6	14.37	14.62	14.62	16.28	15.38	14.91
1-1-7	17.82	18.67	18.67	19.35	17.27	18.55
1-1-8	13.98	14.49	14.49	15.13	14.51	15.80
1-1-9	12.07	11.95	11.95	11.69	11.74	13.88
1-2-1	14.75	14.59	10.83	14.75	12.88	10.26
1-2-2	15.52	15.52	15.52	16.28	17.01	16.02
1-2-3	15.90	16.27	16.27	19.35	18.84	16.86
1-2-4	19.73	20.13	20.13	20.88	19.17	21.49
1-2-5	22.80	16.40	16.40	22.41	21.38	18.12
1-2-6	14.37	20.12	Uncertain	Uncertain	12.89	Uncertain
1-2-7	13.60	25.29	25.29	19.73	24.60	24.44
1-2-8	9.77	25.71	25.71	16.28	26.32	26.75
1-2-9	20.11	27.34	27.34	23.94	29.52	27.95
2-1-1	-9.00	-9.18	-6.54	-10.54	-10.00	-4.22
2-1-2	5.56	5.56	1.86	5.94	4.32	5.18
2-1-3	2.87	3.64	1.71	Uncertain	Uncertain	2.95
2-1-4	15.13	15.36	15.36	Uncertain	12.49	16.63

3-1-1	23.18	23.14	23.14	22.41	22.42	23.80
3-1-2	26.69	26.25	26.68	Uncertain	27.56	11.97
3-1-3	12.45	12.01	12.26	13.60	13.23	13.71
3-1-4	16.28	16.27	16.27	17.43	16.70	16.87
3-1-5	21.65	21.57	21.57	22.80	21.80	23.06
3-1-6	15.13	15.43	13.99	15.52	15.93	13.89
3-1-7	22.03	22.47	22.47	22.80	23.71	23.42
3-1-8	12.07	12.01	11.82	12.45	11.54	12.06
3-1-9	23.18	23.50	23.51	24.33	24.01	24.27
3-1-10	5.94	6.15	5.07	6.70	4.98	5.31
3-2-1	42.72	44.94	44.94	Uncertain	45.05	45.56
3-2-2	22.03	22.57	47.97	Uncertain	Uncertain	47.57
3-2-3	37.36	37.02	37.02	37.74	38.57	37.68
3-2-4	36.59	36.95	36.95	Uncertain	37.62	37.88
3-2-5	44.25	43.28	43.28	Uncertain	44.92	44.14
3-2-6	14.75	19.99	19.99	Uncertain	20.15	20.71
4-1-1	8.62	8.07	8.10	9.39	8.98	9.10
4-1-2	-54.21	-54.82	-47.31	-53.45	Uncertain	-50.77
4-1-3	4.02	4.59	4.15	5.75	4.91	5.05
4-1-4	-2.87	-2.02	-2.13	Uncertain	Uncertain	-2.84
4-1-5	4.78	4.56	4.56	5.17	5.35	-5.30
5-1-1	-38.12	-38.57	-38.57	Uncertain	Uncertain	-41.63
5-1-2	-36.97	-37.17	-37.17	-36.97	Uncertain	-20.99
5-1-3	-29.31	-29.62	-29.62	-28.16	Uncertain	-29.98
5-1-4	-33.14	-34.06	-34.06	Uncertain	-35.12	-34.31
5-1-5	-27.01	-27.07	-27.08	-28.16	Uncertain	-20.50
5-1-6	-37.74	-39.30	-37.79	Uncertain	Uncertain	-38.01
5-1-7	-34.29	-34.15	-34.15	-33.14	-34.53	-34.02
5-1-8	-30.84	-31.33	-31.31	Uncertain	-27.31	-33.84
5-1-9	-38.51	-37.97	-37.97	Uncertain	-38.87	-37.84

# 12. APPENDIX D- ORIGINAL PAPERS

---

- I. Programmable test bench for hemodynamic studies.
  
- II. Synthesized cardiac waveform in the evaluation of augmentation index algorithms.



# Programmable test bench for hemodynamic studies

H.C. Pereira<sup>1,2</sup>, J.M. Cardoso<sup>2</sup>, V.G. Almeida<sup>2</sup>, T. Pereira<sup>2</sup>, E. Borges<sup>2</sup>, E. Figueiras<sup>2</sup>, L.R. Ferreira<sup>2</sup>, J.B. Simões<sup>2,1</sup>, C. Correia<sup>2</sup>

<sup>1</sup>ISA – Intelligent Sensing Anywhere, Portugal

<sup>2</sup>Instrumentation Centre, Physics Department, University of Coimbra, Portugal

*Abstract*— The non-invasive assessment of hemodynamic parameters has been a permanent challenge posed to the scientific community. The literature shows many contributions to this quest expressed as algorithms dedicated to revealing some of its characteristics and as new probes or electronics, featuring some enhanced instrumental capability that can improve their insight.

A test system capable of replicating some of the basic properties of the cardiovascular system, especially the ones related with the propagation of the arterial pressure wave (APW), is a powerful tool in the development of those probes and in the validation of the various algorithms that extract clinically relevant information from the data that they can collect.

This work describes a test bench system, based on the combination of a new programmable pressure wave generator with a flexible tube, capable of emulating some of these properties. It discusses its main characterization issues and demonstrates the system in a relevant case study.

Two versions of the system have been set up: one that generates a short duration pulse-like pressure wave from an actuator operated in a switched mode, appropriate to system characterization; a second one, using a long stroke actuator, linearly operated under program control, capable of generating complex, including cardiac-like, pressure waveforms. This configuration finds its main use in algorithm test and validation.

Tests with a new piezoelectric probe, designed to collect the APW at the major artery sites are shown, demonstrating the possibility of non-invasive precise recovery of the pressure waveform.

*Keywords*— Hemodynamics, test bench, arterial pressure wave, impulse response, deconvolution.

## I. INTRODUCTION

The non-invasive assessment of the arterial pressure waveform (APW) has been, and still remains, a major quest to the scientific community.

In fact, all clinically relevant hemodynamic parameters can be directly connected to its morphology and the literature has been dominated by the discussion of methods to its assessment by non-invasive means. Over the last few years, authors have centered their efforts in the algorithmic interpretation of APW signals obtained either invasively, with catheterized manometers [1, 2], or with different types of

non-invasive probes (electromechanical, optic, ultra sound and others) placed at the major artery sites, in which case the signals are transformed representations of the APW.

Most of the work of these authors evolves in two directions: one related to the efficiency of the algorithm in extracting selected clinically relevant parameters and a second one dealing with probes and electronics developments.

In both cases, a test bench capable of reproducing the major hemodynamic properties of the cardiovascular system, including the variability of its primary ventricular action, is an invaluable tool for measuring and validating all developments.

The physical properties of the media in which waves propagate must be taken into consideration. Latex vessels have been studied by Walker et al [3], proving their adequacy in providing a reliable method of producing physiologically accurate test segments for use in a range of arterial flow models.

Test benches dedicated to pulse wave velocity (PWV) measurement have been described based on different sensing technologies and algorithms: Hermeling et al [4] study PWV over short arterial segments using an ultrasound based bench system and focusing the foot-to-foot class of algorithms; Swillens et al [5] describe a sophisticated phantom for pressure and flow wave simulation and measurement, using linear wave separation and wave intensity analysis.

Several authors address wave separation studies, a major issue in hemodynamics, using data collected in special purpose test benches. Feng and Khir [6] report on an algorithm to separate the velocity waveform into its forward and backward directions, tested with the measured diameter of flexible tube's wall and flow velocity. Wang et al [7] use data from a bench model that produces a solitary wave, that can be repeated reproducibly, to demonstrate the efficiency of wave intensity analysis in wave separation.

Ebenal et al, also introduce a mechanical model of the cardio-systemic circuit system [8] and discuss energy aspects of the heart activity.

Our work demonstrates a test bench with the possibility of generating a programmable pressure waveform capable of mimicking the variability of a range of clinically relevant situations. It also demonstrates the possibility of recovering the propagating pressure waveform using non-invasive sensors and the adequate signal processing tools.

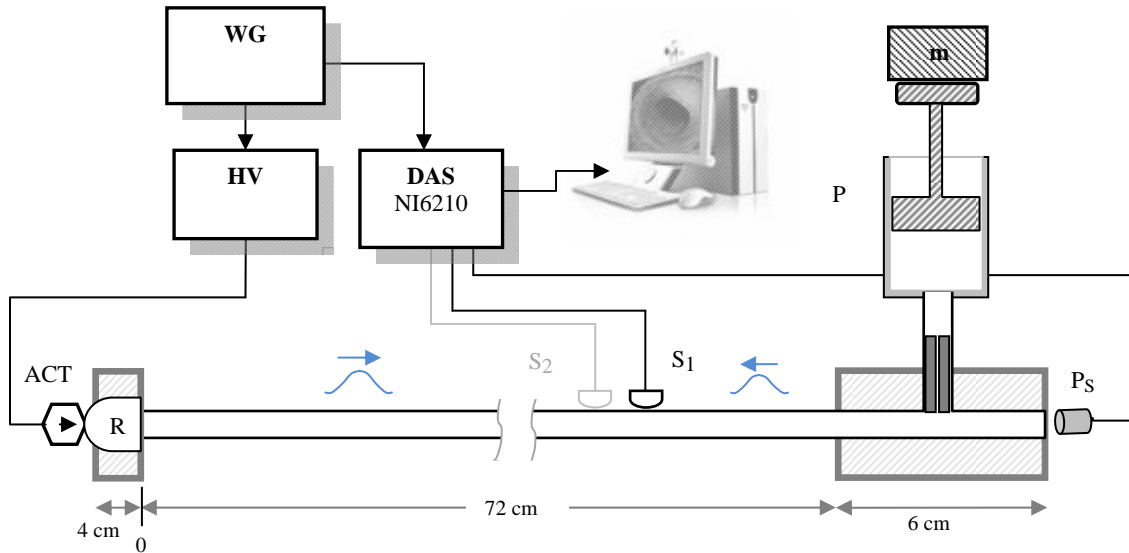


Figure 1 – Schematic drawing of the test bench. The longitudinal pressure wave is imposed by actuator ACT at the rubber interface R, while piston P and mass m set a DC pressure level of 50 mm Hg. Sensors  $S_1$ ,  $S_2$  are placed along the tube and pressure sensor  $P_S$  at its end.

## II. THE TEST BENCH SYSTEM

Figure 1 depicts the main components of the test bench system. An 82 cm long silicone rubber tube (Lindemann, 8 mm inner diameter, 0.5 mm wall thickness) is kept under a DC pressure level of 52 mm Hg by piston P at its right extremity, monitored by pressure sensor  $P_S$  (Honeywell S&C - 40PC015G1A).

The dynamic pressure wave is generated at the other extremity of the tube, by an actuator (ACT) driven by a high voltage power driver (HV). A rubber membrane interface, R, terminates the tube at this end.

Depending on the algorithm and on the sensor under test, two different configurations have been implemented and tested: a fast, short stroke one driven by an electronic switcher, for determining impulse responses; the second is a long stroke configuration, driven by a high-voltage linear amplifier dedicated to generating arbitrary pressure waveforms.

In the first configuration, a 70  $\mu\text{m}$  stroke actuator (Piezomechanik, PSt-HD200/10/45 VS 15) driven by a power switcher (Piezomechanik, HVP200/50) is used.

For the second, a 700  $\mu\text{m}$  actuator (Physik Instrumente GmbH, P-287) is connected to the high-voltage linear amplifier (Physik Instrumente GmbH, E-508).

Both configurations are controlled by an Agilent 33220A arbitrary waveform generator (WG) that also delivers the synchronizing signal that triggers the data acquisition system (DAS).

The DAS, National Instruments USB 6210, can accommodate up to 16 single ended or 8 differential 16 bit resolution data channels with a combined sampling rate up to 250 ksp/s.

## III. RESULTS FROM CONFIGURATION I

The first experiment aims at characterizing the system itself. A very short pressure wave (100  $\mu\text{s}$  width, 0.5 Hz frequency) was sensed at equally spaced (2 cm) locations along the tube, using a new piezoelectric pressure probe, to be described elsewhere, for sensing pressure at the carotid artery site. The impulse response (IR) of the probe had been previously determined in a different experimental set-up.

Figure 2 shows two different representations of the data: raw data in figure 2.a and deconvolved data in figure 2.b.

The forward and backward waves are clearly visible, with higher contrast in the deconvolved data.

The white circles of figure 2.c, generated by a peak detection algorithm, enhance the location (in time and space) of the forward and backward propagating pressure waves. The slopes of their best-straight-line-fittings, dashed black lines, measure the wave propagation velocity.

The forward and backward waves propagate at 20  $\text{m}\cdot\text{s}^{-1}$  for the 52 mm Hg DC pressure. A second forward wave, with a much lower velocity of 5,5  $\text{m}\cdot\text{s}^{-1}$ , very likely represents the slower transversal component of the forward propagating wave.

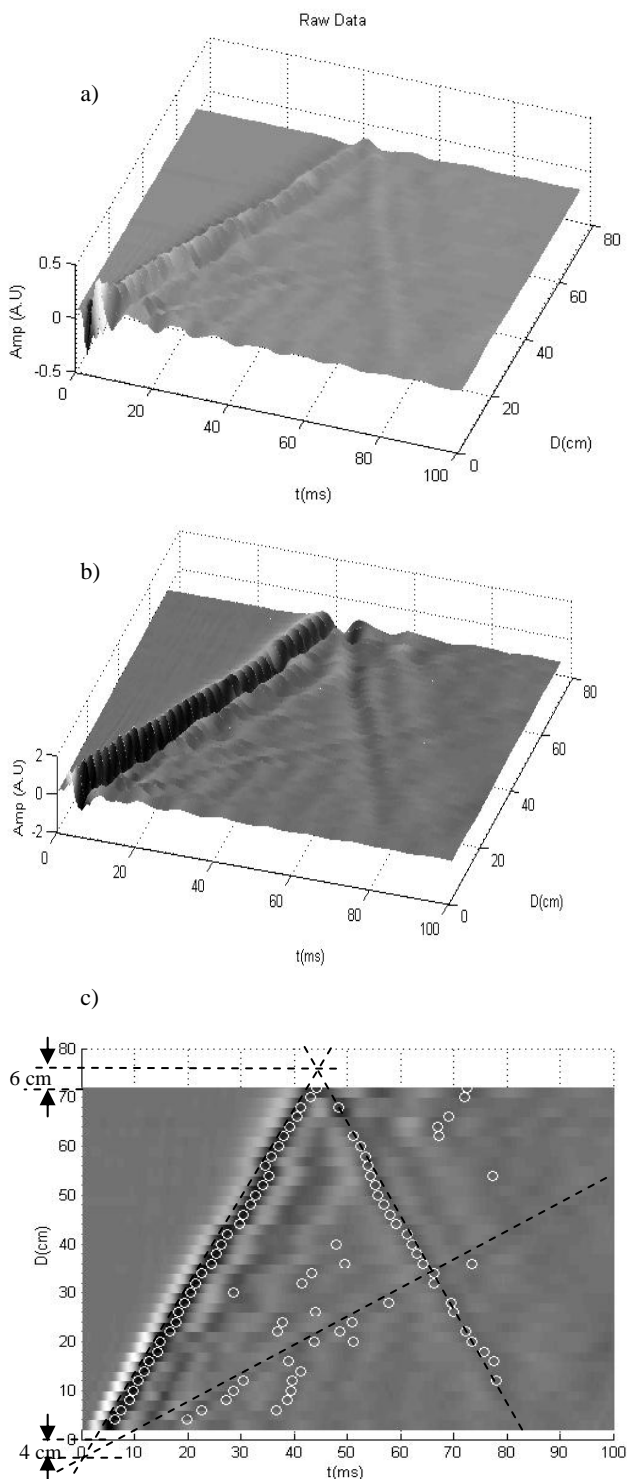


Figure 2 – Raw and deconvolved data are represented in the a) and b) panels, respectively. In c), the white circles and dashed lines result from a peak detection algorithm (see discussion in text).

In figure 2.c, in addition to propagation velocity considerations, evidence of the system geometry can be sorted out. Firstly we notice that the lines converge precisely in the physical reflection site located at 6 cm of the pressure sensor side of the flexible tube. Likewise, the longitudinal and transversal components cross together in the point where they originate, -4 cm. These lengths exactly match the ones of the structures that hold the two tops of the tube (figure 1).

#### IV. RESULTS FROM CONFIGURATION II

The main issue here is to demonstrate the capability of precisely recovering the true pressure waveform from the signal provided by the probe.

To fulfil this endeavour, a cardiac-like signal, shown in figure 3.a, was synthesized and delivered to the system. Deconvolution was used to recover this waveform from the sensor placed at the middle of the tube, using the above referred IR.

Figure 3.b depicts the probe output and the recovered pressure wave showing their striking similarity.

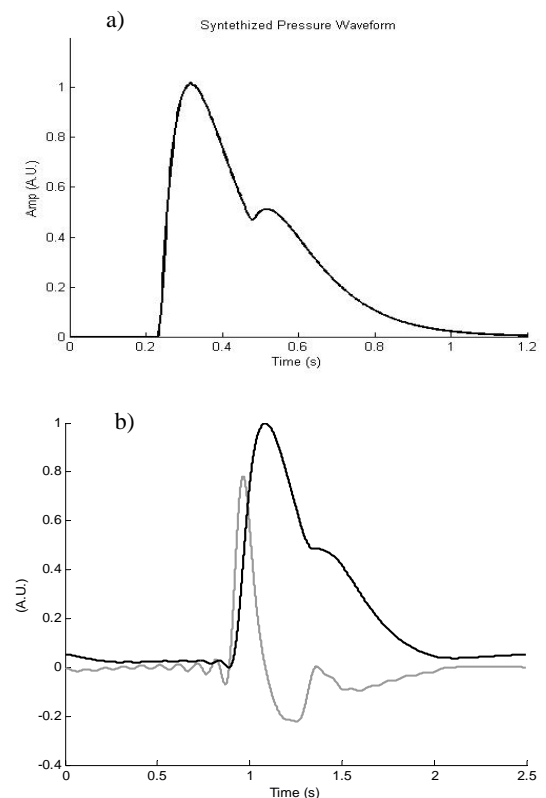


Figure 3 - a) Programmed cardiac-like pressure wave fed to the actuator. b) Probe output (gray), and its deconvolved output (black).

In order to study the influence of reflected waves on the signal, a triangular pressure wave was reproduced by the actuator (for 95 mm Hg DC pressure). The probe was placed at the middle of the tube since the forward and backward travelling waves, from the two reflection sites at the extremities, are more explicitly revealed.

Figure 4 depicts the probe output and its deconvolved waveform, with the time of arrival of the multiple reflected waves signalled by black dots.

The timing associated to the inflection points is consistent with the peaks of the probe signal.

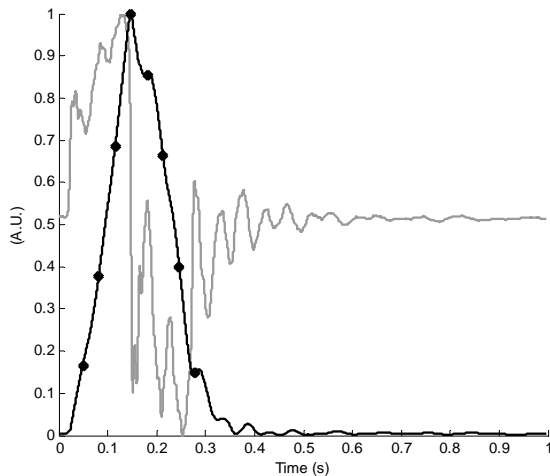


Figure 4 – Evidence of the reflected waves in the shape of the probe signal (gray) and on its deconvolution (black). Black dots denote the timing of arrival of the reflected waves for a  $25 \text{ m}\cdot\text{s}^{-1}$  wave velocity.

Results shown in figure 4 suggest the possibility of developing an algorithm for automatic detection of the reflected waves, using both waveforms.

## V. CONCLUSIONS

A bench system capable of generating arbitrary pressure waveforms under program control was built and operated successfully. Due to its flexibility in generating complex waveforms the system is especially well suited to validate feature-extracting algorithms for hemodynamic studies.

The possibility of recovering APW through deconvolution yielded very satisfactory results and will be naturally pursued up to the clinical tests level. We can still conclude favourably towards the usefulness of the system in probe development and characterization.

Studies in the areas of wave separation, one-point pressure wave velocity, augmentation index and others can be easily implemented and will be pursued as future work.

## ACKNOWLEDGMENTS

We acknowledge support from ISA – Intelligent Sensing Anywhere, from Fundação para a Ciência e Tecnologia and from Instituto de Emprego e Formação Profissional.

## REFERENCES

1. C. D. Bertram, B. S. Gow and S. E. Greenwald (1997) Comparison of different methods for the determination of the true wave propagation coefficient, in rubber tubes and the canine thoracic aorta, *Med. Eng. Phys.* Vol. 19, No. 3. pp. 212-222
2. C.D. Bertram, F. Pythoud, N. Stergiopoulos and J.-J. Meister (1999), Pulse wave attenuation measurement by linear and nonlinear methods in nonlinearly elastic tubes *Medical Engineering and Physics* 21, pp 155–166
3. Richard D Walker, Roy E Smith, Susan B Sherriff and R F M Woodk (1999), Latex vessels with customized compliance for use in arterial flow models, *Physiol. Meas.* **20** (1999) 277–286.
4. Evelien Hermeling, Koen D. Reesink, Robert S. Reneman and Arnold P.G. Hoeks (2007), Measurement of local pulse wave velocity: effects of signal processing on precision, *Ultrasound in Med. & Biol.*, Vol. 33, No. 5, pp. 774–781
5. Abigail Swillens, Lieve Lanoye, Julie De Backer, Nikos Stergiopoulos, Pascal R. Verdonck, Frank Vermassen, and Patrick Segers (2008), Effect of an Abdominal Aortic Aneurysm on Wave Reflection in the Aorta, *IEEE Trans. Biom. Eng.* Vol. 55, no. 5
6. Feng J and Khir AW (2007), Determination of wave intensity in flexible tubes using measured diameter and velocity *Proceedings of the 29th Annual International Conference of the IEEE EMBS, ThP2C2.15*, pp-985
7. Jiun-Jr Wang, Nigel G. Shrive, Kim H. Parker and John V. Tyberg (2009), *Med Biol Eng Comput* 47:189–195
8. Alexander J. Ebenal, Susan Vasana, Corry Clinton, Daniel Cox1 and Timothy Shine (2007), Arterial Blood Pressure System Modeling and Signal Analysis. *Proceedings of the 2007 IEEE International Symposium on Computational Intelligence in Robotics and Automation*, pp 386

Author: Carlos Correia  
 Institute: Centro de Instrumentação  
 Street: University  
 City: Coimbra  
 Country: Portugal

Email: correia@lei.fis.uc.pt

# SYNTHESIZED CARDIAC WAVEFORM IN THE EVALUATION OF AUGMENTATION INDEX ALGORITHMS

## *Case study for a new wavelet based algorithm*

Vânia Almeida, Tânia Pereira, Elisabeth Borges, Edite Figueiras, João Cardoso and Carlos Correia  
*Instrumentation Center, Physics Department, University of Coimbra, R Larga, Coimbra, Portugal*  
vania\_ga@hotmail.com, taniapereira10@gmail.com, elishebabourges@gmail.com, editefigueiras@gmail.com,  
joao.mr.cardoso@gmail.com, correia@lei.fis.uc.pt

Helena Catarina Pereira, José Luís Malaquias and José B. Simões  
*ISA – Intelligent Sensing Anywhere and Instrumentation Center, Physics Department, University of Coimbra, R Larga, Coimbra, Portugal*  
catawina.p@gmail.com, jmalaquias@isa.pt, jbasilio@isa.pt

**Keywords:** Augmentation Index, Arterial Blood Pressure, Wavelets, Probability Density Function.

**Abstract:** We investigate the performance of a new wavelet based algorithm for Augmentation Index (AIx) determination. The evaluation method relies on reference cardiac-like pulses that are synthesized using a weighted combination of exponentially shaped sub-pulses that represent the three main components of real pulses: the systolic stroke, its reflected replica and the carotid reservoir or windkessel effect. The pulses are parameterized so as to reproduce the main types of cardiac waveforms. The values of AIx yielded by the new algorithm are compared with the ones computed directly from the synthesized waveform and with the values produced by standard Probability Density Function (PDF) analysis.

## 1 INTRODUCTION

It has become commonly recognized that, in addition to the the traditional systolic/diastolic pressure values, the morphology arterial pressure waveform (APW) bears a great deal of clinically relevant information.

As a consequence, a trend has emerged inside the hemodynamics research community to extract this information using non-invasive techniques that can circumvent catheterization. Along the years, this quest opened new fields of investigation in sensing techniques and algorithms capable of faithfully rendering the APW, from signals collected at the major artery sites (carotid, brachial, femoral and radial, mainly).

In what concerns the fidelity of APW, the focus of the problem remains on the sensing method adopted to its physical acquisition. Although the non-invasive techniques still rely almost exclusively, on applanation tonometry to collect a representative signal, new ideas are emerging (Mukammala, 2006) (Ciaccio, E., 2008)

On the algorithm side, major areas of interest are under development to extract information from the APW, reflecting the relevance of the clinical parameters they address. Focus on themes such as wave intensity analysis, wave separation, augmentation index, cardiac output have been studied by several authors over the last few years.

Interfacing between signal acquisition and algorithm development, the search for efficient transfer functions capable of rendering the central APW from peripheral data (Hope, 2004) remains an important theme of debate with some authors advocating its accuracy (Chen, 1997; McConnel, 2004) while others show some caution (Hope, 2002; Hope, 2004).

In addition to these two major areas – APW acquisition and algorithm development – new areas of interest have also emerged collaterally along the last few years.

Bench testing is an example. It plays a fundamental role in reproducing one or more features of the arterial system (Khiri A, 2002; Feng J, 2007; Evelien H, 2007) with high enough

repeatability, for testing both, sensing devices and algorithm performance.

Arterial modeling, as another example, has also developed in a multitude of forms. From blood flow and pressure in arteries (Olufsen, M., 1999) to pulse synthesis (Rubins, U., 2008), modeling always shows the possibility of bringing new insights to the problems in study.

The use of the wavelet transform in extracting information from the APW has emerged as a preferred tool due to its decomposition properties (De Melis, 2007). Following this trend, this work focus on studying the performance of a new wavelet based algorithm for determining Aix and explores the virtues of modeling APW with a simple mathematical expression using filtered exponential functions.

## 2 CARDIAC PULSE SYNTHESIS

The usefulness of synthesizing cardiac-like waveforms is associated to their adquacy in playing the role of reference signal for the algorithms under test.

We synthesize the cardiac-like pulse,  $c(t)$ , by summing three exponentially shaped sub-pulses that represent the components of the cardiac waveform with a physiological meaning: the systolic stroke, its reflected replica and the aortic reservoir or windkessel effect. Each sub-pulse is build up with two exponentials that account for the rising and falling edges, respectively.

The general expression of the synthesized pulse is

$$c(t) = \sum_{k=1}^3 A_k \left( \epsilon^{-\frac{t-D_{Rk}}{\tau_{Rk}}} - \epsilon^{-\frac{t-D_{Fk}}{\tau_{Fk}}} \right) \quad (1)$$

Prior to summing, the sub-pulses are submitted to a moving average filtering process in order to smooth the corners that, otherwise, would show up in  $c(t)$ .

In Table 1 a description of the parameters used in equation (1) is provided while Figure 1 depicts a typical cardiac waveform obtained with a suitable selection of these parameters.

Table 1 – Defining parameters for  $c(t)$   
( $k=1$  – systole,  $k=2$  – reflection and  $k=3$  – windkessel)

	$c(t)$ Parameter Description
$A_k$	Amplitude
$D_{Rk}$	Delay of rising exponential
$\tau_{Rk}$	Rising exponential time constant
$D_{Fk}$	Delay of falling exponential
$\tau_{Fk}$	Falling exponential time constant

## 3 AUGMENTATION INDEX

Although Aix carries an important and very intuitive physiological meaning as an index of arterial condition in general, and of arterial stiffness in particular, its prognostic value in clinical practice has not yet reach full potential (Swillens, 2008). This can be a consequence of the compounding nature of its definition where the timing properties of the APW are expressed as a single (possibly misleading) number.

The main purpose of Aix is to quantify the augmentation of the systolic pressure peak (SPP) imparted to the APW by the reflected, or backward propagating, wave.

The commonly accepted definition of Aix is given by the quotient  $Aix = \frac{P_S - P_i}{P_S - P_D}$ , where  $P_S$  is the APW peak pressure,  $P_i$  its pressure at the inflection and  $P_D$  is the diastolic blood pressure. The definition is extended by arbitrarily considering as negative the values of Aix obtained when the reflected wave arrives after the systolic peak (Murgu, 1980). For computational purposes, these values of Aix are given by  $Aix = \frac{P_i - P_S}{P_S - P_D}$ .

The above definition deserves two comments: For one, the physiological meaning of Aix would be better served by the formula  $Aix = \frac{P_S - P}{P_S - P_D}$ , where  $P$  is the increment in pressure imparted to  $P_D$  by the systolic stroke alone, making it clear that  $P$  is the one that can be augmented. Only the fact that  $P$  is unknown (or, at least, very hard to come by) justifies the adopted simplification of taking  $P_i$  instead.

Secondly, the signal convention mentioned above can be misleading. In fact, when the reflected wave arrives shortly after the SPP, the formula yields a negative Aix but, nevertheless, physical augmentation still occurs.

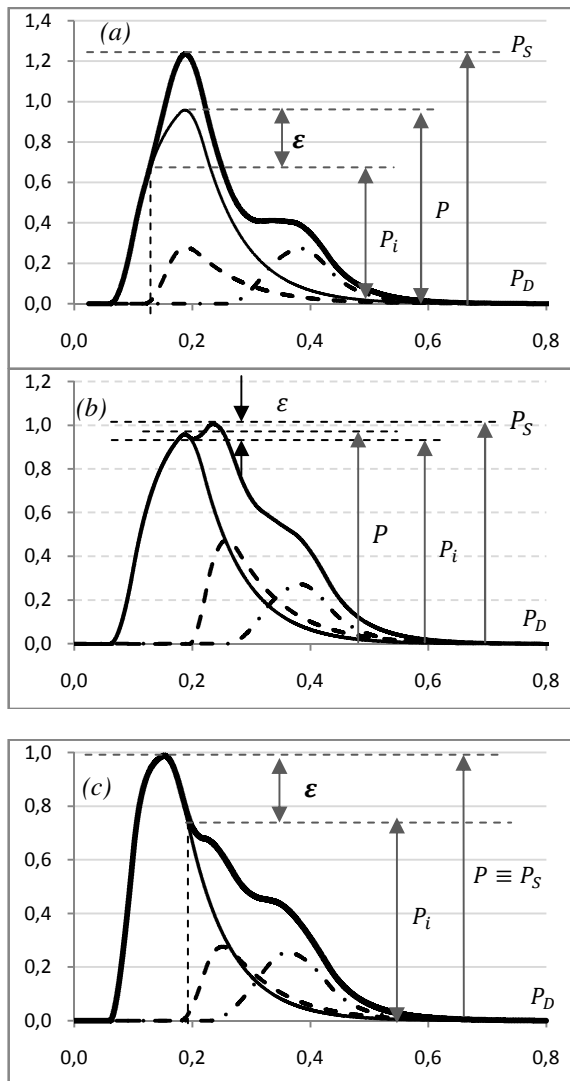


Figure 1 – The panels show the three relevant cases concerning time of arrival of the reflected wave: during systole upstroke (a), shortly after systolic peak (b) and during late systole.

Thin solid line – systolic pressure wave

Dashed line – reflected wave

Dash-point line – windkessel effect.

Thick solid line - APW

Vertical scale – arbitrary units.

Horizontal scale – seconds.

$P_S$  - APW peak pressure,  $P_i$  – pressure at inflection,  $P_D$  - diastolic pressure and  $P$  - increment in pressure imparted to  $P_D$  by the systolic stroke alone

Figure 1 illustrates these comments by plotting three paradigmatic cases: when the reflected wave arrives early during the systolic upstroke, producing an augmentation effect, 1.a, when its arrival occurs shortly after close the systolic peak, still producing augmentation but originating a negative value for AIx, 1.b, and when it arrives during late systole and no physical augmentation, or diminution, occurs but, still, a negative value is delivered by the definition (1.c).

One possible pitfall of the definition lays in the fact that the lawful association of negative values of AIx to a generally favourable arterial condition can configure a misinterpretation of the true physiological situation. This can be particularly important if the undetected condition is clinically addressable by medication.

## 4 ALGORITHM EVALUATION

### 4.1 Test methodology

The key feature of any algorithm for determining AIx is its ability to precisely identify the inflection point associated to the arrival of the reflected wave.

The values of AIx derived from the synthesized waveforms are taken as a reference in all measurements, since these values are not impaired by any identification error.

Evaluation is made by building up a set of waveforms, obtained by gradually varying one of its parameters, in such a way that a range of interesting conditions are swept. In practice, this range of “interesting conditions” must include the limit case where the time of arrival of the reflected wave crosses the systolic peak. This critical transition from positive to negative values of AIx, the so called type A to type C (Murgo et al., 1980) waveforms, unavoidably yields a discontinuity in the output of any of the algorithms.

We use this methodology to evaluate the performance of two intrinsically different algorithms: the PDF and the Bior 1.3 wavelet based one.

Behaviour under noisy conditions is also an important feature that is studied in both cases.

### 4.1.1 Probability Density Function

The working principle of this algorithm (Tsui, 2007) relies on the PDF property of creating a local maximum for the amplitudes close to the inflection point that defines AIx. Unfortunately, other maxima are also created whenever the signal amplitude is slow varying, as happens close to its peaks. To make things worse, these confounding peaks can occur for amplitudes of the same order of magnitude of the inflection point, making the algorithmic identification task very hard to accomplish.

To avoid biasing the results with the error of such an algorithm, we adopted to determine the inflection point using a cursor based interaction. Figure 2 plots a typical result of this procedure.

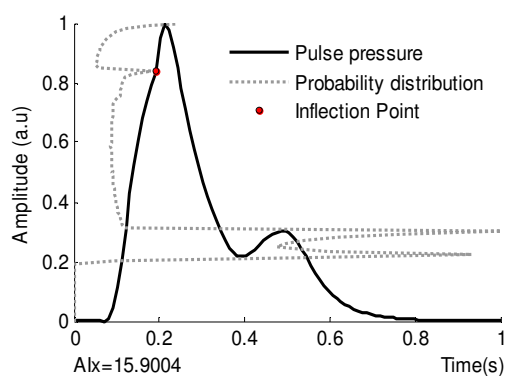


Figure 2 – APW and its associated PDF.

### 4.1.2 Bior 1.3 mother wavelet

The Bior 1.3 mother wavelet represented in Figure 3 (WB1.3) was selected among a few candidates, in a trial and error basis, for its ability in identifying the inflection point, when used in the appropriate scale.

The optimum scale to be used with this mother wavelet in order to maximize the contrast referred to de detection peak. This was determined in several trial-and-error attempts from which the scale 20 (roughly equivalent to a 1.3 ms period) was selected. Figure 4 illustrates a typical detection event characterized by its distinctive narrow peak located in coincidence (vertically aligned) with the inflection point.

The abscissa of the peak is the key to the computation of AIx. Any loss of contrast in the peak definition or any eventual uncertainty in its location (jitter), as happens when noise is present, will reflect in the error magnitude.

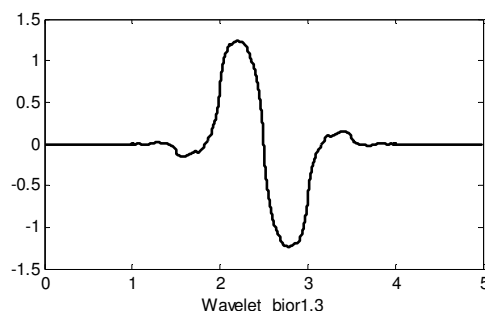
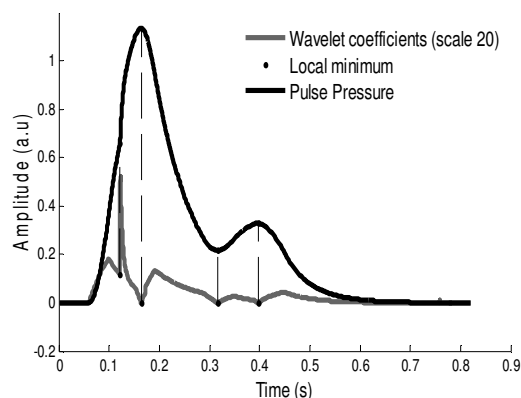


Figure 3 – Mother Wavelet Bior1.3.



The error of the WB1.3 algorithm is studied Figure 4 – Cardiac pulse and its WB1.3 (scale 20) wavelet decomposition (gray curve). Vertical dashed lines show local peaks detected by the WB1.3.

feeding him a family of APWs generated by varying  $D_{R2}$  and  $\tau_{R1}$  in equation 1. These two parameters (systolic wave rise time and the reflected wave delay) probably define the majority of clinical-like interesting conditions. Their variations are selected so as to sweep the interesting region surrounding the APW peak.

Figure 5 depicts the error that affects WB1.3 and allows two conclusions to be drawn: first, an more importantly, the error is very low, always staying below 0.4%. Secondly, yet low, its higher values occur when the reflected waves arrive very soon, low  $D_{R2}$  values, eventually denoting a high pulse wave velocity condition.



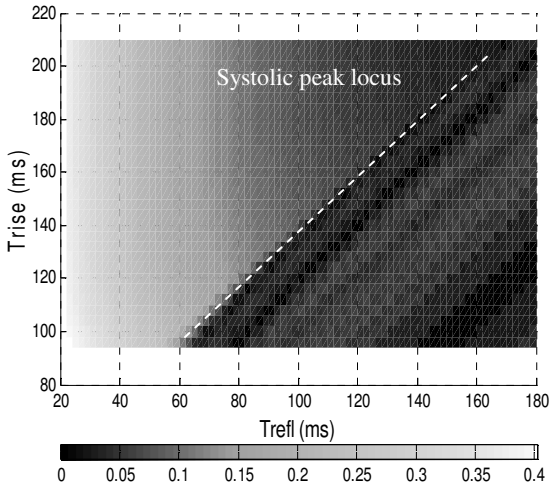


Figure 5 – Plot of Wb1.3 error as a function of  $D_{R2}$  and  $\tau_{R1}$  (denoted respectively as  $T_{refl}$  and  $T_{rise}$ ).

## 4.2 Results

Tests are carried out by feeding a set of cardiac pulses as the input to the PDF and the WB1.3 algorithms in order for them to produce the pressure values required to AIX computation, and comparing the results with the ones obtained when the pressure values directly derive from the synthesized waveforms.

Figure 6 depicts results for a family of cardiac pulses, where  $D_{R2}$  sweeps the interesting area that crosses the systolic peak, showing a discontinuity point created as a result of the definition, as discussed in section 3.

Notice the magnitude of the errors shown in the middle and lower panels, where the superior performance of the WB1.3 algorithm shows up when we compare the maximum errors that are less than 0.5% for the WB1.3 and greater than 2% in the PDF case.

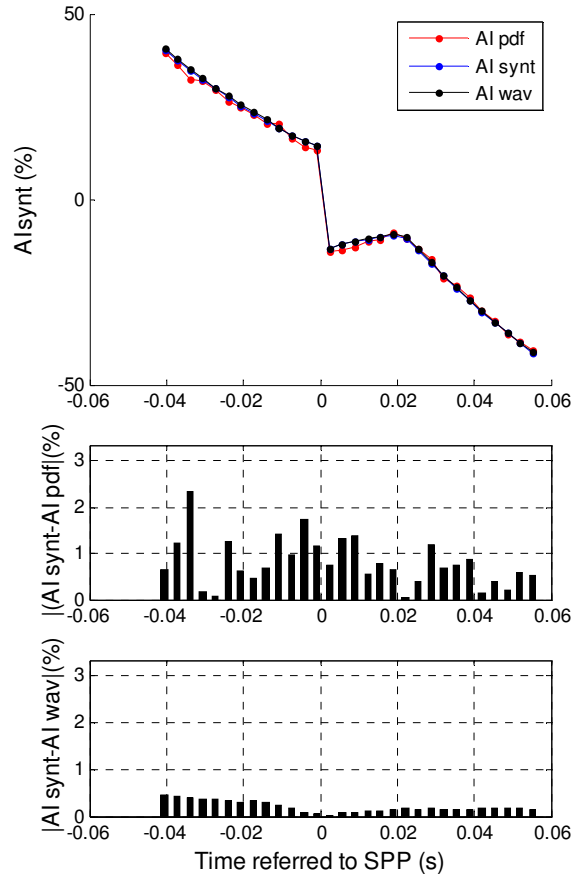


Figure 6 – AIX results yielded by the three methods (upper panel) and plot of errors of PDF and WB1.3 algorithms (middle and lower panels, respectively). Time scale is referred to the systolic pressure peak.

## 4.3 Influence of noise on performance

As expected, the performance of the algorithms is impaired when noise is added to the cardiac pulses. Eventually, a limit can be attained where the discrimination capability of any algorithm is lost. Figure 7 shows the output of the WB1.3 algorithm for a 36 dB signal to noise ratio.

As a general description of noise effects, it scatters and rises the values of AIX, and widens the peak of the WB1.3 output, shown in Figure 4.

It also is noticeable that the characteristic discontinuity of the AIX curve vanishes away in the WB1.3 output, since noise impairs its peak detecting capability.

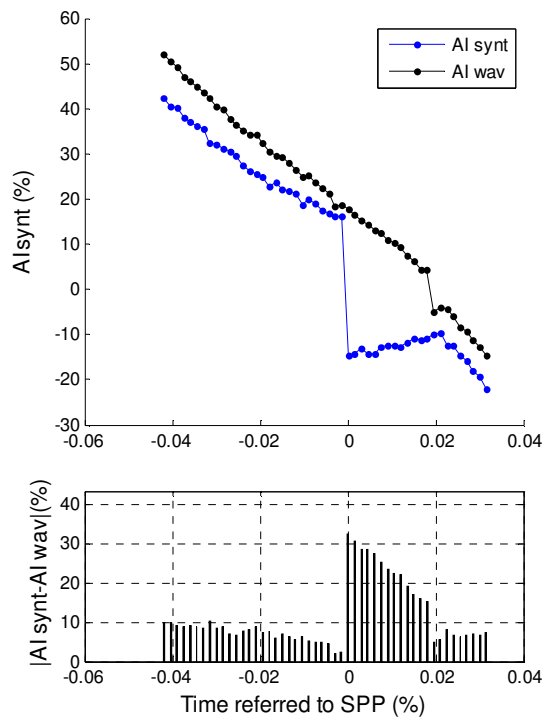


Figure 7 – Consequences of noise added to the APW.

#### 4.4 Sampling frequency

An important question that arises when the cardiac pulses are acquired by the data acquisition system, is to determine the adequate sampling frequency. Oversampling can originate unnecessarily large data files while undersampling will lose information necessary to locate the inflection point.

The issue also casts important consequences on the processing time and on the requirements of the data acquisition system.

The problem can be summarized in a single question: what is the minimum bandwidth required to keep the algorithmic visibility of the inflection point?

Figure 8 shows the absolute value of the error resulting from lowering the signal sampling frequency,  $f_s$ .

The reference for computing the error is a signal sampled at a very high frequency (20kHz).

Even for  $f_s = 1\text{kHz}$ , this error never exceeds 0.6% and, on the other hand, there is no much point in rising this frequency above 5 kHz since no significant improvement in performance is attained.

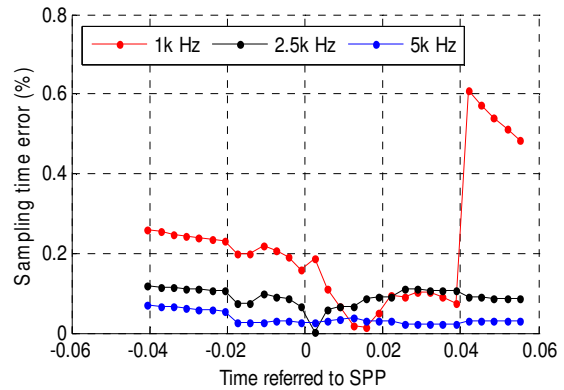


Figure 8 – Error due to different sampling frequencies taking .

## 5 ELECTRONIC IMPLEMENTATION

The fact that AIx depends only on the morphology of the APW, and not on its absolute values, makes it independent of any calibration procedures, hence, very adequate to a simplified implementation.

Current generation microcontrollers available from several manufacturers, contain all resources required to implement a very low component-count electronic AIx instrument. Just a small signal conditioning stage has to be added to match the amplitude of the sensor output to the ADC input.

As in other real time architectures the FIFO shown in Figure 9 plays an important role in interfacing the external signal with the processing unit.

Its capacity must allow the buffering of at least one cardiac cycle, until the current data, another cardiac cycle, is being processed. This figure can only be determined if the sampling rate (SR) of the ADC is known. For a 2 kHz SR, twice the minimum found in 4.4, 2 s long cardiac pulses require a 20 k buffer. This requirement puts a severe constrain in the selection of the microcontrollers for the job. As an example, however, a few members of the PIC32MX family provide, in addition to 32k of RAM, a 10 bit ADC and the USB port.

From the firmware point of view, apart from the basic wavelet decomposition algorithm that takes around 500 ms to run under Matlab, only a routine for start-of-pulse identification has to be added to obtain a fully working device.

Power for the device operation will require a current well below 100 mA that can be borrowed from the USB link.

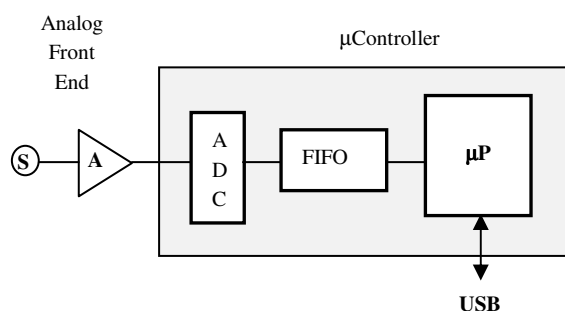


Figure 9 – Diagrammatic view of the electronic circuit.

## ACKNOWLEDGEMENTS

We acknowledge support from Fundação para a Ciência e Tecnologia and from ISA – Intelligent Sensing Anywhere.

## REFERENCES

- Chen, C. (1997). Estimation of Central Aortic Pressure Waveform by Mathematical Transformation of Radial Tonometry Pressure, *Circulation*, 95, 1827-1836
- Ciaccio, E., (2008), Tonometric Arterial Pulse Sensor With Noise Cancellation, *IEEE Transactions on Biomedical Engineering*, 34 (5), 2388-2396
- De Melis, M., et al. (2009). Blood pressure waveform analysis by means of wavelet transform, *Medical and Biological Engineering and Computing*, 47, 165–173.
- Evelien H. (2007), Measurement of local pulse wave velocity: effects of signal processing on precision, *Ultrasound in Med. & Biol.*, 33(5), 774-781
- Feng J. (2007). Determination of wave intensity in flexible tubes using measured diameter and velocity *Proceedings of the 29th Annual International Conference of the IEEE EMBS*, ThP2C2.15, 985-988
- Hope, S. (2002), Comparison of generalized and gender-specific transfer functions for the derivation of aortic waveforms, *Am J Physiol Heart Circ Physiol*, 283, H1150–H1156.
- Hope, S. (2004). Use of Arterial Transfer Functions for the Derivation of Central Aortic Waveform

Characteristics in Subjects With Type 2 Diabetes and Cardiovascular Disease, *Diabetes Care*, 27 (3), 746-751

- Khair, A. (2002), Measurements of wave speed and reflected waves in elastic tubes and bifurcations, *Journal of Biomechanics*, 35, 775–783.
- McConnel, K. (2004). Central Aortic Pressure Wave Changes with Sleep Stage and Disordered Breathing in Children Estimated by Application of an Arterial Transfer Function to Peripheral Blood Pressure, *Proceedings of the 26th Annual International Conference of the IEEE EMBS*, 3864-3866
- Mukkamala, R. (2006), Continuous Cardiac Output Monitoring by Peripheral Blood Pressure Waveform Analysis, *IEEE Transactions on Biomedical Engineering*, 53(3), 459-467.
- Murgo, J.P., Westerhof, N., Giolma J.P., Altobelli, S.A. (1980), Aortic input impedance in normal man: relationship to pressure wave forms. *Circulation*, 62, 105-116
- Olufsen, M. (1999). Structured tree outflow condition for blood flow in larger systemic arteries. *Am J Physiol Heart Circ Physiol*, 276, 257-268.
- Swillens, A. (2008). Assessment of arterial pressure wave reflection: Methodological considerations. *Artery Research*, 2 (4), 122-131
- Rubins, U. 2008. Finger and ear photoplethysmogram waveform analysis by fitting with Gaussians, *Med Biol Eng Comput*, 46, 1271–1276.
- Tsui, P. et al. (2007). Arterial pulse waveform analysis by the probability distribution of amplitude. *Physiol.Means*, 28, 803-812.

# 13. REFERENCES

1. World Health Organization. [Online] 09 08 2009. [http://www.who.int/cardiovascular\\_diseases/en/](http://www.who.int/cardiovascular_diseases/en/).
2. Instituto Nacional de Estatística. [Online] 29 12 2008. [www.ine.pt](http://www.ine.pt).
3. *Expert consensus document on arterial stiffness: methodological issues and clinical applications. Special article.* **Laurent S, et al.**, 25 September 2006, European Heart Journal, p. 18.
4. *Associating between arterial stiffnes and artherosclerosis - The Rotterdam Study.* **van Popele NM, et al.**, 2001, Stroke, Vol. 32, pp. 454-460.
5. Complior (Site in construction). [Online] 09 08 2009. [www.complior.com](http://www.complior.com).
6. AtCor Medical. [Online] 09 08 2009. <http://atcormedical.com/sphygmocor.html>.
7. SEER Training Modules. [Online] [Cited: 13 08 2009.] <http://training.seer.cancer.gov/anatomy/cardiovascular/heart/structure.html>.
8. **Van De Graaff KM**, *Human Anatomy*. s.l. : Mc Graw Hill, 2002. p. 840 .
9. *Arterial Blood Pressure System Modeling and Signal Analysis.* **Ebenal AJ, et al.**, 2007, Proceedings of the 2007 IEEE International Symposium on Computational Intelligence in Robotics and Automation Jacksonville, FL, USA, June 20-23, 2007.
10. **Nichols WW and O'Rourke MF**, *McDonald's Blood Flow in Arteries: Theoretical, Experimental and Clinical Principles*. 5 th ed. London : Hodder Arnold, 2005.
11. *Changes in Arterial Stiffness and Wave Reflection With Advancing Age in Healthy Men and Women: The Framingham Heart Study.* **Mitchell GF, et al.**, 2004, Hypertension, Vol. 43, pp. 1239-1245.
12. *Methods and devices for measuring aterial compliance in humans.* **Pannier BM, Avolio AP and Hoeks A**, 2002, AJH, Vol. 15, pp. 743-753.
13. **Mackenzie IS, Wilkinson IB and Cockcroft JR**. Assessment of arterial stiffness in clinical practice. *Q J Med.* 95, 2002, pp. 67-74.
14. *Assessment of pulse wave velocity.* **Boutouyrie P, et al.**, 2009, Artery Research, Vol. 3, pp. 3-8.

15. DiaTecne. *PulsePen*. [Online] [Cited: 18 08 2009.] [www.pulsepen.com](http://www.pulsepen.com).
16. **Safar ME and O' Rourke MF**. *Arterial Stiffness in Hypertension*. p. 624. Vol. 23, Google livros. Available at: [http://books.google.pt/books?id=h8ao-fkUZ1UC&printsec=frontcover&source=gbs\\_navlinks\\_s#v=onepage&q=&f=false](http://books.google.pt/books?id=h8ao-fkUZ1UC&printsec=frontcover&source=gbs_navlinks_s#v=onepage&q=&f=false) (13-08-2009).
17. *Validation of a new non-invasive portable tonometer for determining arterial pressure wave and pulse wave velocity: determining arterial pressure wave and pulse wave velocity: the PusePen device*. **Salvi P, et al.**, 2004, *Journal of Hypertension*, Vol. 22, pp. 2285-2293.
18. *Central Aortic Pressure Wave Changes with Sleep Stage and Disordered Breathing in Children Estimated by Application of an Arterial Transfer Function to Peripheral Blood Pressure*. **McConnell KB, et al.**, San Francisco, CA, USA : s.n., 2004. Proceedings of the 26th Annual International Conference of the IEEE EMBS. pp. 3864-3866.
19. *Estimation of central aortic pressure waveform by mathematical transform of radial tonometry pressure*. **Chen-Huan C, et al.**, 1997, *Circulation*, Vol. 95, pp. 1827-1836.
20. *Comparison of generalized and gender-specific transfer functions for the derivation of aortic waveforms*. **Hope S**, 2002, *Am J Physiol Heart Circ Physiol*, Vol. 283, pp. H1150-H1156.
21. *Clinical Measurement of Arterial Stiffness Obtained From Noninvasive Pressure Waveforms*. **Nichols WW**, 2005, *AJH*, Vol. 18, pp. 3S-10S.
22. *Wave propagation in a model of the arterial circulation*. **Wang JJ and Parker KH**, 2004, *Journal of Biomechanics*, Vol. 37, pp. 457-470.
23. [http://www.daviddarling.info/images/anatomy\\_of\\_aorta.gif](http://www.daviddarling.info/images/anatomy_of_aorta.gif). [Online] 27 06 2009.
24. *Aortic input impedance in normal man: relationship to pressure wave forms*. **Murgo JP, et al.**, 1980, *Circulation*, Vol. 62, pp. 105-116.
25. *Normal vascular aging: differential effects on wave reflection and aortic pulse wave velocity: the Anglo-Cardiff Collaborative Trial (ACCT)*. **McEniery CM**, 2005, *J Am Coll Cardiol*, Vol. 46, pp. 1753-1760.
26. *Assessment of arterial pressure wave reflection: Methodological considerations*. **Swillens A and Segers P**, 2008, *Artery research*, Vol. 2 (4), pp. 122-131.
27. *Arterial stiffness and prediction of cardiovascular risk*. **Kingwell BA and Gatzka CD**, 2002, *Journal of Hypertension*, Vol. 20, pp. 2337-2340.
28. *Arterial pulse waveform analysis by the probability distribution of amplitude*. **Tsui P, et al.**, 2007, *Physiological measurement*, Vol. 28, pp. 803-812.

29. **Milnor WR.** *Cardiovascular Physiology.* p. 520. Google Books. Available at: [http://books.google.pt/books?id=1duFI886FxlC&sitesec=buy&source=gbs\\_navlinks\\_s\\_s](http://books.google.pt/books?id=1duFI886FxlC&sitesec=buy&source=gbs_navlinks_s_s) (13-08-2009).
30. *The arterial windkessel.* **Westerhof N, et al.,** 2009, *Med Biol Eng Comput*, Vol. 47, pp. 131-141.
31. *Systemic venous circulation. Waves propagating on a windkessel: relation of arterial and venous windkessel to systemic vascular resistance.* **Wang J, et al.,** 2006, *Am J Physiol Heart Circ Physiol*, Vol. 290, pp. H154-H162.
32. National Heart Lung and Blood Institute. Diseases and conditions Index. [Online] [Cited: 4 Fevereiro 2009.] [http://www.nhlbi.nih.gov/health/dci/Diseases/Atherosclerosis/Atherosclerosis\\_WhatIs.html](http://www.nhlbi.nih.gov/health/dci/Diseases/Atherosclerosis/Atherosclerosis_WhatIs.html).
33. Cardiovascular Media Library. [Online] American Heart Association. [Cited: 4 Fevereiro 2009.] <http://medmovie.com/mmdatabase/MediaPlayer.aspx?ClientID=65&TopicID=0>.
34. *Pulse pressure: a predictor of long-term cardiovascular mortality in a French male population.* **Benetos A, et al.,** 1997, *Hypertension*, Vol. 30, pp. 1410-1415.
35. *Isolated systolic hypertension: prognostic information provided by pulse pressure.* **Domanski MJ, et al.,** 1999, *Hypertension*, Vol. 34, pp. 375-380.
36. Piezoelectric sensors. [Online] 25 07 2009. <http://ccrma.stanford.edu/CCRMA/Courses/252/sensors/node7.html>.
37. **Borges E.** *Assessment of Hemodynamic Parameters.* Departamento de Física, Universidade de Coimbra. 2008.
38. **Gautschi G.** Google Book Search. *Piezoelectric Sensorics.* [Online] [Cited: 24 02 2009.] [http://books.google.com/books?id=-nYFSLcmc-cC&printsec=frontcover&source=gbs\\_summary\\_r&cad=0#PPP1,M1](http://books.google.com/books?id=-nYFSLcmc-cC&printsec=frontcover&source=gbs_summary_r&cad=0#PPP1,M1).
39. Piezoelectric sensors. *Wikipedia.* [Online] [Cited: 25 07 2009.] [http://en.wikipedia.org/wiki/Piezoelectric\\_sensor](http://en.wikipedia.org/wiki/Piezoelectric_sensor).
40. **Tadinada Akhila.** Piezo film sensors for capture of arterial wave pulse. [Online] [Cited: 25 07 2009.] <http://cnx.org/content/m15671/latest/>; <http://cnx.org/content/m15664/latest/>; <http://cnx.org/content/m15670/latest/>.
41. *Piezoelectric sensor determination of arterial pulse wave velocity.* **McLaughlin J,** 2003, *Physiological measurement*, Vol. 24, pp. 693-702.
42. *Blood pressure waveform analysis by means of wavelet transform.* **De Melis M, et al.,** 2009, *Med Biol Eng Comput*, Vol. 47, pp. 165-173.
43. *Wavelet transform to quantify heart rate variability and to assess its instantaneous changes.* **Pichot V.,** s.l. : *J Appl Physiol*, 1999, Vol. 86, pp. 1081-1091.

44. **Misiti M, et al.**, *Wavelet Toolbox 4. User's Guide*.
45. *A theory for multiresolution signal decomposition: the wavelet representation*. **Mallat SG**, 1989, IEEE T Pattern Anal, Vol. 11 (7), pp. 674-692.
46. *Cuffless and Noninvasive Estimation of Blood Pressure Based on a Wavelet Transform Approach*. **Lee CM and Zhang YT**, 2003. IEEE EMBS Asian-Pacific Conference on Biomedical Engineering. pp. 148-149.
47. *Dicrotic notch detection using wavelet transform analysis*. **Antonelli L, Khamlach R and Ohley W**, 1994. Proceedings of the 16th Annual International Conference of the IEEE. pp. 1216-1217.
48. *Wavelet transform analysis of the arterial pressure waveform*. **Antonelli L, Khamalach R and Ohley W**, 1994. Proceedings of the IEEE-SP International Symposium on Time-Frequency and Time-Scale Analysis. pp. 568-571.
49. *A novel approach in R peak detection using Hybrid Complex Wavelet (HCW)*. **Moghadam PJ, et al.**, 2008, Intrnation Journal of Cardiology, Vol. 124, pp. 250-253.
50. *Wavelete theory-based analysis of high-frequency, high-resolution electrocardiograms:a new concept for clinical uses*. **Ishikawa Y and Mochimaru F**, 2002, Progress in biomedical research, Vol. 7(3), pp. 179-184.
51. **Pereira HC**, *Cardioaccelerometry*. Departamento de Física, Universiadade de Coimbra. 2007.
52. *Latex vessels with customized compliance for use in arterial flow models*. **Walker RD, et al.**, 1999, Physiol Meas, Vol. 20, pp. 277-286.
53. *Multi-branched model of the human arterial system*. **Avolio AP**, 1980, Med Biol Eng Comput, Vol. 18, pp. 709-718.
54. *Effect of an Abdominal Aortic Aneurysm on Wave Reflection in the Aorta*. **Swillens A**, 2008, IEEE Trans Biom Eng, Vol. 55(5).
55. *Determination of wave intensity in flexible tubes using measured diameter and velocity*. **Feng J and Khir AW**, 2007. Proceedings of the 29th Annual International, Conference of the IEEE EMB. pp. 985-988.
56. *"Wave" as defined by wave intensity analysis*. **Wang J**, 2009, Med Biol Eng Comput , Vol. 47, pp. 189-195.
57. *Measurements of wave speed and reflected waves in elastic tubes and bifurcations*. **Khir AW and Parker KH** 2002, Journal of Biomechanics, Vol. 35, pp. 775-783.
58. Sirp . *Loudspeaker analyser*. [Online] 27 07 2009. <http://www.tolvan.com/sirp/SirpUsersGuide.htm>.

59. *Finger and ear photoplethysmogram waveform analysis by fitting with Gaussians.* **Rubins U**, 2008, *Med Biol Eng Comput*, Vol. 46, pp. 1271-1276.
60. *Continuous Cardiac Output Monitoring by Peripheral Blood Pressure Waveform Analysis.* **Mukkamala R, et al.**, 2006, *IEEE Trans Biom Eng*, Vol. 53(3), pp. 459-467.
61. *Forward and Backward Running Waves in the Arteries: Analysis Using the Method of Characteristics.* **Parker KH and Jones CJH**, 1990, *Journal of Biomechanical Engineering*, Vol. 112, pp. 322-326.
62. *Chasing the wave. Unfashionable but important new concepts in arterial wave travel.* **Bleasdale RA, Parker KH and Jones CJH**, 2003, *Am J Physiol Heart Circ Physiol*, Vol. 284, pp. H1879–H1885.
63. National Instruments. [Online] 15 February 2009. <http://www.ni.com/>.